RADIATION STUDIES ON AL-RELATED DEFECT CENTERS IN QUARTZ CRYSTALS

By

HO BYONG HWANG

Bachelor of Science
Jeonbug National University
Jeonju, Jeonbug, Korea
1974

Master of Science
Oklahoma State University
Stillwater, Oklahoma
1985

Submitted to the Faculty of the
Graduate College of the
Oklahoma State University
in partial fulfillment of
the requirements for
the Degree of
DOCTOR OF PHILOSOPHY
May, 1987

RADIATION STUDIES ON AL-RELATED DEFECT CENTERS IN QUARTZ CRYSTALS

Thesis Approved:

Joel J. Martin
Thesis Adviser

Timothy M. Wilson

Larry E. Halliburton

Zahir A. Iskander

Norman N. Durham
Dean of the Graduate College

ACKNOWLEDGEMENTS

I would like to take this opportunity to thank Profs. Joel J. Martin, Larry E. Halliburton, Timothy M. Wilson, and Zuhair Al-Shaieb for serving as the members of my committee. Special thanks are due to Dr. Joel J. Martin, my adviser and committee chairman, for his advice, help, and patience.

Further acknowledgement is extended to the Solid State Science Division, RADC, U.S. Air Force Hanscom AFB and Sandia National Laboratories which sponsored this work.

Lastly, I must thank my grandmother, my parents, my wife, and my daughter, Jeong In, for their understanding and sacrifice.

TABLE OF CONTENTS

LIST OF TABLES

LIST OF FIGURES

CHAPTER I

INTRODUCTION

1. Quartz

Silicon dioxide, SiO_2, exists in several crystalline phases as well as an amorphous phase. Alpha-quartz, sometimes called "low-quartz," is one of the phases which crystallize at temperatures below 573°C at atmospheric pressure. It transforms from alpha-quartz to beta-quartz at 573°C at atmospheric pressure. Under stress it transforms at lower temperatures. Beta-quartz, sometimes called "high-quartz," does not change its structure at temperatures between 573°C and 870°C under atmospheric pressure. Alpha-quartz has a trigonal structure while beta-quartz has a hexagonal structure. We are concerned with alpha-quartz and will refer to it simply as "quartz." Both right-handed and left-handed quartz are found in nature. They are mirror images of each other. Sometimes quartz is named as rose quartz, smoky quartz, amethyst, or other gems by its color which is due to traces of foreign matter. Among the other forms of SiO_2 are tridymite, cristobalite, and silica (the fused amorphous form). High-quality natural quartz is found in nature, especially in Brazil. However, the limited supply and the high cost of natural quartz have resulted in

the development of a cultured quartz industry. In these days cultured quartz, or synthetic quartz, is used for most applications.

The brothers Pierre and Jacques Curie discovered the direct piezoelectric effect in 1880. The direct piezoelectric effect can be defined as the electric field generated by mechanical stress especially in a crystalline substance, as quartz; electric polarization can be induced by simply squeezing the crystal along a certain axis. The inverse piezoelectric effect was predicted in 1881 by the French physicist Lippmann on the basis of the principle of conservation of electricity. It was verified in the same year by the brothers Curie. The inverse piezoelectric effect is the strain caused by an applied electric field; the application of polarizing electric fields may cause the crystal to experience a longitudinal or shearing stress. Although many crystals exhibit the piezoelectric effect, very few are useful, and quartz alone provides the necessary combination of mechanical, electrical, and thermal properties required for making piezoelectric elements for the electrical communication field. By using the piezoelectric properties of quartz, in 1916 Paul Langevin piezoelectrically excited quartz plates to generate acoustic waves in water for use in submarine detection. About the same time the piezoelectric resonator was developed, and quartz proved to be the most suitable material [1]. The quartz resonator vibrates over an extremely narrow range of

frequencies. Quartz crystal can be used as an oscillator or a filter which operates with a combination of the direct and inverse piezoelectric effects. It is used to control and manage the frequencies of the carrier signals in electronic communications. No other method of frequency control has been devised which competes with the vibrating quartz piezoid in accuracy, convenience, and reliability. The quartz piezoid is an electromechanical transducer, i.e., it provides coupling between the mechanical resonance frequency of the piezoid and the electric circuit.

2. Quartz Resonators

Since the physical properties of the crystalline solid are generally dependent upon direction, it is necessary to choose reference directions within the crystal for use in specifying their values. Such directions are called the crystal axes. A crystal axis is not a line but a direction in the crystal. The axial directions are chosen to describe the crystalline properties as simply as possible. Different axial systems may be used to describe the same crystal. However, one axial system may be convenient for one purpose and another system for another purpose. For example, the Bravais-Miller axial system is convenient to specify the natural faces and atomic planes in quartz while an orthogonal coordinate system is more convenient for purposes of computations involving the piezoelectric and mechanical properties of quartz. Figure 1 shows the idealized quartz

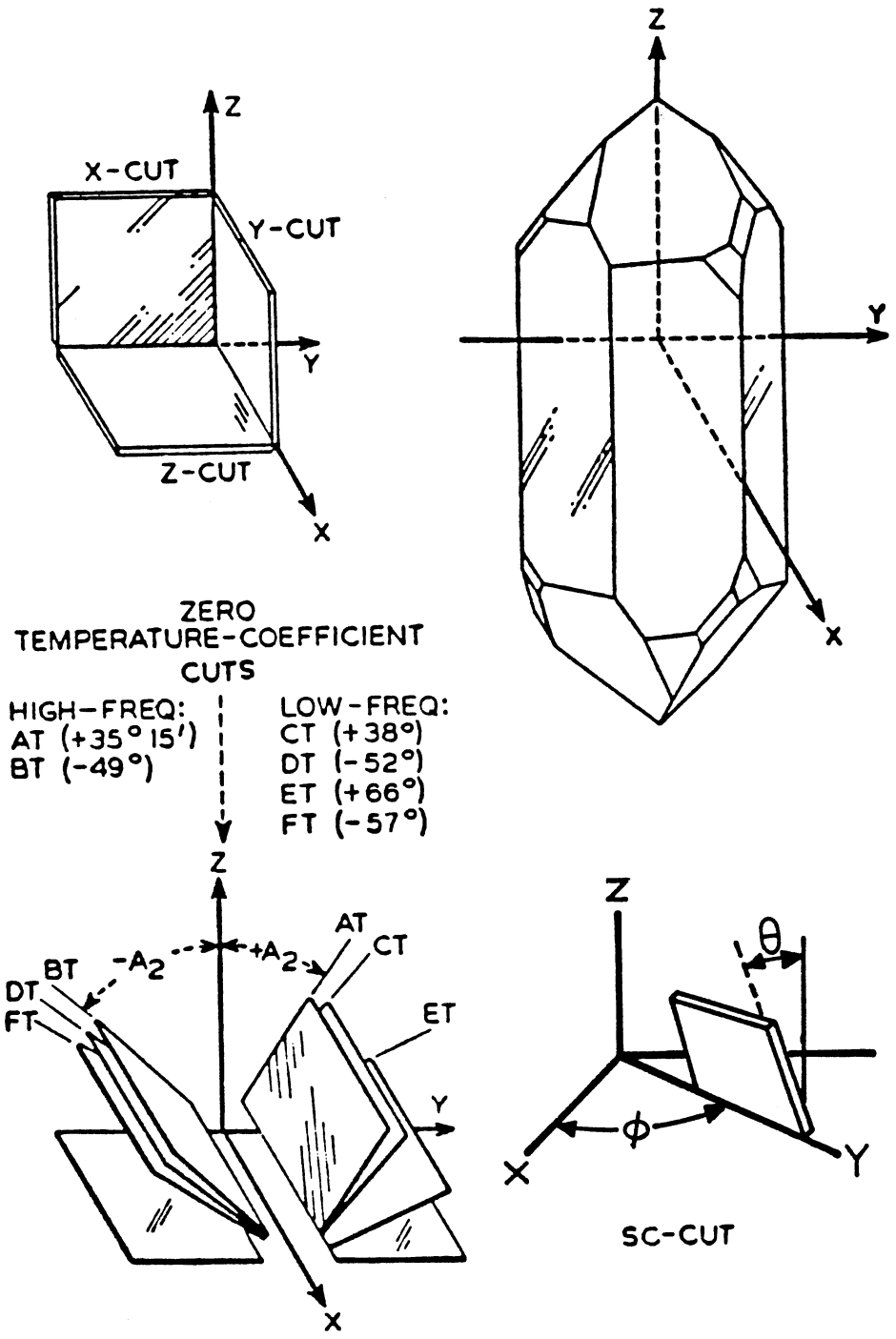

Figure 1. Idealized Quartz Crystal and Principal Cuts

crystal with the orthogonal, or rectangular, coordinate system indicated on it and various cuts. The X-axis of the orthogonal coordinate system is one of the three electric axes which have two-fold symmetry or are parallel to a line bisecting the angles between adjacent hexagonal prism faces. The positive X-direction is chosen to be the direction in which the extension resulting from tension produces a positive charge. The Z-axis is taken along the axis of the hexagonal prism, or the optical axis, c, which has three-fold symmetry. The positive Z-direction is chosen in either end of the Z-axis since the X-axis is an axis of two-fold symmetry. Then, the Y-axis is chosen to form the orthogonal coordinate system. The Y-axis is not a polar axis and no electric polarization results from an extensional strain in the Y-direction.

For a frequency control devices, the quartz stone is cut into plates which become the frequency-determining elements. The first quartz resonator was simple quartz plate cut from the crystal in such a way that the normal to the plate is parallel to the X-axis. Such a quartz plate, called an X-cut plate, has a temperature coefficient of frequency of about -20Hz/(MHz)(^{o}C). This means that the frequency decreases 20 ppm for each degree rise in temperature. The Y-cut plate, which is perpendicular to the Y-axis, has certain advantages over the X-cut plate. It is only about two-thirds as thick as an X-cut plate of the same frequency. It also has fewer undesirable modes of vibration

and is less affected by air damping. Its fabrication is also somewhat simpler when Y-bar synthetic quartz is used. Its most important advantage is that it can be clamped for mounting. However, the Y-cut has two disadvantages; the temperature coefficient of frequency is about 100 ppm/^{o}C and the device often refuses to operate or change frequency abruptly as the temperature is changed. These plates can have a number of modes of vibration and, often, each mode will have a different temperature dependence. However, the primary vibration of the X-cut is a longitudinal along the thickness direction while the Y-cut vibrates primarily in a thickness-shear mode.

The X- and Y-cuts have relatively poor temperature-frequency characteristics. Thus, singly rotated cuts were developed to improve the poor temperature-frequency characteristics of the X- and Y-cuts. The first zero-temperature-coefficient cut is the AT-cut which is a Y-cut plate containing the X-axis and rotated about the X-axis by approximately 35^{o}20'. The rotation angle of 35^{o}20' about the X-axis is chosen so that the temperature coefficient of frequency is zero or very small at the desired operating temperature range, which is usually between 25^{o}C and 70^{o}C. The second zero-temperature-coefficient cut is the BT-cut which is the Y-cut plate rotated about the X-axis by -49^{o}. It is 50 percent thicker than the AT-cut for a given frequency. The AT-cut is preferred since it has a smaller frequency excursion over the wide temperature range required

by modern communication systems. Other singly rotated cuts, such as CT-cut, DT-cut, ET-cut, and FT-cut, were discovered later as a result of the search for orientations for which the frequency is immune to temperature changes. However, the AT-cut is still the most widely used cut of all the quartz cuts. The primary vibration of these singly rotated cuts is a thickness-shear mode with atomic displacements in the X-direction.

Although the AT-cut has a zero-temperature-coefficient of the frequency at certain temperature range, it is sensitive to mechanical stress bias such as caused by sudden small temperature changes and forces of acceleration. The frequency stabilization under highly adverse conditions required the development of the crystal unit much less affected by a variety of thermally and physically induced stresses. In 1976, EerNisse [2] predicted theoretically that a doubly rotated cut should be free of frequency changes due to any mechanical stress bias. He concluded that the frequency-stress coefficient should depend on the rotation angle about the Z-axis, ϕ, while the first-order frequency-temperature coefficient should be determined almost entirely by the rotation angle about the X-axis, θ. He called the new doubly-rotated cut the SC-cut which means the stress-compensated cut. In 1977, Kusters *et al.* [3] showed experimentally that the results predicted by EerNisse were obtained with a cut having the orientation angles $\phi=21.93^{\circ}$ and $\theta=34.11^{\circ}$. Therefore, the SC-cut has a number

of advantages over the singly rotated AT-cut and BT-cut plates for a variety of thermally and physically induced sresses. The predominant mode of vibration in the SC-cut is a quasi-shear c-mode which is analogous to the AT-cut.

3. Review of Acoustic Loss Literature

Acoustic loss studies for high frequency precision quartz resonators began at the Bell Telephone Laboratories in 1955. H. E. Boemmel, W. P. Mason, and A. W. Warner [4, 5] first found the two loss peaks, one near 23K and the other 53K in 5 MHz AT-cut quartz resonators. They assigned incorrectly these 23K and 53K loss peaks to dislocation relaxations and oxygen vacancies respectively. J. C. King [6, 7] introduced annealing, electrolysis and irradiation techniques. He found another loss peak near 135K in quartz containing a large 53K loss peak. He also found that electrolysis removed the 53K loss peak and induced a 85K loss peak. C. K. Jones and C. S. Brown [8] reported that the 53K loss was increased and the 23K loss peak decreased with increasing growth rate of the quartz stone. D. B. Fraser [9] diffused the various alkali ions into resonators by electrodiffusion technique. He found the 50K and 135K loss peaks with the Na^+-diffused natural quartz which was similar to those of the synthetic z-minor quartz. The Li^+-diffused resonator showed a reduction of the 53K loss peak while the K^+-diffused resonator showed the large 53K loss peak. This last result is understandable because the Na^+

ions present at the furnace or the anode material could move more readily in the case of electrodiffusion of the large K^+ ions than in the case of the Li^+-diffusions. J. C. King [6, 7] and Fraser [9] showed that the Al-Na^+ center is responsible for the 53K loss peak by using irradiation and electrodiffusion techniques. J. J. Martin [10] swept Li^+- and H^+-, or D^+-ions into AT-cut resonators made from high-aluminum-content Premium Q grade quartz and measured the acoustic loss in the temperature range from 4.5K to 370K. The small 53K loss peak present in the as-received sample was removed by the electrodiffusion but no new loss peaks were introduced in this temperature range. Therefore, he concluded that the Al-Li^+ and the Al-OH^- centers have no loss peaks in this temperature region.

J. C. King [6, 7] found that the size of the 53K loss peak was reduced and a new 100K loss peak was produced after irradiating the resonators with 50KV X-rays. King and Sander [11] produced the 100K loss peak and the broad loss peak between 125K and 165K by irradiating the AT-cut resonator at liquid nitrogen temperature and measuring the losses as the resonator was warmed up, and attributed these loss peaks to the Al-hole center. J. J. Martin, L. E. Halliburton, and R. B. Bossoli [12] described this broad loss as a single peak centered at 135K. J. J. Martin and S. P. Doherty [13] suggested that the 23K loss peak is also due to the Al-hole center. Infrared studies by W. A. Sibley, J. J. Martin, and M. C. Wintersgill *et al.* [14] and ESR studies

by M. E. Markes and L. E. Halliburton [15] on well-characterized synthetic quartz show that in the presence of an ionizing radiation field, hydrogen is mobile at all temperatures; but sodium and the other alkalis are mobile only at the temperatures above 200K. Acoustic loss studies under irradiation by Doherty and Martin [16] also show that sodium becomes mobile above 200K. L. E. Halliburton, N. Koumvakalis, and M. E. Markes *et al.* [17] reported that the room temperature irradiation breaks up the Al-Na^+ centers and produced a mixture of the Al-hole and Al-OH^- centers. They suggested that these radiation-induced Al-hole centers are responsible for the loss peaks at 23K, 100K, and 135K. J. J. Martin, H. B. Hwang, and H. Bahadur [18] reported new radiation-induced loss peaks at 305K in Li-swept samples and 340K in samples which contained significant amount of sodium.

4. Purpose of Investigation

Quartz crystals are often used in electronic instruments as filters and frequency control devices. The performance of such electronic devices in space can be degraded by ionizing radiation [11]. Therfore, investigation of the effects of ionizing radiation on quartz resonator is of considerable importance.

The substitutional aluminum in quartz requires a charge compensating ion which is usually an interstitial alkali ion. Irradiation at room temperature destroys the Al-M^+

centers in quartz and produces a mixture of the Al-hole and $Al\text{-}OH^-$ centers [17]. These Al-related defects, both growth and radiation-induced defects, play a important role in the performance of quartz oscillators.

The frequency shift caused by the removal of the $Al\text{-}Na^+$ centers and by the production of the Al-hole centers is not desirable. Thus, it is very important to know how the defects are modified or produced by the ionizing radiation. The $Al\text{-}Na^+$ center causes the 53K loss peak, but the $Al\text{-}Li^+$ center does not have a loss peak below 370K. Radiation-induced loss peaks at 100K and 135K appear to be related to the Al-hole centers while the $Al\text{-}OH^-$ centers do not show acoustic loss peaks below 370K [10]. Ionizing radiation also introduces the 23K loss peak.

Unswept, Na-swept, Li-swept, and H-swept samples of AT-, BT-, or SC-cut crystal will be used for this study to investigate the destruction of the $Al\text{-}Na^+$ centers and the production of the Al-hole centers as a function of radiation dose at room temperature. Also initial low temperture irradiation and subsequent low temperature irradiation after room temperature irradiation to saturation will be performed to study the production of the defects causing acoustic loss. The 100K loss peak is probably caused by the Al-hole center. The defect responsible for the 23K loss peak is, at the present time, unknown; it usually appears along with the 100K loss peak. The frequency shift due to the removal of the 53K loss peak or the introduction of the 100K loss peak

will be studied. These frequency related data can be used to predict the radiation response of the quartz resonator.

CHAPTER II

INTERNAL FRICTION

1. Anelasticity and Internal Friction: Review

When a stress is applied to a solid, the orientation of point defects changes with time to a new equilibrium state: when the stress is removed the change is reversed and with time the original state of order is restored. This process, known as "stress-induced ordering," produces the anelastic behavior of the solid [19]. Acoustic loss or internal friction is one manifestation of anelasticity of the solid. An ideal elastic solid, which is described by Hooke's law, satisfies the following conditions; an unique equilibrium relation, "instantaneous," and "linearity." However, if among these three conditions, the condition, "instantaneous," is discarded and time-dependence is introduced, the solid is anelastic.

Nowick and Berry have reviewed the theory of anelasticity [20]. In the case of the dynamic experiments such as where the stress and the strain change sinusoidally, the strain will lag behind the applied stress by a phase angle ø in an anelastic system. This phase angle ø is found to be

$$\tan \phi = \frac{1}{2\pi} \frac{\Delta W}{W} \tag{1}$$

where ΔW is the energy density dissipated in a full cycle and W is the maximum stored energy density [20]. Equation (1) shows that tan ϕ is a measure of the energy dissipated or energy loss in a cycle due to the anelasticity of the material. The quantity ϕ (or tan ϕ) is often called the "internal friction" or the "acoustic loss." The quality factor, Q, of a vibrating system is defined as

$$Q = 2\pi \frac{W}{\Delta W} \tag{2}$$

so long as the damping is small [21], and Equation (1) can be rewritten as follows

$$\phi = Q^{-1} = \frac{1}{2\pi} \frac{\Delta W}{W}, \quad \phi << 1 \tag{3}$$

The complex elastic modulus M^* of the anelastic solid can be written as

$$M^* = M^* \exp(i\phi) = M_1 + iM_2 \tag{4}$$

where ϕ is the loss angle, M_1 describes the "storage," and M_2 the "loss." The internal friction then follows, from the above Equation (4).

$$\tan \phi = M_2/M_1 \tag{5}$$

Suppose that the solid "relaxes" at a rate, τ, from its unrelaxed state with modulus M_u to a relaxed state with modulus M_r upon the application of a step function stress.

Nowick and Berry [20] showed that in the case of small loss angle

$$M_1 = M_u - \frac{\delta M}{1+\omega^2\tau^2}, \qquad M_2 = \frac{\delta M}{1+\omega^2\tau^2} \tag{6}$$

where $\delta M = M_u - M_r$. Figure 2 shows the real M_1 and imaginary M_2 parts of the complex elastic modulus M^* plotted against the logarithm of $\omega\tau$. By substituting Equations (6) into Equation (5) we can find the acoustic loss or internal friction for the case of small losses as follows

$$Q^{-1} = \phi = \frac{\Delta}{1+\Delta}\frac{\omega\tau}{1+\omega^2\tau^2}, \quad \phi<<1 \tag{7}$$

where Δ, which is called "relaxation strength," is defined as $\Delta = \delta M/M_r$. However, since the relaxation strength, Δ, is very small ($\Delta<<1$) Equation (7) can be rewritten as follows

$$Q^{-1} = \frac{\Delta\omega\tau}{1+\omega^2\tau^2}, \quad \phi<<1 \tag{8}$$

This form is first suggested by Zener in 1948. For the case of point defects, the anelastic behavior of a solid often shows a single relaxation process, and follow a single Debye peak such as Equation (8). Often the relaxation process is due to the thermally activated jumping of an atom or defect between equivalent orientations. When this assumption holds, the probability of a jump per second, τ^{-1}, can be described by an Arrhenius relation:

$$\tau^{-1} = \tau_o^{-1}\exp(-\Delta H/kT) \tag{9}$$

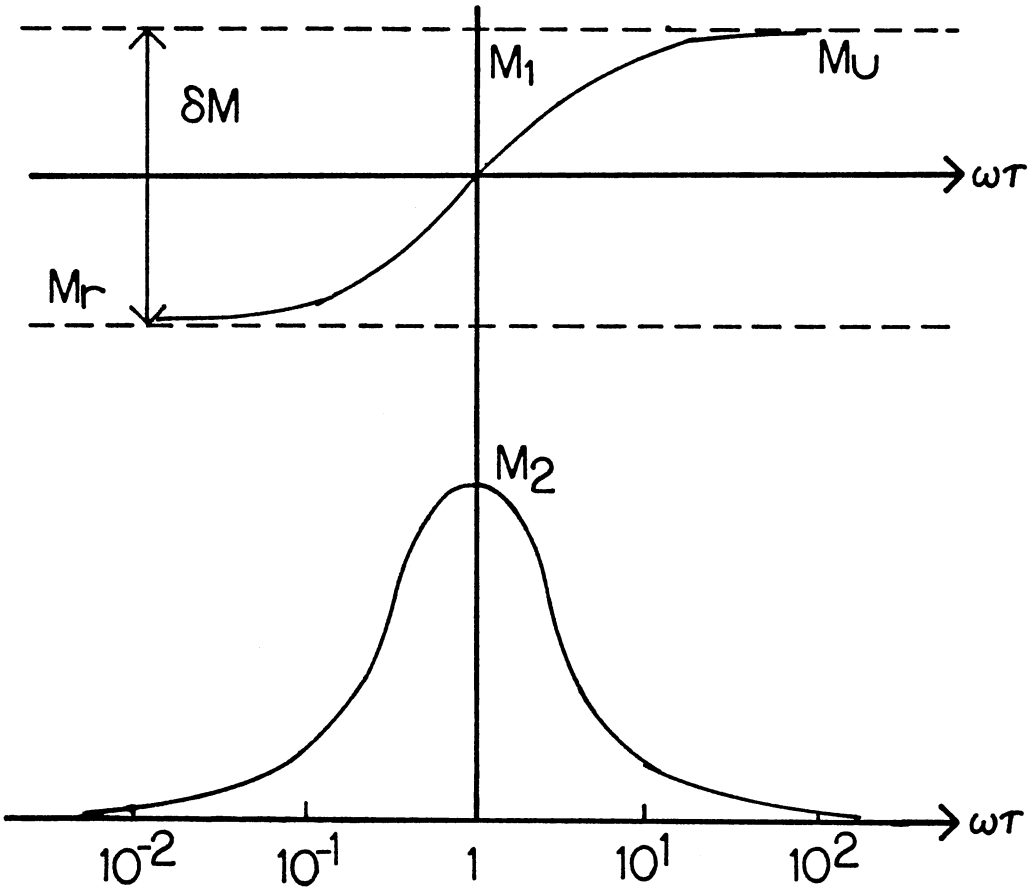

Figure 2. The Variation of M_1 and M_2 as a Function of Angular Frequency, ω, where M_1 and M_2 are the Real and Imaginary Parts of the Complex Elastic Modulus, M^*, of an Anelastic Solid

where τ^{-1} is the product of a vibrational frequency and an entropy factor, ΔH the height of the potential barrier between the equivalent sites, k Boltzmann's constant, and T the absolute temperature. Acoustic loss measurements are usually made with the sample vibrating on one of its normal modes. Thus, instead of varying ω, τ can be varied over a wide range by changing the temperature. Figure 3 shows M_1 and M_2 plotted as a function of temperature with fixed ω. One way to obtain the activation energy is to measure the loss versus temperature spectrum for a number of harmonically related modes at T_p. Equation (9) can be rewritten as follows

$$\ln \omega = \ln \tau_o^{-1} - \frac{\Delta H}{k} \frac{1}{T_p} \qquad (10)$$

So a plot of ω versus $1/T_p$ should yield a straight line of slope, $-\Delta H/k$. Another method is to numerically fit Equation (8) with Equation (9) to the experimental loss versus temperature curve at one frequency.

When a sample goes through one loss peak the frequency shifts according to the following form [22]

$$(f-f_b)/f_b = (Q^{-1})_{max}/(1+\omega^2\tau^2) \qquad (11)$$

At a temperature where $\omega\tau=1$ the frequency shift is $(Q^{-1})_{max}/2$, at low temperature where $\omega\tau>>1$ it approaches to $(Q^{-1})_{max}$, and at high temperature where $\omega\tau<<1$ it approaches to zero. Thus, the maximum frequency shift is $(Q^{-1})_{max}$ when the sample goes over a loss peak. If more than one loss

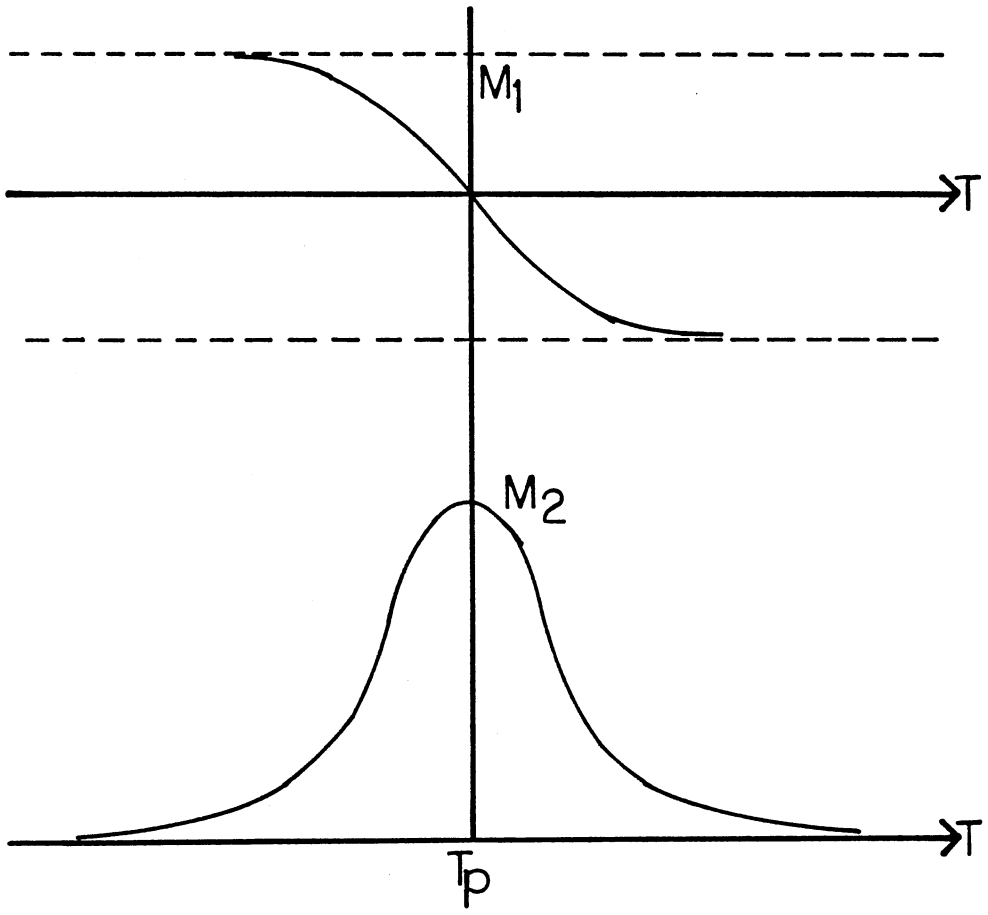

Figure 3. The Variation of M_1 and M_2 as a Function of Temperature

peak is present at temperature below the operating temperature of the sample then the frequency shifts for all of the loss peaks below that temperature are summed as follows [23]

$$\sum_{i=1}^{n} \Delta f_i / f = \sum_{i=1}^{n} (Q_{max}^{-1})_i \qquad (12)$$

2. Log-decrement Technique

The measurement of acoustic loss as a function of temperature is a useful technique for the identification of point defects in both natural and synthetic quartz crystals. This measurement also provides a direct connection to the performance of the crystal in an oscillating circuit. The acoustic losses are caused by an interaction of the crystal lattice vibration with the thermal phonons and also a relaxation of a point defect. The log-decrement technique, one way to measure the acoustic loss or internal friction of a sample, is to drive it on one of its normal modes of vibration, remove the drive and then measure the free decay of the amplitude. The vibration of this free decay can be expressed by the equation of motion describing an one-dimensional anelastic spring such as, according to Nowick and Barry [20],

$$m\ddot{x} = -k^* x = -k_1(1+i\tan\phi)x \qquad (13)$$

where m is the mass attached to the end of the anelastic spring, k^* a complex spring constant, ϕ the loss angle, k_1

is a constant. The solution to Equation (13) is found to be

$$x = x_o \exp\left[-\sqrt{\frac{k_1}{m}}\left(\frac{\tan\phi}{2}\frac{3\tan^3\phi}{48}+\cdots\right)t\right]\exp\left[i\sqrt{\frac{k_1}{m}}\left(1+\frac{\tan^2\phi}{8}+\cdots\right)t\right] \quad (14)$$

When the loss angle ϕ is very small, the natural angular frequency ω_o in free decay becomes simple; that is $\omega_o = \sqrt{\frac{k_1}{m}}$. Then Equation (14) can be rewritten as follows

$$x = x_o \exp\left[-\omega_o \frac{\phi}{2} t\right]\exp(i\omega_o t), \quad \phi << 1 \quad (15)$$

If a piezoelectric sample resonator is driven at its resonator frequency and then allowed to freely decay, the decaying voltage will decrease exponentially as

$$V = V_o \exp(-t/t_o)\exp(i\omega_o t) \quad (16)$$

where t_o is the relaxation time. Comparing the damping term in Equation (16) with that of Equation (15), we find that

$$\phi = \frac{1}{\pi f_o t_o} \quad (17)$$

where $f_o = \omega_o/2\pi$ is used. When we measure the time $T_{1/2}$ taken for the amplitude of vibration to fall to a half of its initial value, the relaxation time t_o is found to be

$$t_o = \frac{T_{1/2}}{0.693} \quad (18)$$

Combining Equation (3), Equation (17), and Equation (18) we can write the acoustic loss as follows

$$Q^{-1} = \phi = \frac{0.693}{\pi f_o T_{1/2}}, \quad \phi << 1 \quad (19)$$

where f_o is a tuned frequency and $T_{1/2}$ is obtained from the

timer.

3. Transmission Technique

An electro-mechanical oscillatory system can be described by an analog electric network consisting of a series R, L, C, circuit shunted by a second capacitance C_1 as shown in Figure 4. The motional R, L, C elements describe the mechanically vibrational part while C_1 is caused by the electrodes and associated cables. The Q factor of the oscillating system can be expressed in terms of the equivalent electrical constants as the following [1]

$$Q = \frac{\omega L}{R} \tag{20}$$

where ω is an oscillating frequency in the neighborhood of a natural frequency.

The transmission technique, another way to measure acoustic loss of a sample, measures the motional equivalent-circuit elements, R and L, of the sample and calculates acoustic loss from Equation (20). The sample crystal is placed in a resistive pi-network circuit as shown in Figure 20 in Chapter IV. By analyzing this pi-network circuit using Thevenin's equivalent circuit theorem with R_1=30 ohm, R_2=20 ohm, and R_L=50 ohm, the crystal impedance, Z_c, is found as follows

$$Z_c = R + jX \tag{21}$$

$$\text{where } R = 4(V_A/V_{Bmax})\cos \phi - 28 \tag{22}$$

$$X = -(4V_A/V_{Bmax})\sin \phi \tag{23}$$

where V_A is the measured voltage at point A and V_{Bmax} the measured voltage at point B when the phase angle, ϕ, is adjusted to zero. The crystal is usually described in terms of the electrical analog as shown in Figure 4. By assuming that the "static" capacitance, C_1, is very small, expressing the motional capacitance, C, in terms of the resonance frequency, f_s, and the motional inductance, L, expanding the crystal impedance, Z_c, in terms of δ ($=f-f_s$), and taking only the first order of δ since δ is very small in a quartz resonator, the crystal impedance, Z_c, becomes

$$Z_c \simeq R + j4\pi L\delta \tag{24}$$

Comparing Equation (21) with Equation (24) and setting $\sin\phi \simeq \phi$, since the phase angle, ϕ, is very small during the measurement the motional inductance, L, in Henry is found as follows

$$L = (V_A/V_{Bmax})(-(\frac{d\phi}{d\delta})/180) \tag{25}$$

We usually take several data of the phase angle, ϕ, and the frequency deviation, δ, from the resonance frequency and plot the data on graph to calculate the slope of ϕ and δ for averaging. When the phase angle, ϕ, is adjusted to zero Equation (22) follows

$$R = 4(V_A/V_{Bmax})-28 \tag{26}$$

Therefore, if V_A and V_{Bmax} are monitored by tuning the frequency to zero phase angle, the motional equivalent-

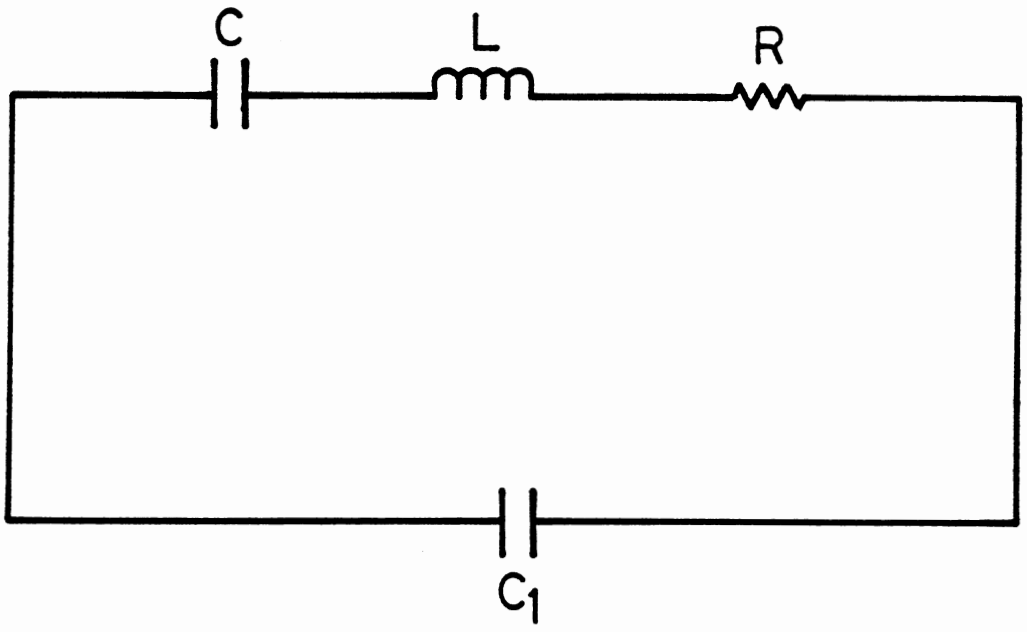

Figure 4. Electrical Equivalent of a Quartz Crystal Resonator

circuit elements, L and R, can be calculated from Equation (25) and Equation (26) respectively. Acoustic loss or internal friction is then calculated from Equation (20).

CHAPTER III

BACKGROUND LOSS

1. Model

When a sound wave travels in quartz, the attenuation due to the phonon-phonon interactions are always present in addition to that due to impurities and structural defects. The phonon-phonon interactions are related to the anharmonic character of the solid. The acoustic loss due to the phonon-phonon interactions is the expression of the anharmonic character of the solid, and the phonon-phonon interactions determine the background loss in a perfect crystal containing no impurities.

The microscopic theory of sound absorption by Landau and Rumer (1937) treats the case, resulting when the product of the angular frequency of the acoustic wave by the relaxation time, τ, is greater than unity. Klemens has made it clear that for $\omega\tau \gg 1$ the attenuation is caused by the direct interaction of the acoustic wave with individual phonons [24].

However, for a condition $\omega\tau \ll 1$, direct interaction of the sound wave with phonons cannot be followed, but the effect of the sound wave on the assembly of thermal phonons as a whole is considered. The phonon gas can be described

by a number of macroscopic parameters which vary periodically under the influence of the sound wave. So the applied sound wave modulates the phonon gas assembly and throws it out of equilibrium. Attainment of equilibrium occurs with an increase in entropy of the phonon assembly; this irreversible process is the cause of the absorption of energy from the sound wave. A theory of this type was proposed by Akhieser [25] and further developed by Boemmel and Dransfeld [26] and by Woodruff and Ehrenreich [27]. All of their derivations take the form of the equation

$$A = \frac{C T \gamma^2 \omega^2 \tau}{2 \rho V^3 (1 + \omega^2 \tau^2)} \tag{27}$$

where the relaxation time, τ, is the time required to equilibrate the interchange of acoustic energy with thermal energy. Using the well known formula for the relation between the attenuation and the internal friction, we find

$$Q^{-1} = \frac{2VA}{\omega} = \frac{C T \gamma^2 \omega \tau}{\rho V^2 (1 + \omega^2 \tau^2)} \tag{28}$$

It is demonstrated by W. P. Mason [28] that the relaxation time, τ, is closely equal to the thermal relaxation time, τ_{th}, for shear waves. We rewrite the above eqation as follows

$$Q^{-1} = \frac{\gamma^2 C T}{\rho V^2} \frac{\omega \tau_{th}}{(1 + \omega^2 \tau^2)} \tag{29}$$

where γ is a Gruneisen constant which is picked to fit the data at room temperature, C is the specific heat per unit volume, V is the velocity of the applied sound, ρ is the

circular frequency of the applied sound, and is the density of specimen. To calculate Equation (29) the thermal relaxation time, τ_{th}, was calculated from the expression

$$\tau_{th} = \frac{\int_0^{\frac{\Theta}{T}} \tau x^4 e^x (e^x-1)^{-2} dx}{\int_0^{\frac{\Theta}{T}} x^4 e^x (e^x-1)^{-2} dx} \qquad (30)$$

where $x = \frac{\hbar\omega}{kT}$. An 8 point Gaussian numerical quadrature method from the IBM scientific subroutine package was used to do the above integrations. In above eqation τ is the combined relaxation time for the various phonon scattering processes which limit the lattice thermal conductivity. It was taken as

$$\tau^{-1} = V/L + A\omega^4 + (B_1 + B_2 \exp(-T_1/T)\omega^2 T \qquad (31)$$

where the first term represents boundary scattering, the second point defect scattering, and the third phonon-phonon scattering. The parameters L, A, B_1, B_2, and T_1 can be adjusted to fit experimental data. The specific heat per unit volume, C, is calculated from the eqation

$$C = \frac{3k^4T^3}{2\pi\hbar^3V^3} \int_0^{\frac{\Theta}{T}} x^4 e^x (e^x-1)^{-2} dx \qquad (32)$$

which is derived from Debye model of the lattice heat capacity. During calculations of Q^{-1} the sound velocity V was taken to be 4650 m/s, the Debye temperature Θ = 470 K,

the Gruneisen constant γ = 1.5, the density of specimen ρ = 2649 Kg/m, and the applied frequency f=5 MHz.

2. Results of the Calculations

Background acoustic losses were calculated from Equation (29) using the above model. Figure 5 shows a general shape of the calculated background acoustic loss, with the parameters L, A, B_1, B_2, and T_1 in Equation (31) adjusted to fit the experimental data for Premium Q cultured quartz by M. Jalilian-Nosraty and J. J. Martin [6]. It also shows the acoustic loss versus temperature curves which is plotted from the experimental data for Premium Q cultured Quartz. We see that the low temperature peak is sharper than that of an experimental background loss curve.

Figure 6 shows the backround loss curves calculated with only one of the phonon scattering terms in Eqation (31) considered for each curve; the p-defect curve is the result of calculations in which only point-defect scattering term in Equation (31) is considered and so on. Both curves calculated with only point-defect scattering term and only boundary scattering term go up high as temperature increases. However, the curve calculated with only phonon-phonon scattering term behaves like the original background loss curve, that is calculated with all phonon scattering terms considered. Therefore, the sharpness at low temperature does not have any relation with the boundary scattering parameter, L, or the point defect parameter, A.

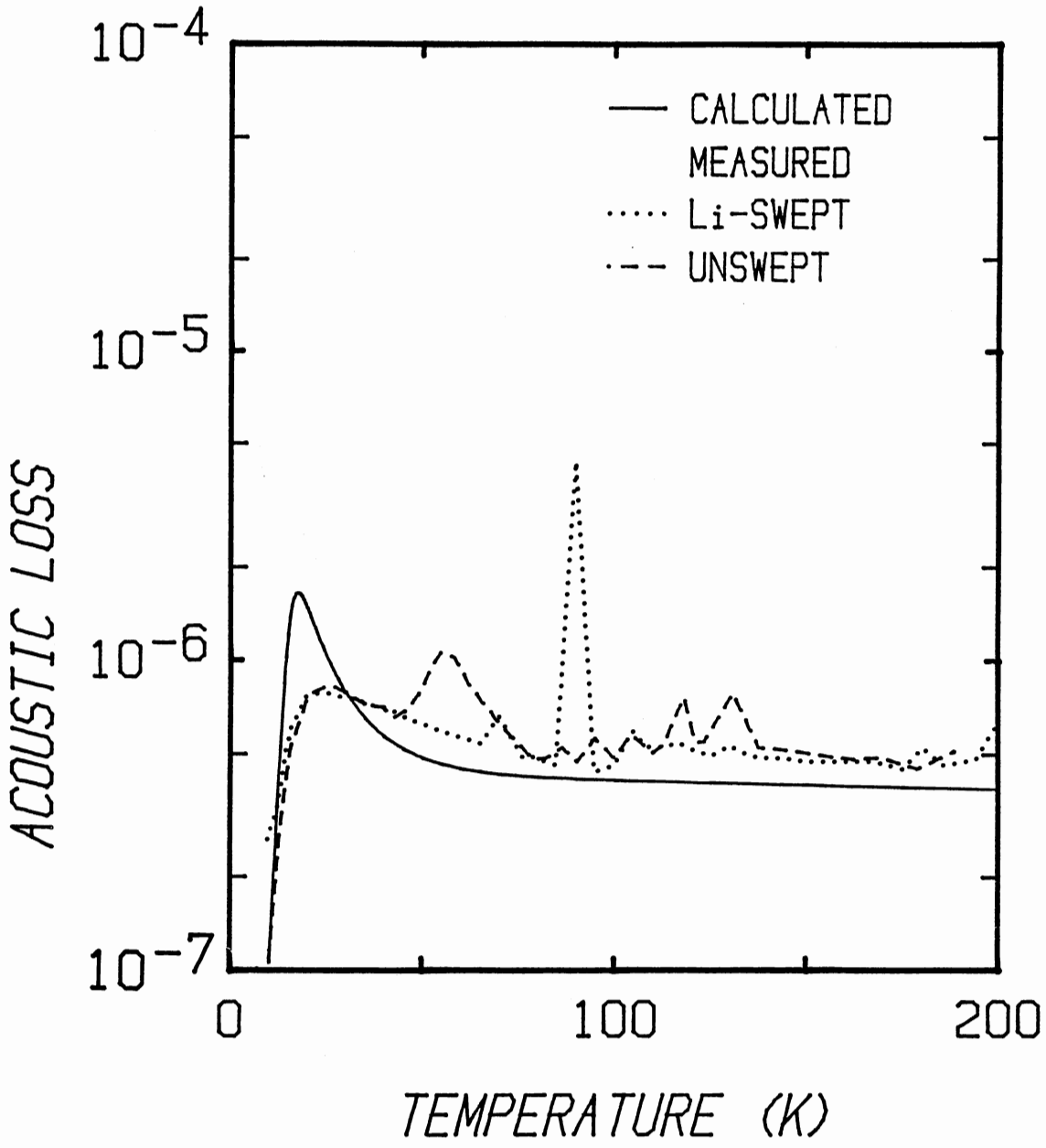

Figure 5. A General Shape of the Calculated Background Acoustic Loss with the Parameters L, A, B_1, B_2, and T_1 in Equation (31) to fit the Experimental Data for Premium Q Cultured Quartz

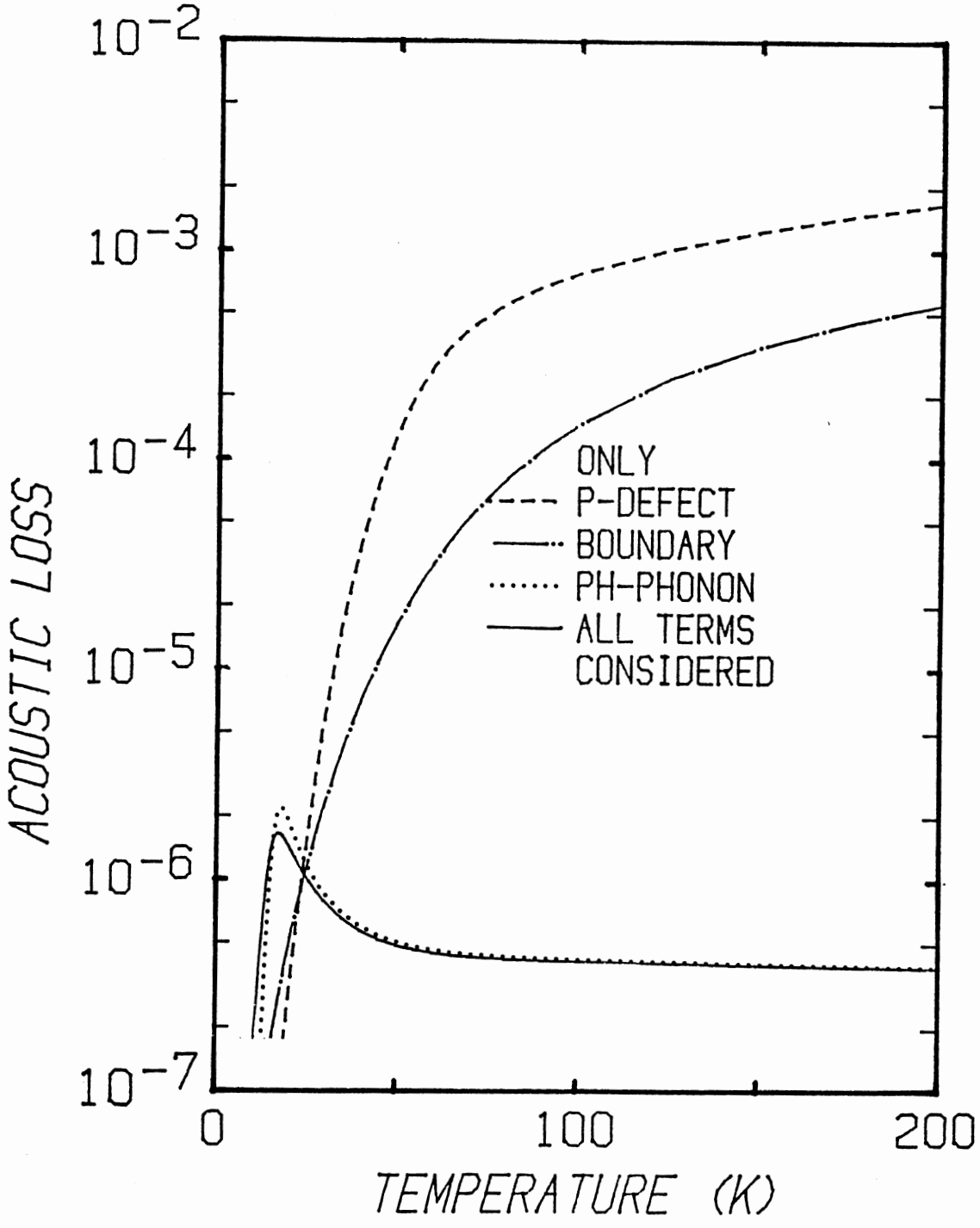

Figure 6. Calculated Background Loss Curves with One of the Phonon Scattering Terms, Point Defect, Boundary, or Phonon-Phonon, Considered for Each Curve

Figure 7 shows calculated background loss curves with changes in B_1, which is one of the phonon-phonon scattering term parameters B_1, B_2, and T_1. Increasing the parameter B_1 slightly increases the background losses below 20 K and decreases the losses above 50 K, but decreases the losses between 20 K and 50 K considerably. The peak appears to be saturated above B_1=5.8E-23.

Figure 8 shows calculated background loss curves with 3 different values of the parameter B_2. Decreasing the parameter B_2 does not affect the background losses below 20 K but incereases the losses above 20 K.

Figure 9 is the results of the background losses calculated with changes in T_1, which is one of the phonon-phonon scattering term parameters in Equation (31). Increasing the parameter T_1 does not affect the background losses below 20 K and slightly increases the losses around 200 K, but increses the peak considerably. Also we see that the peak temperature shifts to the high temperature side as the parameter T_1 goes up.

The calculated background loss curve is well fitted to the measured background loss curve except the sharp peak near 23K. The sharp peak can not be eliminated as we see in the above figures. Also another sets of combinations in phonon scattering parameters we tried, gave the same results.

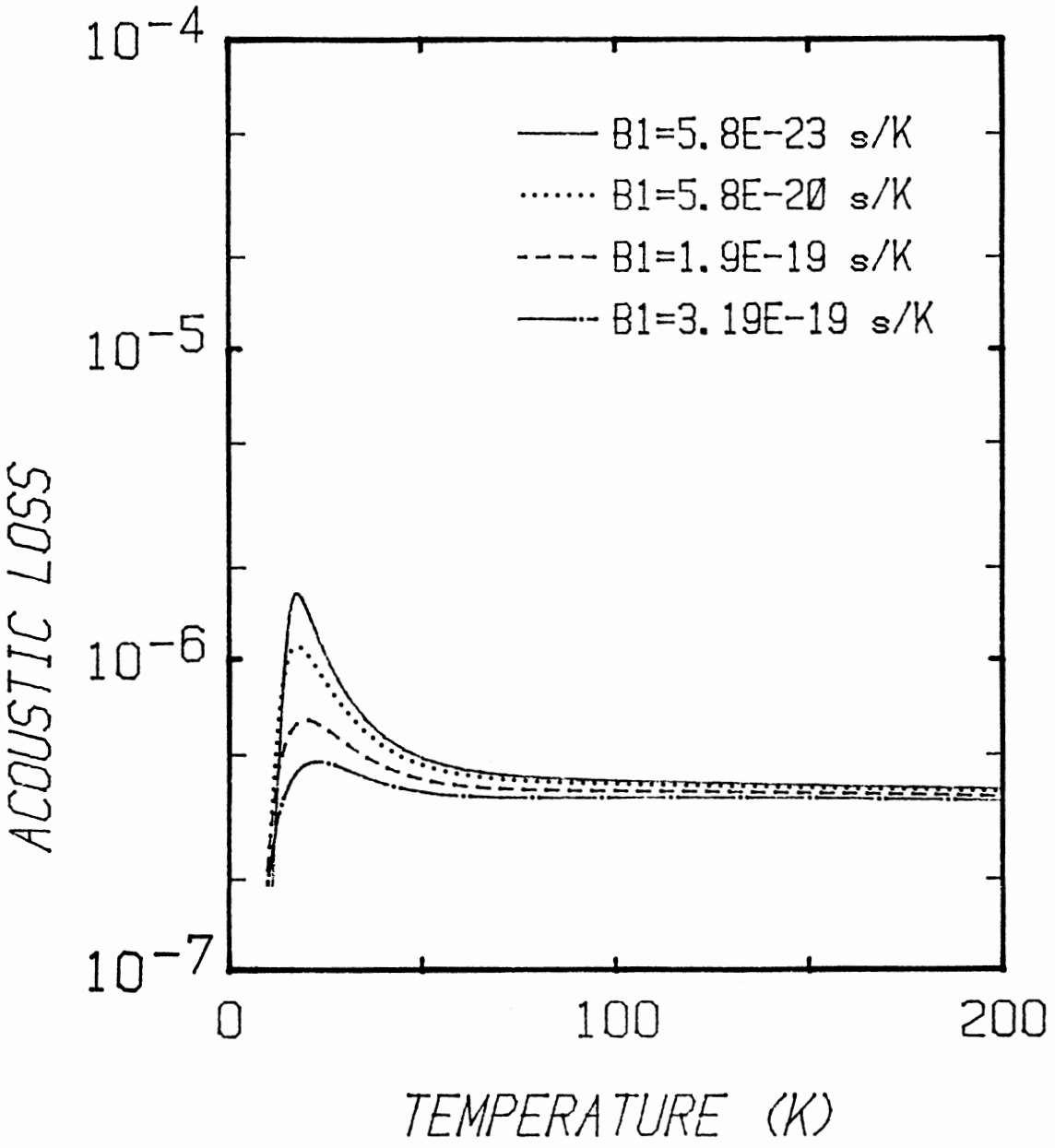

Figure 7. Calculated Background Loss Curves with Changes in B_1 which is One of the Phonon-Phonon Scattering Term Parameters

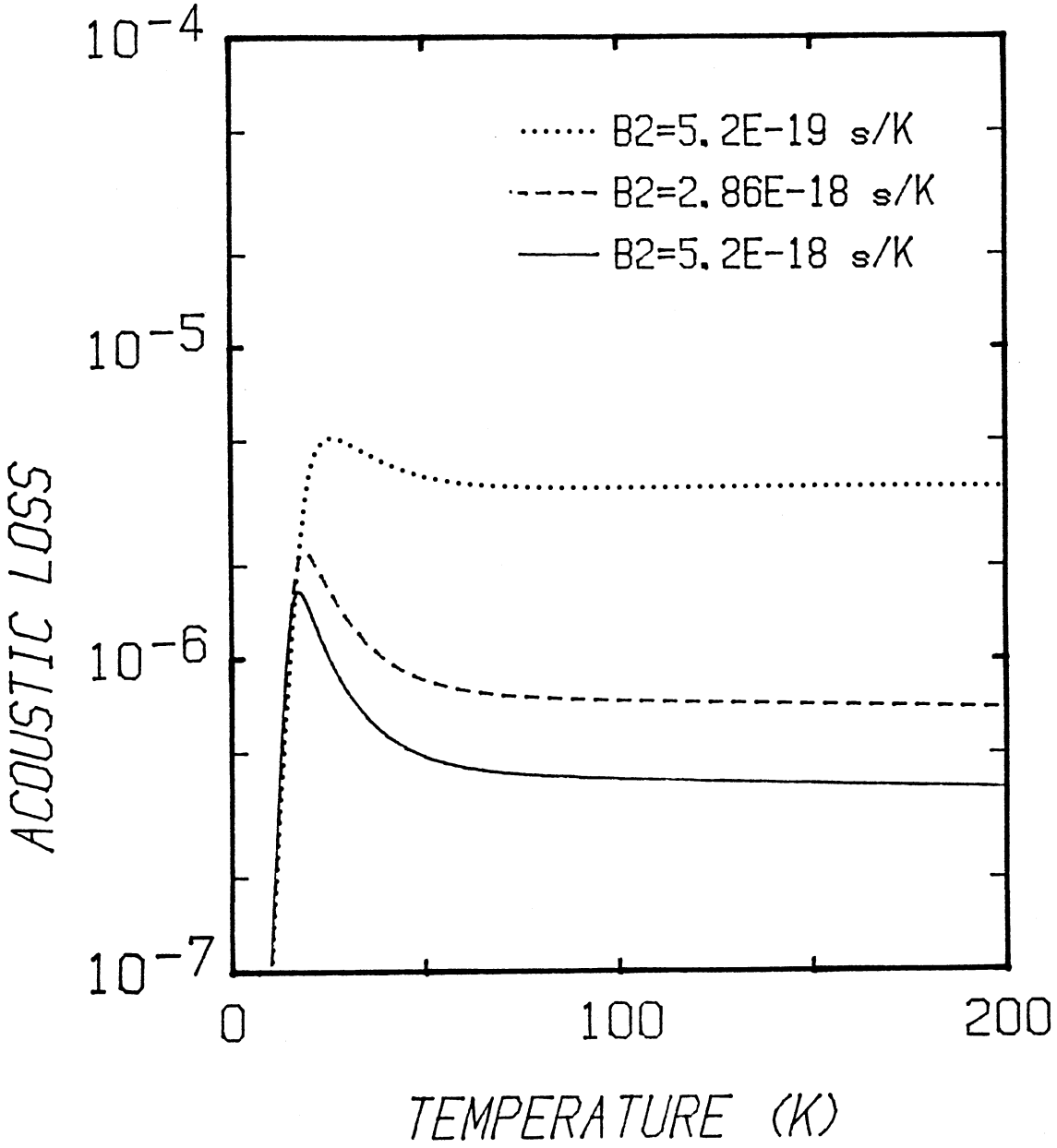

Figure 8. Calculated Background Loss Curves with 3 Different Values of B_2

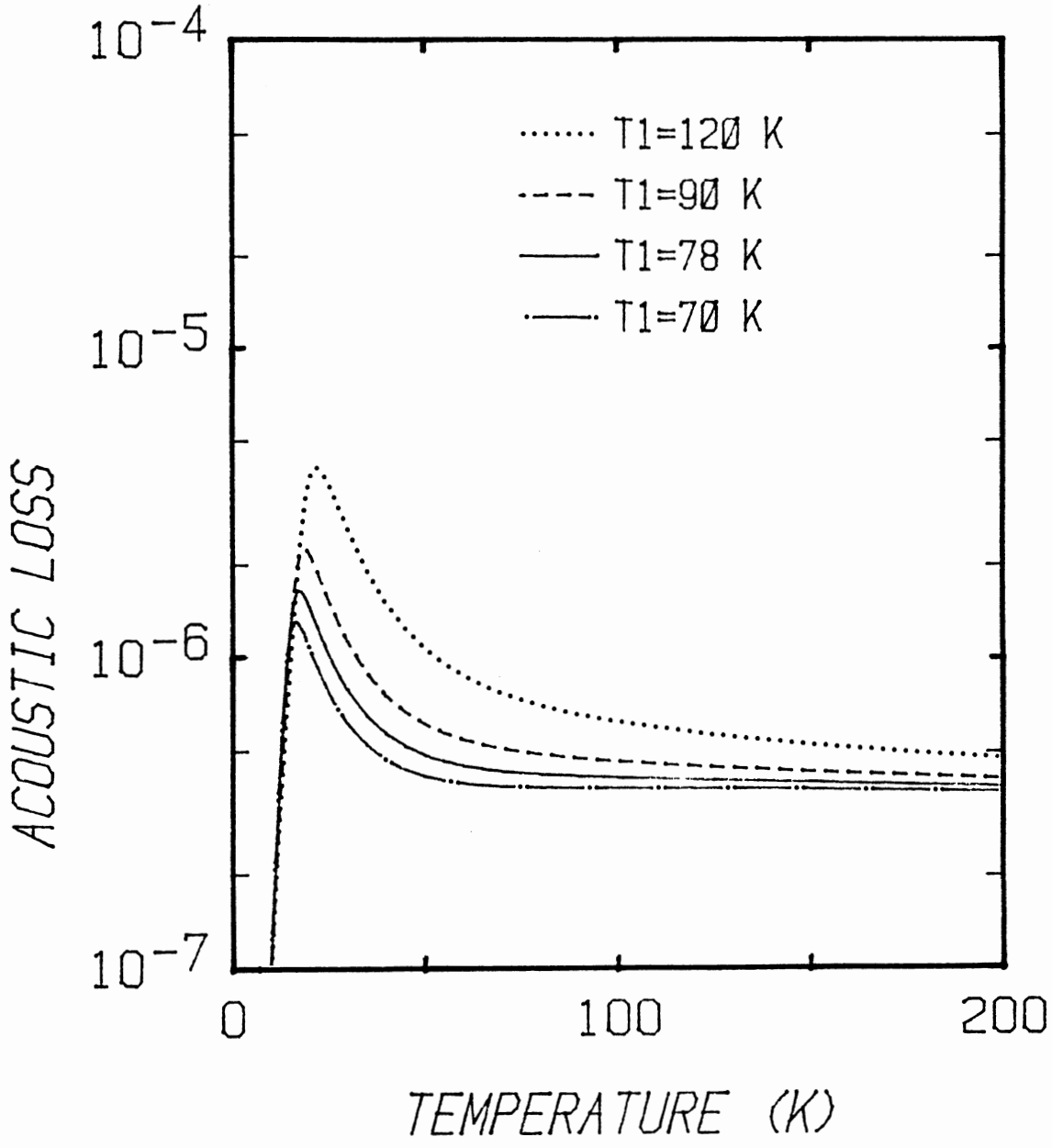

Figure 9. The Results of the Background Losses Calculated with Changes in T_1

3. Discussion

As shown in Figure 5, the general shape of the calculated background losses with essentially the same L, A, B_1, B_2, and T_1 values as the thermal conductivity calculations done by M. Jalilian-Nosraty and J. J. Martin [29], agrees well with that of measured background losses except the sharp peak at low temperature. The sharpness of the peak could not be eliminated by any set of combinations in the phonon scattering parameters we tried.

Equation (29) was derived considering Ahkieser effect which attributes background acoustic losses to the interations of sound waves with the assembly of the thermal phonons. Thus the calculated background losses are only due to elastic phonon-thermal phonon interactions; no other mechanism is involved. Equations (30) and (31) tell the thermal relaxation time, τ_{th}, is related to phonon-boundary, phonon-point defect, phonon-phonon scattering; note that these are thermal phonons. Thus the background losses calculated from Equation (29) are also related to them. In Figure 6 the dotted curve which is calculated with only the phonon-phonon scattering term in Equation (31), is very similar to the solid curve calculated with all phonon scattering terms while both of the dashed curves which are results of considering only the boundary and point defect scattering terms respectively are quite different from the solid curve. Therefore, we conclude that the calculated background losses are mostly governed by the thermal phonon-

thermal phonon interactions and so does the low temperature peak.

The sharpness of the low temperature peak may be real and the absence of sharpness in measured background losses is due to the presence of coupled modes around 30 K or an unknown defect. These coupled modes were sometimes observed when we ran sythetic quartz resonators.

The model may be not perfect. The thermal relaxation time, τ_{th}, is calculated from Equation (30) which is derived from the following equation

$$\tau_{th} = \frac{3K}{V^2 C} \tag{33}$$

where K is the thermal conductivity, C is the specific heat per unit volume, and V is the sound velocity. M. Jalilian-Nosraty and J. J. Martin [29] were able to fit their thermal conductivity data with the phonon scattering parameters in Figure 5. Hence the thermal conductivity integral in Equation (30) looks correct. C in Equation (33) is the specific heat at constant pressure but we used the specific heat at constant volume. This might give us an incorrect thermal relaxation time, τ_{th}, and incorrect losses. Also, using the specific heat at constant volume might cause incorrect losses in Equation (29). Mason [28] shows that γ is a slowly varying function of temperature. It can be determined from the measured values of the third-order elastic moduli. But the third-order elastic moduli were not measured for quartz, and we introduced an arbitrary

constant, γ, in the loss calculations. This might be a problem of the sharpness in the low temperature peak.

CHAPTER IV

EXPERIMENTAL PROCEDURE

1. Description of Samples

The substitutional aluminum is compensated by the interstitial alkali, Na^+ or Li^+, for electrical neutrality in as-grown synthetic quartz. Toyo Supreme Q labeled bar, SQ-B, of the pure Z-growth synthetic quartz contains approximately 10 to 15 ppm aluminum as impurities, of which 33% are compensated by Na^+-ions and 67% by Li^+-ions. Sawyer Premium Q labeled bar, SP-DD which is the Sawyer autoclave run D14-45, contains less than 1 ppm aluminum.

The sample crystals used in this study are Warner design 15 mm diameter plano-convex circular AT-, BT-, or SC-cut blanks as shown in Figure 10(a). The 3rd overtone blanks were fabricated from the Toyo Supreme Q bar SQ-B by Frequency Electronics Inc. and the 5th overtone blank by the Sawyer Premium Q bar SP-DD by Piezo Crystal Co. as described in Table 1. After sweeping each blank with Na^+-, Li^+-, or H^+-ions at OSU 5 mm-diameter gold electrodes were vapor deposited on these blanks with the connecting "tab" oriented along the Z'-direction as shown in Figure 10(b). The electrode thickness was such that the frequency of the resonator was 3 to 5 kHz below that of the blank. Then the

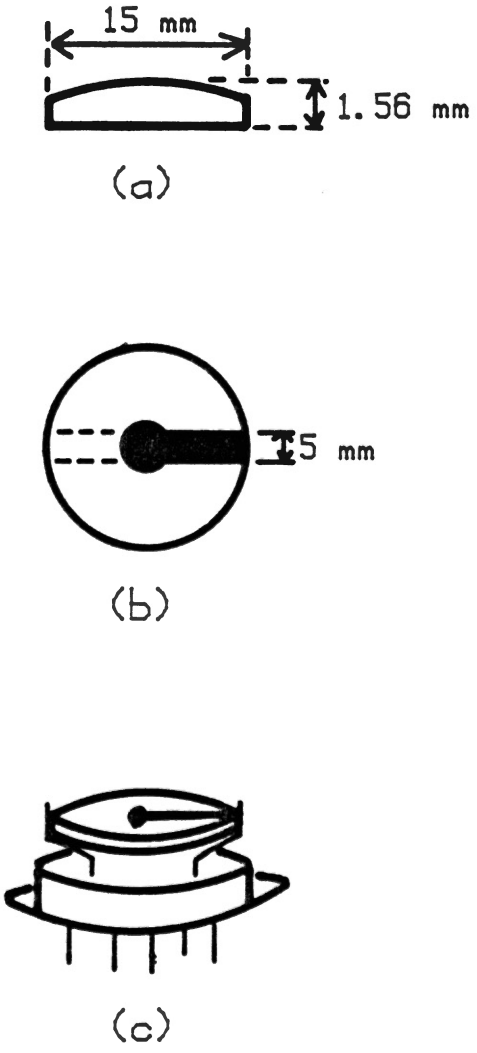

Figure 10. Warner Design Plano-convex Circular Blank (a) Side view (b) Top view (c) Its Mounting in HC49U Crystal Holder

TABLE I

LIST OF SAMPLES USED IN THIS STUDY*

sample name	sweeping condition	cut	operating overtone	bar	aluminum content
SC1U	unswept	SC-	5MHz 3rd	SQ-B Toyo	10-15ppm
SQBR7	Li^+-swept	AT-	5MHz 3rd	SQ-B Toyo	10-15ppm
BT2L	Li^+-swept	BT-	5MHz 3rd	SQ-B Toyo	10-15ppm
SQBR10	H^+-swept	AT-	5MHz 3rd	SQ-B Toyo	10-15ppm
SQBR8	Na^+-swept	AT-	5MHz 3rd	SQ-B Toyo	10-15ppm
SP-DDR6	Na^+-swept	AT-	5MHz 5th	SP-DD Sawyer	<1ppm

* Toyo Crystals are fabricated from Frequency Electronics Inc. and Sawyer Crystals from Piezo Crystal Co.

gold-plated blanks were mounted in HC49U crystal holders with Epotek P-1011 or Transene PDA-D-500 silver filled polyimide epoxy as shown in Figure 10(c). Only two of the four mounting tabs were cemented to the blank: these two tabs were connected to the pi-network.

2. Cryogenics Systems

The acoustic loss versus temperature data were obtained using two different measurement techniques which will be described below and two different cryogenic systems. The first cryogenic system which covers the 5K to 300K temperature range is a variable temperature liquid helium cryostat. Figure 11 shows the schematic diagram of the variable temperature liquid helium dewar. It consists of a cold finger and heater, a heat leak chamber, an inner helium chamber, an outer nitrogen chamber, and a thin-walled stainless steel enclosure which is connected to a vacuum system. The inner dewar, outer dewar, and stainless steel enclosure are insulated from each other and the surroundings by the vacuum of at least 5×10^{-6} Torr. The sample can be thermally connected to the cryogenic fluid in the inner dewar by filling the heat leak chamber with a small amount of helium gas which acts as a heat exchange medium. The heater system consists of a 14 ohm constantan wire wound on the cold finger and a HP 6201B DC power supply. A model DRC-80C digital cryogenic thermometer/controller with a model DC-500-DRC silicon diode sensor from Lake Shore

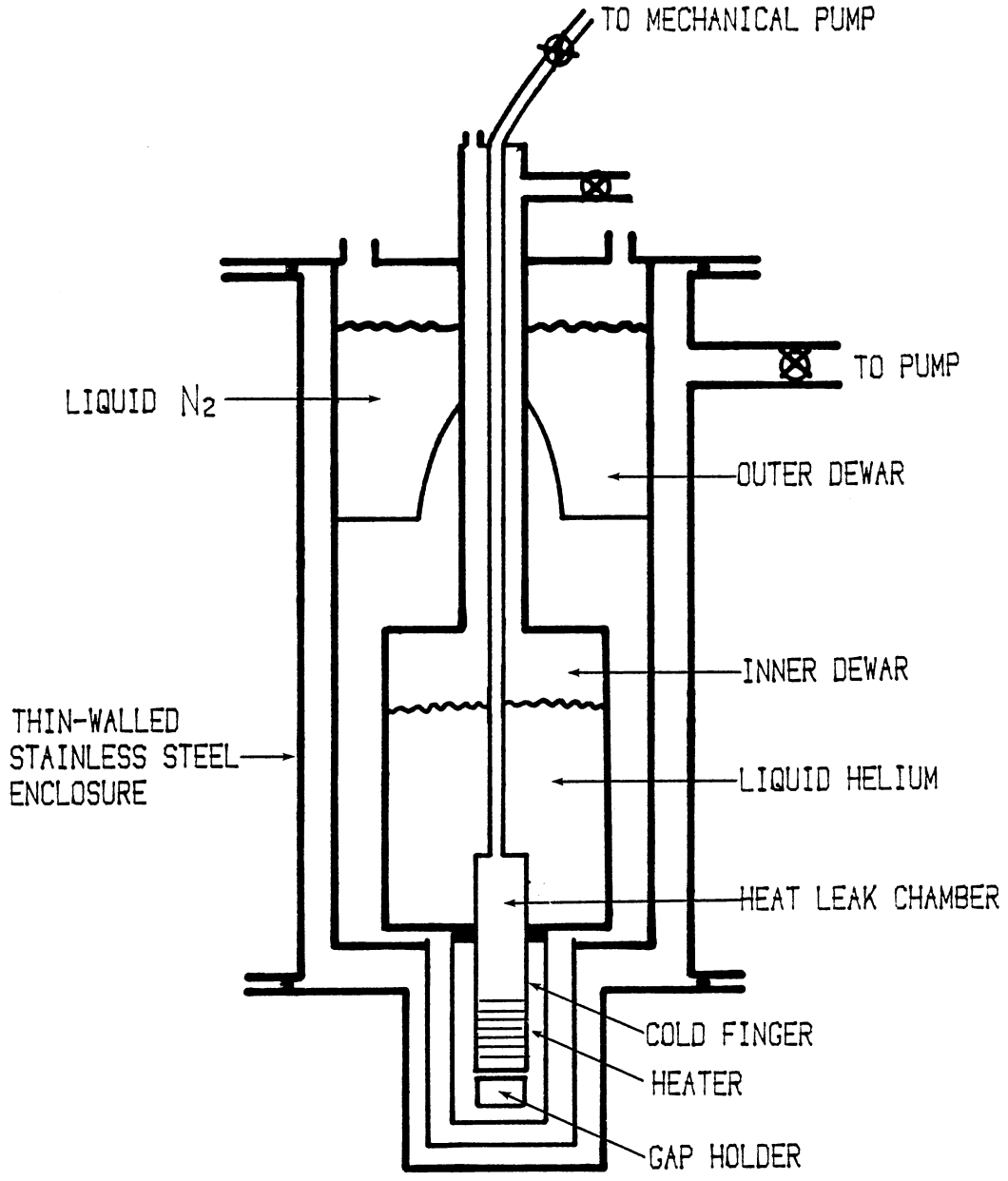

Figure 11. A Variable Temperature Liquid Helium Dewar

Cryotronics, Inc. were used to monitor the sample's temperature.

To cool down the sample from room temperature to 4.5 K, liquid nitrogen was poured into the inner and outer dewars after the heat leak chamber was filled with a helium gas. When the whole system reached equilibrium at 80K, the liquid nitrogen was removed from the inner dewar and then liquid helium was transferred. The holder and resonator blank then cooled to approximately 4.5K. Data were taken starting at low temperatures and then going up to higher temperatures. The temperature was raised by applying heater current and reducing the helium pressure in the heat leak chamber. Once 20K was reached the heat leak chamber was pumped continuously and the current was increased to bring the sample to the desired temperature. The HC49U crystal holder was fastened to the cold finger with a small aluminum clamp.

The second cryogenic system was a CTI Closed cycle refrigerator with a TRI 2000 temperature controller. Figure 12 shows the cold finger details. The sample crystal is mounted on the end of the second-stage cold station of the refrigerator as shown in the Figure 12. The Cryocal CD-301 Silicon Diode Sensor is attached near the sample crystal and connected to the temperature controller so that the sample's temperature can be monitered. The heater wire which is 6 ft long of 32 gauge Manganin wire is wound around the second-stage cold station, and connected to the temperature controller.

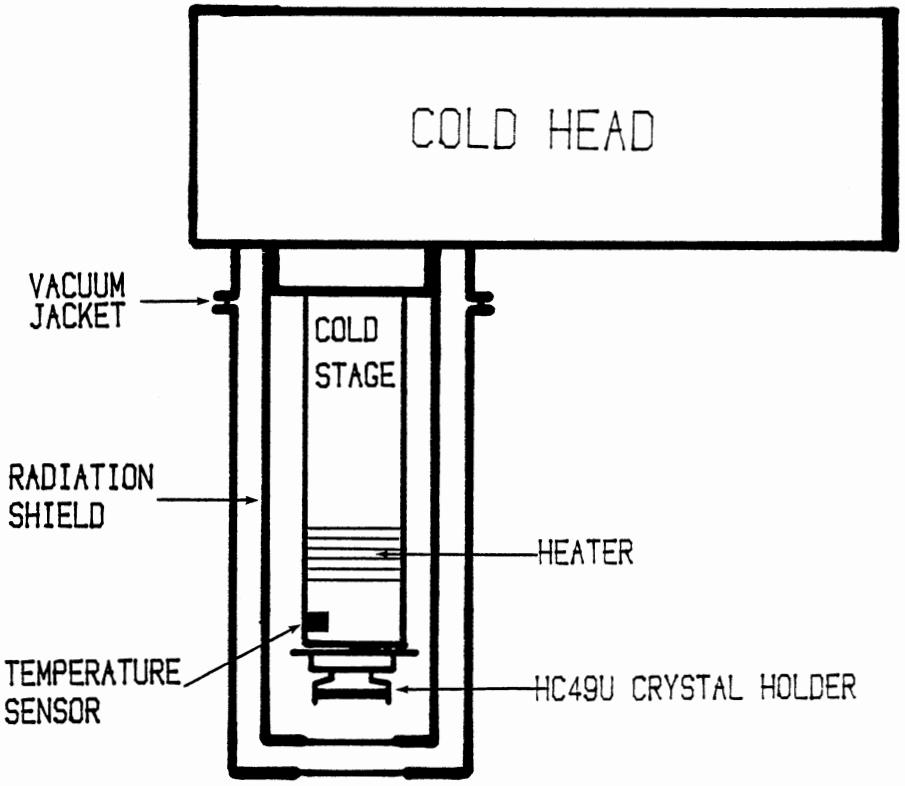

Figure 12. Mounting Structure of a Sample in Transmission System

3. Radiation Techniques

The samples were irradiated using either a Van De Graaff electrostatic accelerator or a ^{60}Co gamma-cell with a dose rate of approximately 250 rad/min. To irradiate the sample, SQBR8, which was run in the variable temperature liquid helium cryostat, the sample was removed from the holder on the cold finger, placed in a small bottle with a helium gas atmosphere, and then the bottle with the sample was put into the ^{60}Co gamma-cell. The initial irradiation was for 2 hours. Subsequent irradiations were repeated for longer times after finishing the acoustic loss measurement for total times up to 104 hours.

To irradiate the samples mounted on the refrigerator, the refrigerator rack was placed 3.5" in front of the aluminum window of the Van De Graaff electrostatic accelerator as shown in Figure 13. The electron beam passed through two 0.13 mm aluminum foil vacuum windows and two 0.033 mm aluminum foil thermal shield windows before striking the sample. Irradiations were carried out at either room temperature or low temperature, 80K to 100K, with a 1.75 Mev electron beam. The beam current was set to 10 uA initially but changed to about 8 uA during the shots. This reduction of the beam current during the shots is due to the three aluminum foil windows and the complicated geometry of the cold head of the refrigerator. The current density on the sample was measured to be 0.34 uA/cm by replacing the sample blank with the same size of conducting

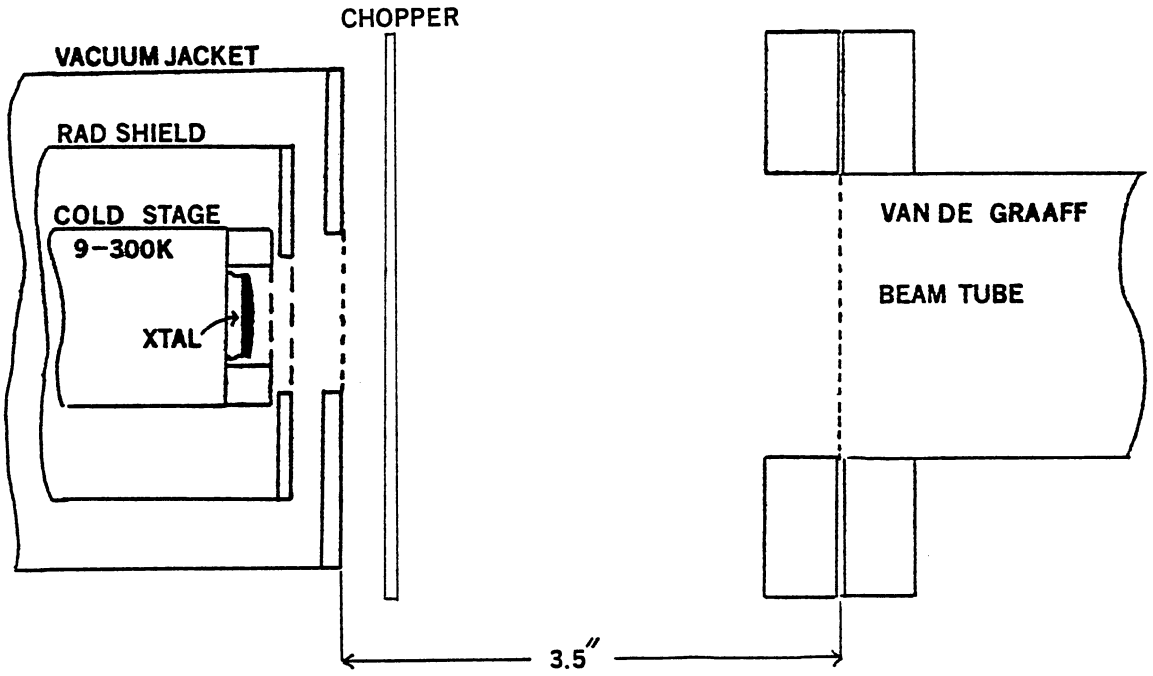

Figure 13. The Geometry of the Irradiation of a Sample Crystal by Van de Graaff Electrostatic Accelerator

metal. The radiation dose rate was calculated to be about 0.15 Mrad/sec from this measured current density by assuming that all electrons were stopped in the sample. Electrons passing through quartz lose their energy in the process of bremsstrahlung, the excitation and ionization of bound electrons, or elastic collisions with nuclei. However, energy losses due to the elastic collisions with nuclei is known to be very much less than either electronic or bremsstrahlung losses at all energy levels with relativistic electrons, and the electronic losses are dominant over the radiative losses at the low energy levels such as 1.75 MeV [30]. Thus, most of the 1.75 MeV electrons lose their energy by the collisions with bound electrons and are deflected from their trajectories. In this way a flood of the free electrons and holes is produced. The simple experiment of irradiating through a stack of three pieces of high aluminum quartz and monitoring Al-OH centers with an IR spectrophotometer showed that more than one half of the shot electrons passed through the first sample with thickness of 1.57 mm. The thickness of the resonator blanks used during this study is about 1.56 mm. Thus, most of the electrons pass through the samples and the actual dose rate is expected to be much smaller than the calculated value, 0.15 Mrad/sec. However, it is observed that even this smaller dose rate is sufficient to cause significant sample heating, especially at low temperatures where the specific heat of the sample is reduced. The heat produced in this

irradiation process might give an annealing effect on the sample, which is not desirable because we want to monitor a pure irradiation effect. To fix this heating problem, the Gralab model 900 programable timer was used to control irradiation time and give pulsed-electron shots on the sample. The sample, SP-DDR6, was irradiated at room temperature for two second intervals with the beam off for 5 seconds and the sample, BT2L, for 0.5 second intervals with the beam off for 5 seconds.

The Gralab timer worked fine, but switching on and off the beam frequently caused the breakage of the cotter pin inside the Van De Graaff electrostatic accelerator. Thus, a rotating wheel beam chopper was used to irradiate the samples, SQBR7 and SC1U. It is mounted on the vacuum jacket of the cold head besides the aluminum window and gives 0.5 second pulses repeated every two seconds.

To irradiate the sample at low temperature, the control rack was wheeled into place near the Van De Graaff control console. A sample's temperature was monitored and controlled to a desired temperature by the control rack. The increment of temperature during the low temperature , 80K or 100K, irradiation was kept within 1.5K range of temperature by using both of the pulsed-electron techniques. The irradiation of the samples was performed with 0.5-1 second pulsed shots spaced 30-60 seconds by using the Gralab timer and with 0.5 second pulsed shots with the beam off for 2 seconds by using the wheel chopper.

4. Log-decrement Technique

Internal friction of quartz was determined by using either the log-decrement or the transmission techniques. The log-decrement technique was used especially for the samples with large Al-Na loss peak because it works better for the measurements of high acoustic losses such as 10^{-4}. However, it has poorer frequency resolution and the transmission technique has an advantage over the log-decrement technique in the sense that it can be easily automated. Thus, most of the samples was run with the transmission technique. Both of the internal friction measurement techniques agreed well each other within a experimental error. All measurements were made with the sample in a vacuum of about 5 X 10^{-6} Torr.

When measuring internal friction using the log-decrement system the variable temperature helium dewar was used to control sample's temperature. A schematic diagram of the acoustic loss measuring system is shown in Figure 14. The radio frequency ($f_o \approx$ 5MHz) signal from a HP 3325A synthesizer/function generator goes to the gate which is opened for 10 ms every 0.5, 1, 2, or 5 seconds by the gate control. The sample resonator is driven at its resonant frequenvy and then allowed to freely decay. This decaying RF($f_o \approx$ 5MHz) signal is fed into the mixer after amplification by a wide-band pre-amplifier, and there mixed with the RF(f_o ±455KHz) signal from the local oscillator. The mixer output, which is 455KHz, is amplified by the two

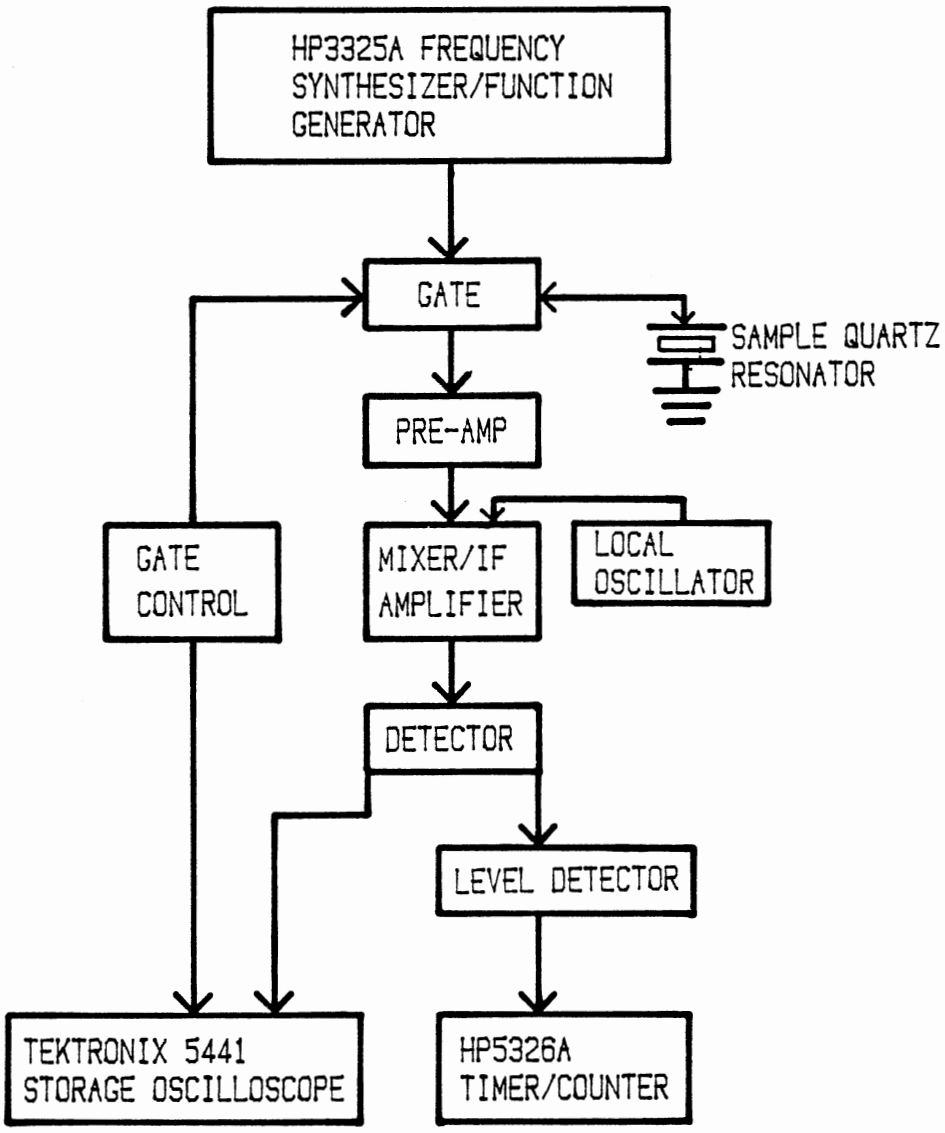

Figure 14. A Schematic Diagram of the Acoustic Loss Measuring System

stage intermediate frequency amplifier. This decaying IF signal is rectified with a precision operational amplifier detector and displayed on a Tektronix 5441 storage oscilloscope. The rectified signal from the detector also goes to a pair of level detectors which start the timer function of a HP 5326A timer-counter at 8V and stop it at 4V. Hence, the timer reading yields the half-time $T_{1/2}$ of the exponential decay. Then the acoustic loss, Q^{-1}, is calculated from Equation (17) in Chapter II.

5. Transmission Technique

The transmission technique gives the great convenience of taking acoustic loss data automatically. It measures the motional equivalant-circuit elements, R and L, of the sample crystal from which the acoustic loss is calculated by Equation (20) in Chapter II. The block diagram of the transmission system is shown in the Figure 15. The transmission system consists of the control rack and the refrigerator rack. The control rack contains a TRI Resesrch T-2000 Temperature Controller, a HP 3325A Frequency Synthesizer, a HP 5616A Universal Counter, a HP 3438 DVM, a HP 59307A VHF Switch, and a HP Integral Personal Computer. All components are connected to the computer by the IEEE-488 bus, so that this system can be controlled by the computer. The refrigerator rack contains a CTI Closed-cycle Helium Refrigerator, a HP 8405A Vector Voltmeter, and a pi-network. The resistors are connected to the probe A and B of the

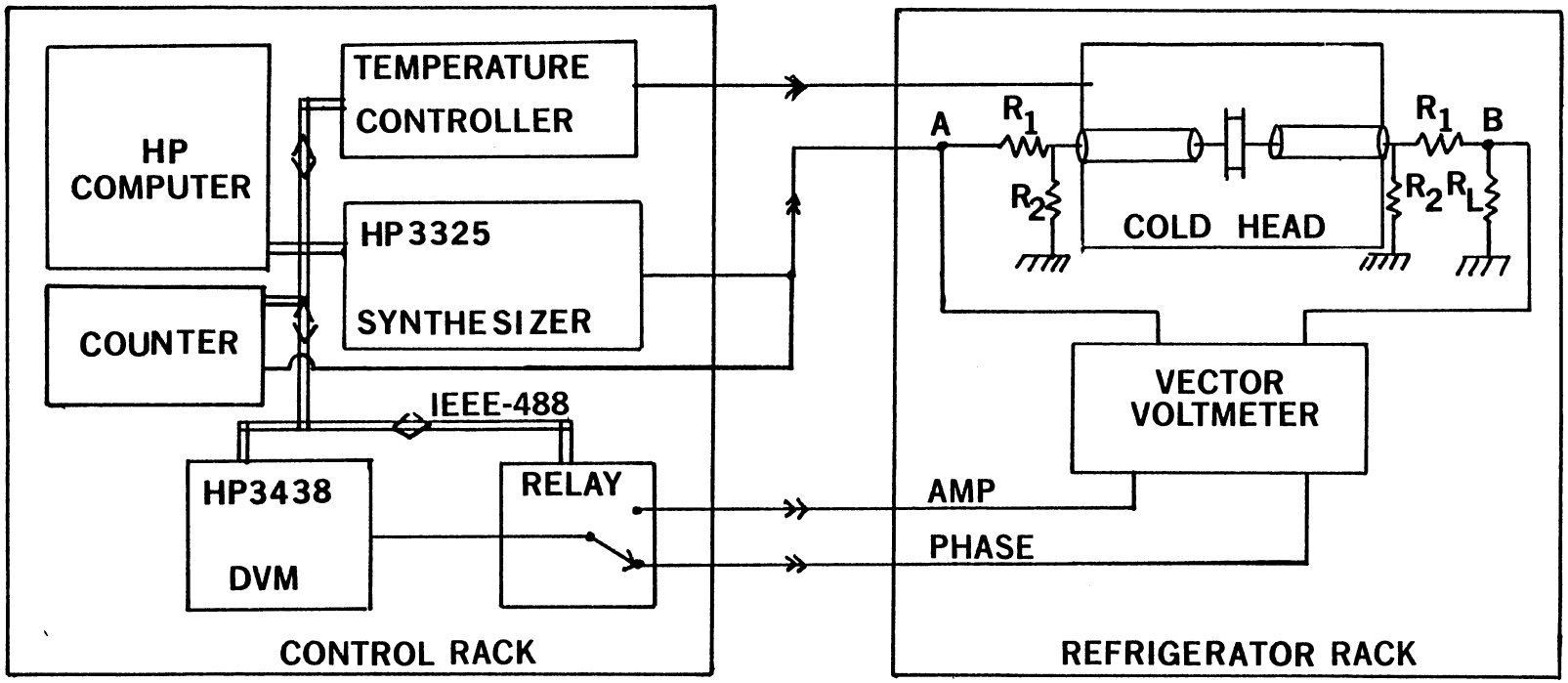

Figure 15. Block Diagram of the Transmission System used for Computer-Controlled Crystal Resistance Measurements

Vector Voltmeter and to the leads of the crystal by using BNC connectors, so that the pi-network is formed.

The transmission circuit signals from the synthesizer are fed into the crystal and also to the counter by the RG-58 coaxial cable. The vector voltmeter monitors the voltages Va and Vb at the points A and B as shown in Figure 16, and the phase angle at the point B with respect to the point A. The amplitude and phase outputs from the vector voltmeter are fed into the switch which connects the phase output of the vector voltmeter to the DVM for tuning the resonant frequency, and the amplitude output to the DVM for measuring the Vb alternately.

The computer keeps the system tuned to "zero-phase" by using a digital feedback loop as shown in Figure 17. The loop uses the digital phase of the DVM as an error signal. Figure 18 shows the computer flowchart for taking the series resistance versus temperature data. The computer also keeps track of the temperature by periodically increasing the set point temperature of the temperature controller. When the temperature has been changed by the desired amount, usually 2 or 3K, and the phase is in tune, the computer trigers the counter for the frequency measurement and reads the temperature, TEMP1. Then it connects the amplitude output of the vector voltmeter to the DVM by controlling the switch and reads the amplitude of the voltage at the point B, Vb, from the DVM; during this process the computer stops tuning the frequency, but it is done fast enough that the drift

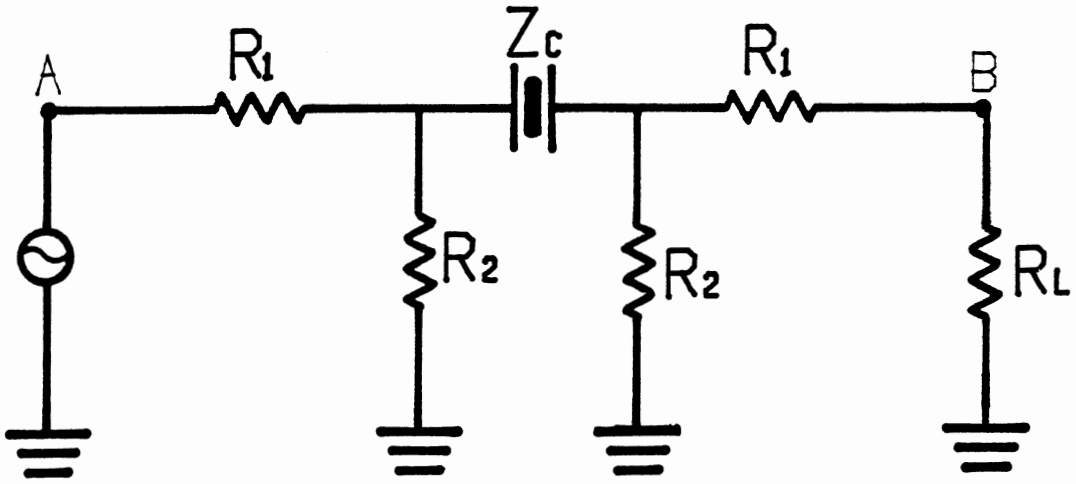

Figure 16. The Pi-network used in the Transmission System to measure a Series Resistance, R, of a Sample Crystal

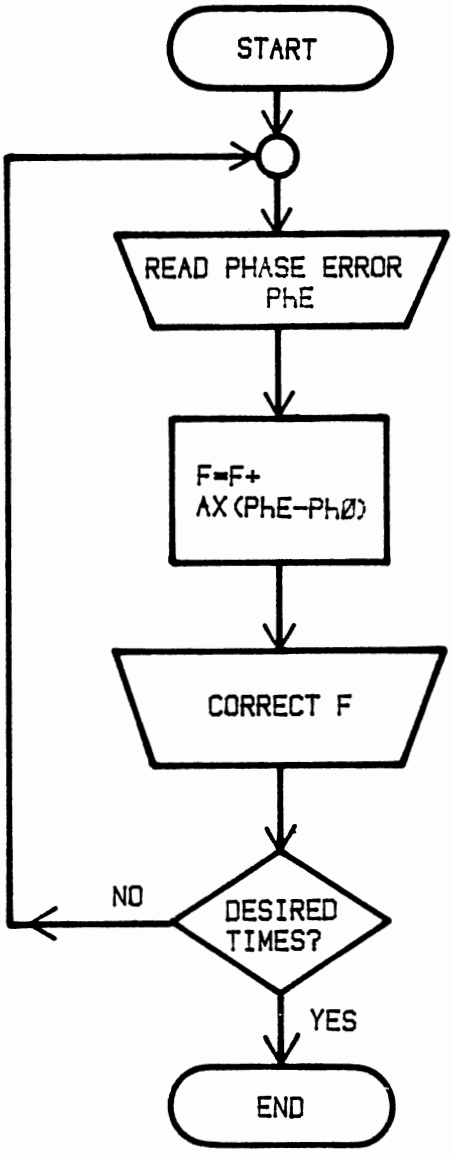

Figure 17. The Digital Feedback Loop of Subroutine Program, "Tune Phase"

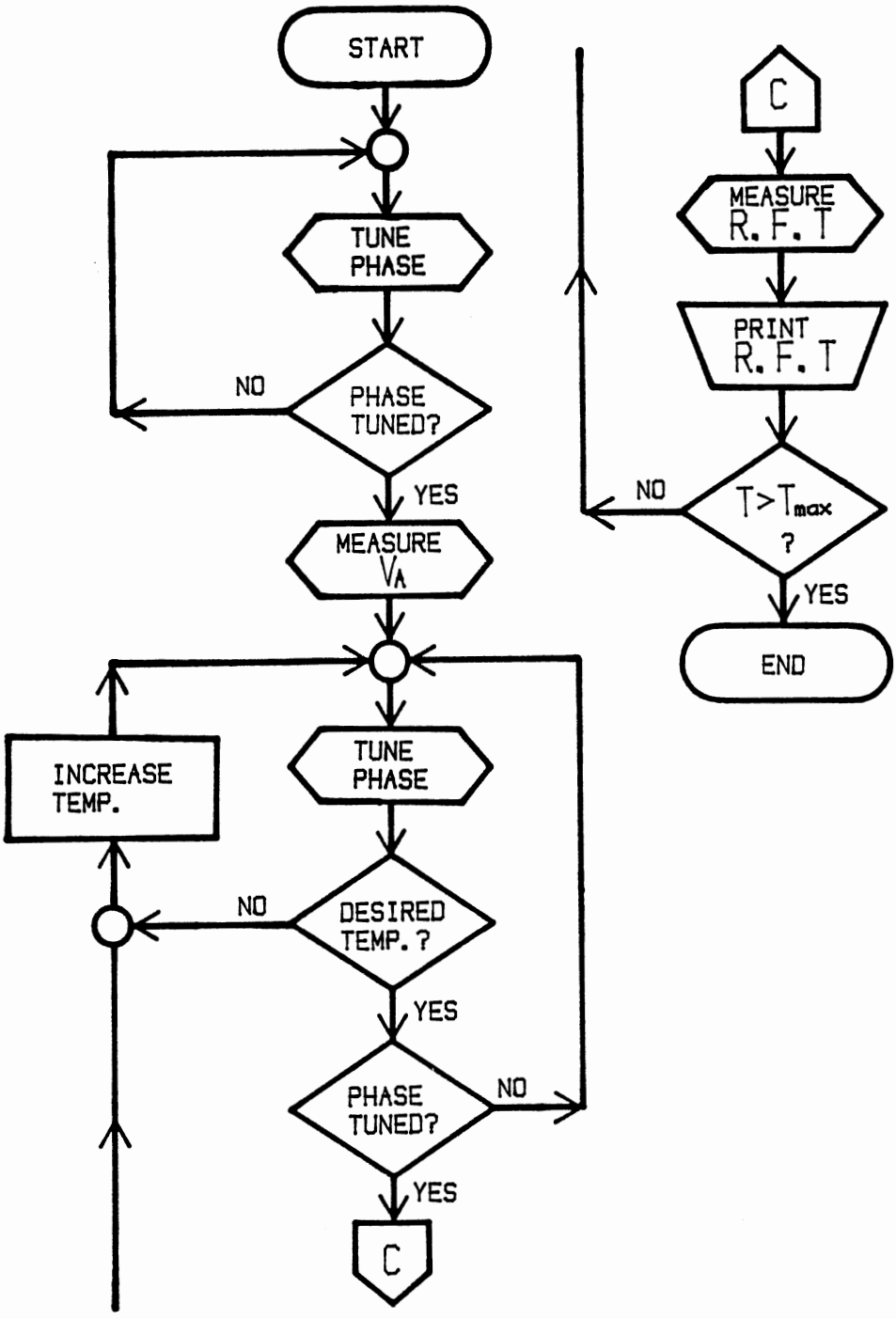

Figure 18. Flowchart for taking the Series Resistance versus Temperature Data

from "zero-phase" is negligible. After reading Vb the computer connects the phase output to the DVM again by controlling the switch, reads the temperature, TEMP2, and the frequency, F, and calculates the average temperature, T of the TEMP1 and TEMP2, and the series resistance, R. Then it increases the set point of the temperature controller if the measured temperature is less than the maximum temperature of the measurement, and starts tuning again for the next measurement. It stops taking data if the measured temperature is larger than the maximum temperature.

6. Statement of Errors

Uncertainties may exist in the process of irradiating samples with Van De Graaff electrostatic accelerator. The generating voltmeter itself of the accelerator has an accuracy of ±0.05% and the meter calibration is accurate within around ±5%. The accelerating voltage can be read to ±0.025 MV. Thus, the adjustment of the accelerating voltage has an uncertainty of ±1.4%. The beam current meter can be read to ±0.1 uA; however, sometimes the current drifts ±0.5 uA during an irradiation. The uncertainty in the beam current is estimated at ±5%. The irradiation time has been controlled by a Gralab model 900 programable timer or a rotating wheel chopper. The Gralab timer is accurate within ±0.015% at one minute. The rise and fall time of the beam current is observed to be around 10 m sec. which gives the uncertainty of 1%. The speed of the rotating wheel chopper

is expected to be constant within the uncertainty of 2%. Consequently, the error due to the adjustment of the accelerator voltage, the beam current, and the irradiation time turns out to be around ±14%.

The AECL 2000 ^{60}Co gamma-cell at OSU has been calibrated with an accuracy of ±3%. The most significant error of irradiations in ^{60}Co gamma-cell is due to irradiation time for which a sample stays in the gamma-cell. The uncertainty of irradiation in the gamma-cell is estimated to be around ±4%.

The cleaning and mounting techniques for both the log-decrement method and the transmission method were developped to minimize their effects on the acoustic loss. Since we typically achieve acoustic Q's, $>10^7$, at 5K, we are reasonably certain that the holder and cleaning procedures are not limiting the measurements at higher temperature.

The Lake Shore model DRC-80 thermometer and controller which was used with the variable temperature helium cryostat displays temperature with ±0.5K accuracy from 4K to 330K. The temperature was increased in a rate of 0.13K/minute during the measurements. The TRI T-2000 Cryo Controller was used with the CTI Closed-cycle helium refrigerator. The TRI Cryo temperature controller uses a silicon diode cryogenic temperature sensor, model CD301 Cryo Diode, which is accurate within ±0.01K between 1.5K and 25K and ±0.1K between 25K and 380K. The TRI Cryo temperature controller increased the sample's temperature in a rate of 0.6K/minute

during the measurements. Therefore, the displayed temperature on both of the temperature controllers was reasonably closed to the sample's temperature.

The uncertainty of the acoustic loss measurement exists in both the log-decrement method and the transmission method. The error of the acoustic loss measurement by the log-decrement method could occur due to the reading error of the decay time, $T_{1/2}$, and the tuning error of the resonance frequency. Since the frequency could be adjusted within ±5Hz, the frequency error did not contribute significantly to the calculation of the acoustic loss. The decay time was not stable but fluctuated within approximately ±0.5 ms at $T_{1/2}$ = 10 ms and ±1 ms at $T_{1/2}$ = 20 ms. The uncertainty of the acoustic loss measurement by the log-decrement method is expected to be about ±5%.

Errors in the acoustic loss measurements by the transmission method might take place in tuning the resonance frequency and measuring the resistance and inductance, and deriving the equation for the resistance due to inaccuracy of the resistors. During the measurements, the resonance frequency was tuned so that its phase angle lies between -3.24 and +1.44 degrees. Within this range of the phase angle, the frequency was off from the resonance frequency less than ±0.5 Hz from 9K to 320K, which is too small to affect the measured acoustic loss. The uncertainty in the ratio of V_A/V_{Bmax} due to the off-tuning caused -0.34% error in the calculation of the series equivalent resistance of

the sample and, therefore, the acoustic loss. However, this limitation of the phase angle was sometimes relaxed upto ±15 degrees, which gives around -4.5% error. The error of the inductance due to using the approximation equation gives about -2.2% and the error of the inductance measurement is figured out to be around ±5.4%. The resistors used in the pi-network have 1% tolerance, so the equation for the equivalent series resistance can give around 1% error between -3.24 and +1.44 degrees of the phase angle. The uncertainty of the acoustic loss measurement by the transmission method is figured out to be less than ±9% at the temperature range of 9K and 320K.

Therefore, the uncertainty involved in the experiment is estimated to be around ±10% to ±13% for the log-decrement method and around ±14% to ±17% for the transmission method.

CHAPTER V

RESULTS AND DISCUSSION

The samples used in this study are Na^+-, H^+-, and Li^+-swept AT-cuts, a Li^+-swept BT-cut, and an unswept SC-cut blanks which have been fabricated by Frequency Electronics Inc. from the same Toyo Supreme Q labeled bar, SQ-B, and a Na^+-swept AT-cut blank which has been fabricated by Piezo Crystal Company from Sawyer Premium Q labeled bar, SP-DD(D14-45). The Toyo bar SQ-B comtains 10-15 ppm aluminum and the Sawyer bar SP-DD less than 1 ppm aluminum. These samples were swept using the OSU Electrodifussion facility.

The Na^+-swept AT-cut Toyo, and Na^+-swept AT-cut Sawyer, and unswept SC-cut Toyo blanks were used to investigate the reduction of the Al-Na^+ centers and the production of the 23K and 100K loss peaks as a function of the radiation dose at room temperature. The Li^+-swept AT-cut and Li^+-swept BT-cut Toyo blanks were used to investigate the growth of the 100K and 23K loss peaks as a function of the radiation time at room temperature. Also, the frequency shift which is mostly due to the reduction of the Al-Na^+ 53K loss peak was studied. The comparison between the Li^+-swept AT-cut, Li^+-swept BT-cut, and unswept SC-cut samples was made.

The H^+-swept and Li^+-swept AT-cut Toyo blanks were used to study the production of the 100K and 23K loss peaks by an initial low temperature irradiation at 80K. For the Na^+-swept AT-cut Sawyer, Li^+-swept AT- and BT-cut Toyo, and unswept SC-cut Toyo samples, subsequent low temperature irradiations following the room temperature irradiation to saturation were carried out at 80K or 90K to investigate the growth patterns of the 100K and 23K loss peaks and to identify the defect responsible for the 100K and 23K loss peaks. Also, the frequency shift due to the reduction of the Al-Na^+ 54K loss peak and the growth of the 100K and 23K loss peaks was studied.

For the Na^+-swept AT-cut Toyo sample, the log decrement technique with the sample in the variable temperature liquid helium dewar was used to measure acoustic losses as a function of temperature. The sample was irradiated in the ^{60}Co gamma source with the sample removed from the cold finger of the variable temperature liquid helium dewar.

For all samples except the Na^+-swept AT-cut Toyo, the acoustic loss versus temperature spectrum was measured using transmission method with the sample mounted on the cold head of the closed-cycle helium refrigerator. The irradiations were carried out using the Van De Graaff electron accelerator without removing the sample from the cold head of the refrigerator. To minimize the sample heating, a Gralab programmable timer which gave 0.5-2 second pulsed shots spaced 5 seconds was used to irradiate the samples

except for the Na^+-swept AT-cut Toyo and unswept SC-cut sample. Irradiations of the unswept SC-cut Toyo sample were carried out using a rotating wheel chopper which gave 0.5 second shots repeated every 2 seconds to improve the irradiation performance and to prevent the breakage of the cotter pin inside Van de Graaff electrostatic accelerator.

1. Loss Spectra: Room Temperature Irradiations

Figure 19 shows the acoustic loss versus temperature curves of the Na^+-swept AT-cut Toyo blank in the as-swept condition, after 120 krad and 2.08 Mrad irradiations at room temperature. The curve for as-Na^+-swept condition shows a 53K loss peak of 2.3 X 10^{-4}. Since this peak is about three times as large as the one in the unswept AT-cut blank taken from the same Toyo bar SQ-B [23], the Al-Na^+ concentration is about three times that of the unswept crystal. The Al-Na^+ concentration is estimated to be 9.2-13.8 ppm, which accounts for really all of the aluminum, using the following equation found by Martin

$$C = [\ 5(\pm 20\%)X10^4]\ \Delta Q_{53K}^{-1} \qquad (34)$$

where C is the concentration of the Al-Na^+ centers and ΔQ_{53K}^{-1} is the height of the 53K loss peak [15]. A 135K Al-Na^+, β, peak is shown as high as 1.9 X 10^{-6} even though it is obscured by interfering modes at 150K. The curve after 120 Krad irradiation shows that a 23K loss peak has been produced, but the peak is obscured by the interfering mode

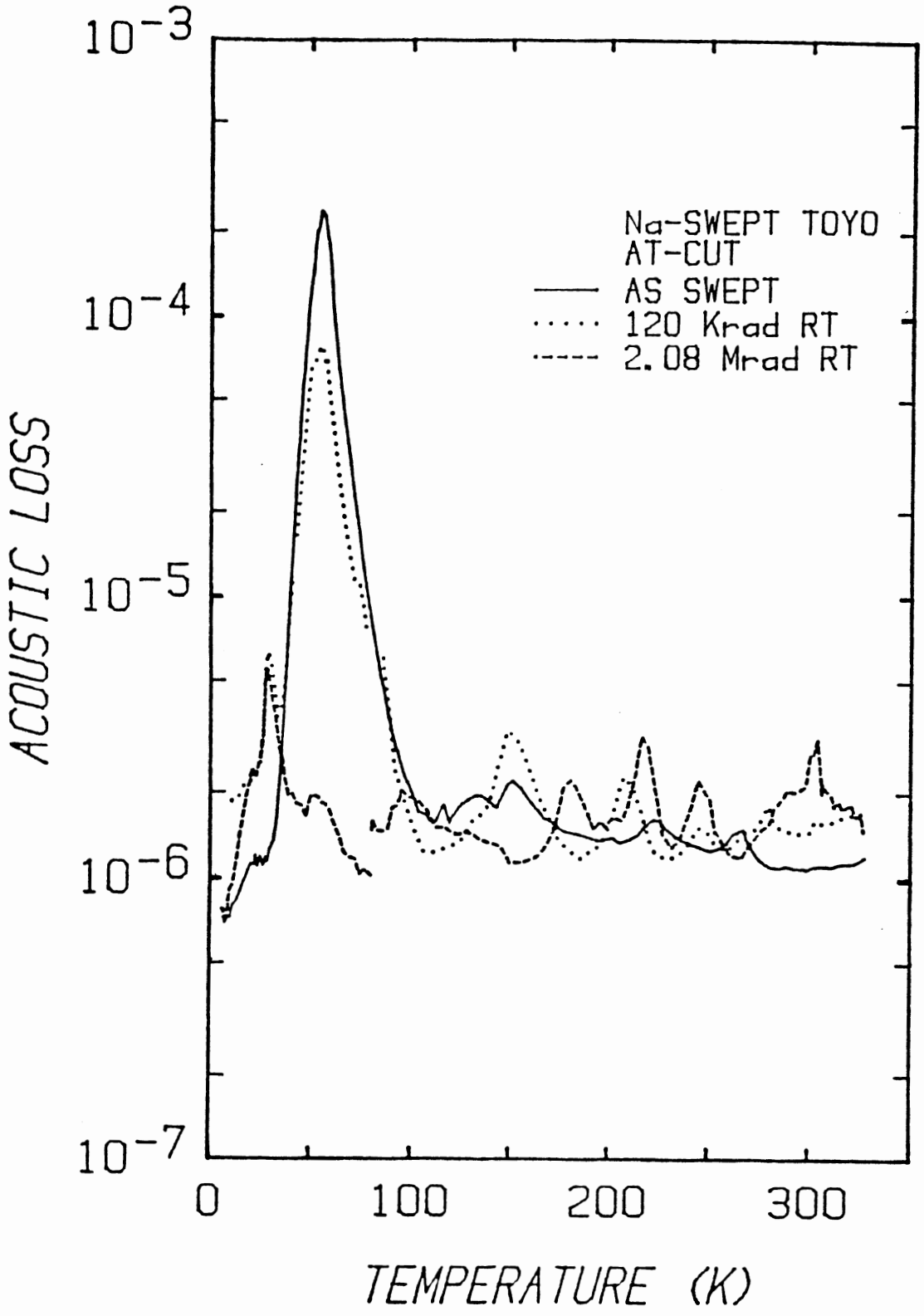

Figure 19. The Acoustic Loss of a Na^+-swept AT-cut Blank taken from Toyo Bar, SQ-B, as a Function of Temperature in the As-Na^+-swept Condition and After Two Gamma Irradiations

at 30K. The 54K loss peak was reduced to 7.43 X 10^{-5} by the irradiation. This shows that the Al-Na^+ centers were destroyed and the defect centers responsible for the 23K loss peak produced by the irradiation. A 100K loss peak, probably due to Al-hole centers, is hidden by the large 54K loss peak in this Na^+-swept sample. The 135K Al-Na^+, β, loss peak is completely obscured by the interfering mode at 150K. The curve after 2.08 Mrad irradiation shows a very small 54K loss peak of 1.9 X 10^{-6}, which means that most of the Al-Na^+ centers have been converted into Al-hole and Al-OH^- centers by the 2.08 Mrad total dose [22]. The 135K Al-Na^+, β, loss peak has disappeared. The 100K loss peak is present, but no further growth in the 23K peak was observed for the 2.08 Mrad irradiation.

Figure 20 shows the acoustic loss versus temperature spectra for the Na^+-swept AT-cut Sawyer crystal in the as-swept condition and after 90 sec and 210 sec room temperature irradiations. The size of the Al-Na^+ 54K loss peak is 1.24 X 10^{-5} in as-Na^+-swept condition and its ratio to the one in the Na^+-swept Toyo sample with high aluminum content described in Figure 19 is about 0.05, which agrees well with the ratio of the Al concentrations of the two samples, the Na^+-swept AT-cut Sawyer and the Na^+-swept AT-cut Toyo crystals. This 54K loss peak is reduced to 4.85 X 10^{-6} by the 90 sec room temperature irradiation and to 1.55 X 10^{-6} by the 210 sec room temperature irradiation. The size of the Al-Na^+ 135K, , loss peak scales with

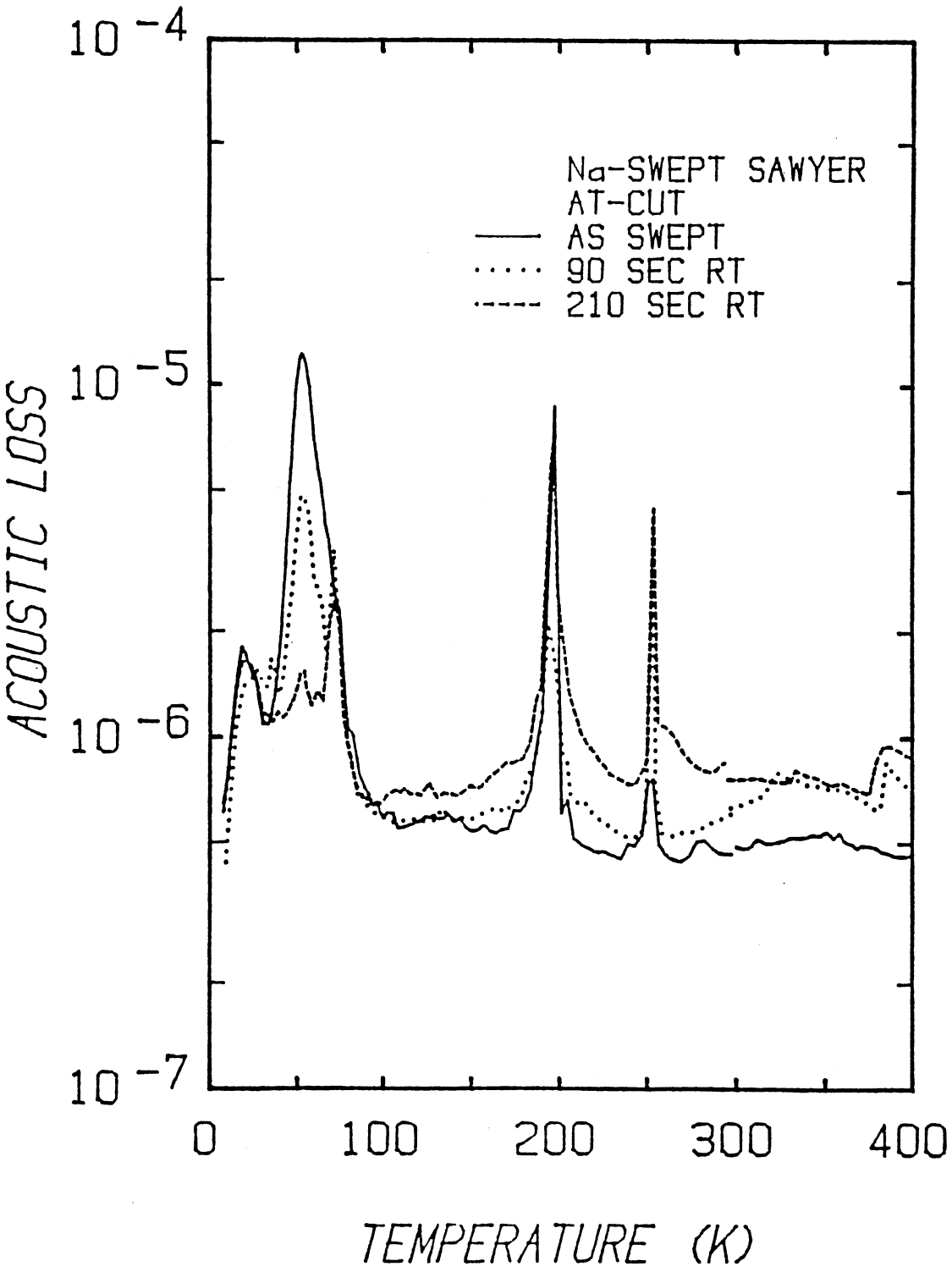

Figure 20. The Acoustic Loss versus Temperature Spectra for a Na^+-swept AT-cut Crystal taken from Sawyer D14-45 Premium Q labeled Bar, SP-DD, in the Na^+-swept Condition and After Several Electron Irradiations at Room Temperature

the Al content of the crystal when compared to the Na^+-swept AT-cut Toyo sample. Because of an interfering mode the 23K loss peak looks too high in the as-Na^+-swept condition. However, it shows that it has been produced by the 90 sec room temperature irradiation and further enhanced by the 210 sec room temperature irradiation. The 100K loss peak is too small to be identified as a peak after the 90 sec irradiation, but it is clearly present after the 210 sec room temperature irradiation. In this sample, as well as the Na^+-swept AT-cut Toyo crystal, the 23K and 100K loss peaks can not be monitored as a function of radiation dose because of the persistent interfering modes and the high 53K loss peaks. The strong peaks at 200K and 250K are due to the interfering modes. The 90 sec room temperature irradiation has produced a loss peak at 340K. This peak goes up and then decreases as the radiation dose increases. It is due to the Na^+-ions, that have been freed from the Al-Na^+ centers and trapped in unknown sites [23].

The above experiments on the Na^+-swept AT-cut Toyo and Sawyer samples showed that the strong 54K loss peak tended to mask the radiation-induced 100K loss peak and that the 100K loss peak was relatively small compared to the 23K loss peak. Therefore, it was very difficult to track the 100K loss peak as a function of radiation dose. J. C. King suggested that the Al-hole 100K loss peak was larger in BT-cut crystals than in AT-cut crystals. Figure 21 shows the acoustic loss versus temperature curves for a Li^+-swept BT-

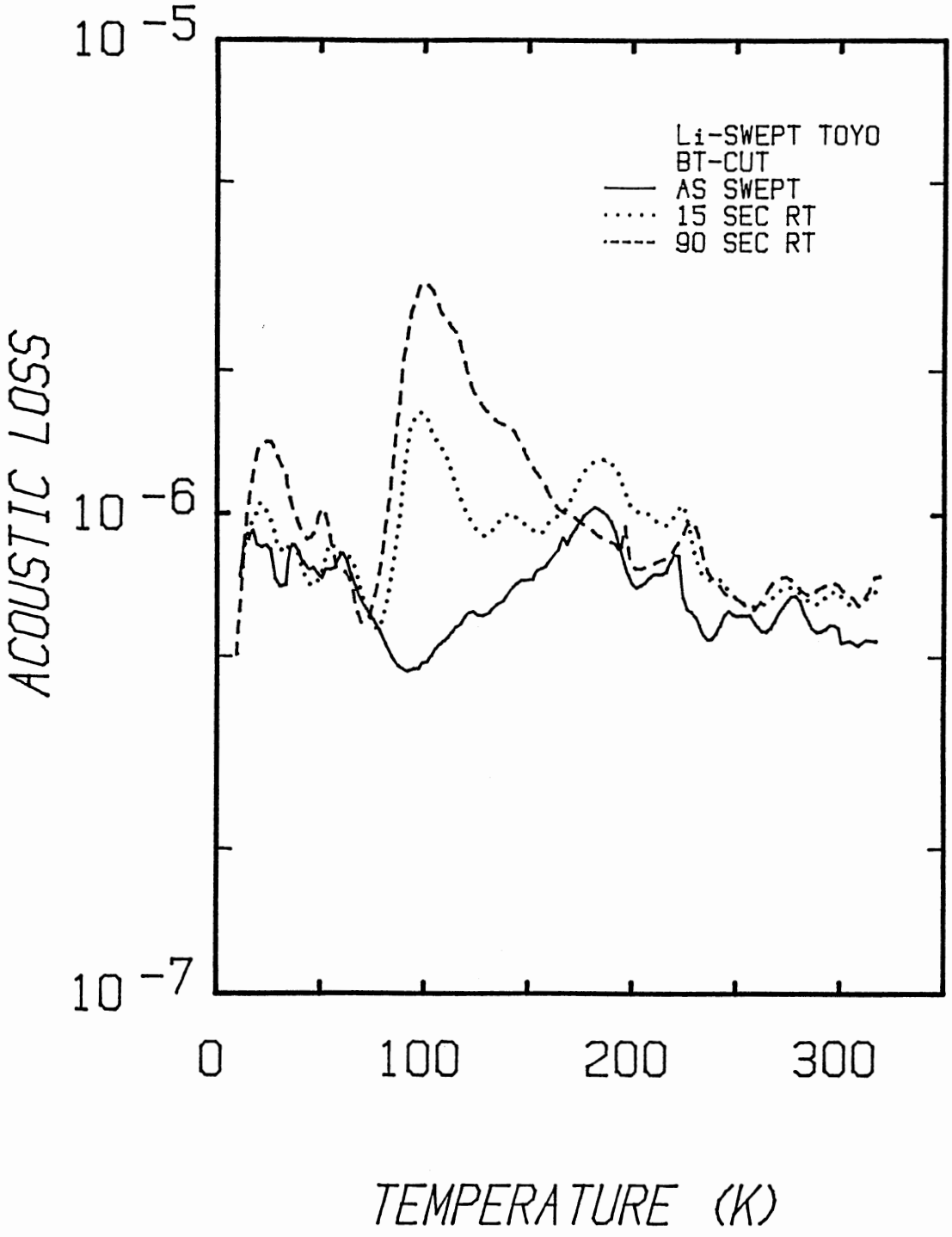

Figure 21. The Acoustic Loss versus Temperature Curves for a Li^+-swept BT-cut Toyo Crystal in As-swept Condition and After 15 sec and 90 sec Electron Irradiations at Room Temperature

cut Toyo crystal in as-Li^+-swept condition and after 15 sec and 90 sec electron irradiations at room temperature. The solid curve in the as-swept condition does not show the 100K and 135K loss peaks as well as a 23K loss peak. The Al-Na^+ 54K loss peak is very small as expected since this sample has been Li^+-swept. The 15 second room temperature irradiation produced the Al-hole 100K loss peak of 1.62×10^{-6}, the Al-hole 135K loss peak of 9.96×10^{-7}, and the 23K loss peak of 1.04×10^{-6} as shown in the dotted curve. The Al-hole 100K loss peak is greater than the 23K peak by a factor of 1.56; we observed the opposite in similar AT-cut crystals. The dashed curve shows the result for the 90 second electron irradiation at room temperature. Both the 100K peak and the 23K loss peak were further enhanced to 3.07×10^{-6} and 1.43×10^{-6} respectively. Also, the 135K loss peak was further enhanced although a part of the 135K loss peak was screened by the large 100K loss peak. The production of the radiation-induced loss peaks explains that the room temperature irradiation has destroyed the Al-Li^+ centers and produced the defects responsible for the 23K, 100K, and 135K loss peaks. The reverse of the size of the 23K and 100K loss peaks in AT-cut and BT-cut samples shows that the defect causing the 100K loss peak, probably Al-hole, is associated with oxygens nearly parallel to the AT-cut plane and the defect causing the 23K loss peak with oxygens nearly parallel to the BT-cut plane. Interfering modes are present above 150K in this sample.

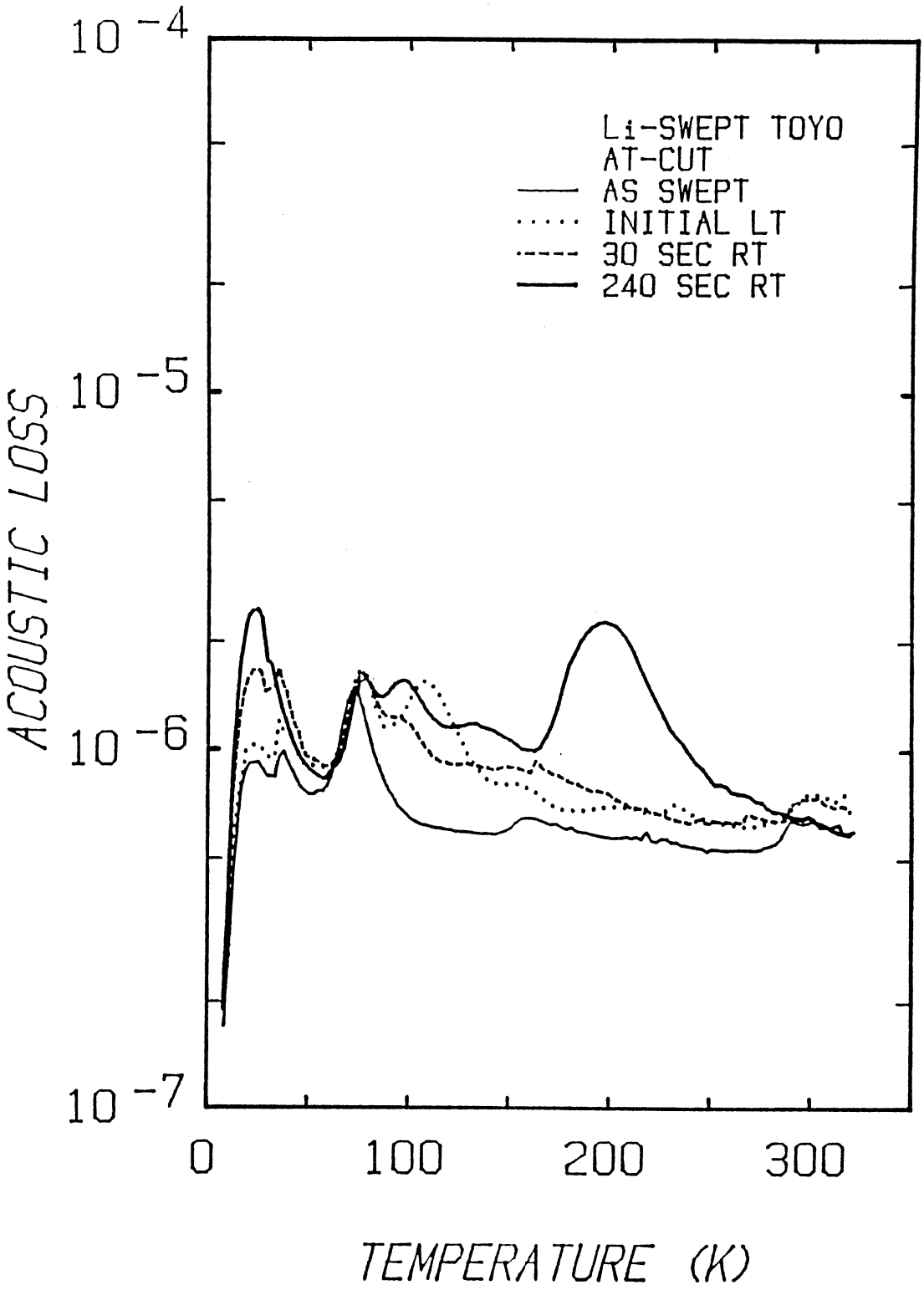

Figure 22. An Initial Low Temperature Irradiation produced a New Loss Peak at 107K in This Li^+-swept Sample. Room Temperature Irradiations produced the 23K and 100K Loss Peak

Figure 22 shows the acoustic loss spectra for a Li^+-swept AT-cut Toyo crystal as a function of temperature in as-Li^+-swept condition, after initial 90 second low temperature irradiation at 90K, and after 30 sec and 240 sec room temperature irradiations. Through out the measurement run on this sample there existed interfering modes at 40K and 80K. The light solid curve shows a smooth background loss except for the two interfering modes at 40K and 80K. It also shows small loss peak at 305K caused by Li^+-ions trapped in unknown site. The initial 90 second low temperature irradiation produced a very small 23K loss peak and a larger previously unobserved loss peak at about 107K, and enhanced the Li^+-related loss peak at 305K as shown in the dotted curve. However, the 100K loss peak was obscured by the large interfering mode at 80K. This 23K loss peak produced by the initial 90 second low temperature irradiation is too small compared to the one produced by the room temperature irradiations. The enhancement of the Li^+-related 305K loss peak indicates that the initial low temperature irradiation has destroyed Al-Li^+ centers; however, the number of Al-Li^+ centers destroyed may be very small since the 305K loss peak can grow with a small radiation dose. The 23K loss peak is also too small compared to the one produced by the low temperature irradiations of samples with high Al-OH^- contents such as the H^+-swept AT-cut Toyo crystal discussed in Figure 25. This result agrees well with the fact that this Li^+-swept sample contains very

few Al-OH^- centers. Consequently, the 23K loss peak is caused by the defect which has been produced in the process of the destruction of Al-Li^+ centers or also Al-OH^- centers. When compared to the curves for the room temperature irradiations, the new 107K loss peak is definitely not the 100K loss peak. The room temperature irradiations caused the 23K loss peak to grow according to the form $3.3 \times 10^{-6}(1-\exp(-t/83))$ and the Al-hole 100K loss peak according to the form $1.5 \times 10^{-6}(1-\exp(-t/50))$. The slower growth rate of the 23K loss peak as compared to the probably Al-hole 100K loss peak is consistent with earlier results [23]. Also the room temperature irradiations produced a 135K loss peak. The newly observed loss peak at 107K was destroyed either by the 15 second room temperature irradiation or by warming the sample to room temperature. The origin of this loss peak is not understood at this time; perhaps it is due to a Li^+ perturbed Al-hole center. The large loss at 200K is due to an interfering mode.

Figure 23 shows the acoustic loss spectra as a function of temperature for the unswept SC-cut Toyo crystal in as-received condition and after a series of room temperature irradiations. The crystal was operated on the "c" mode. The measured frequency was averaged by a HP 5316A universal counter. In the as-received condition the Al-Na^+ 53K loss peak is about 50% lower than for unswept AT-cut Toyo crystals taken from the same bar [23]. This difference may be due to differences between SC-cut and AT-cut; or it may

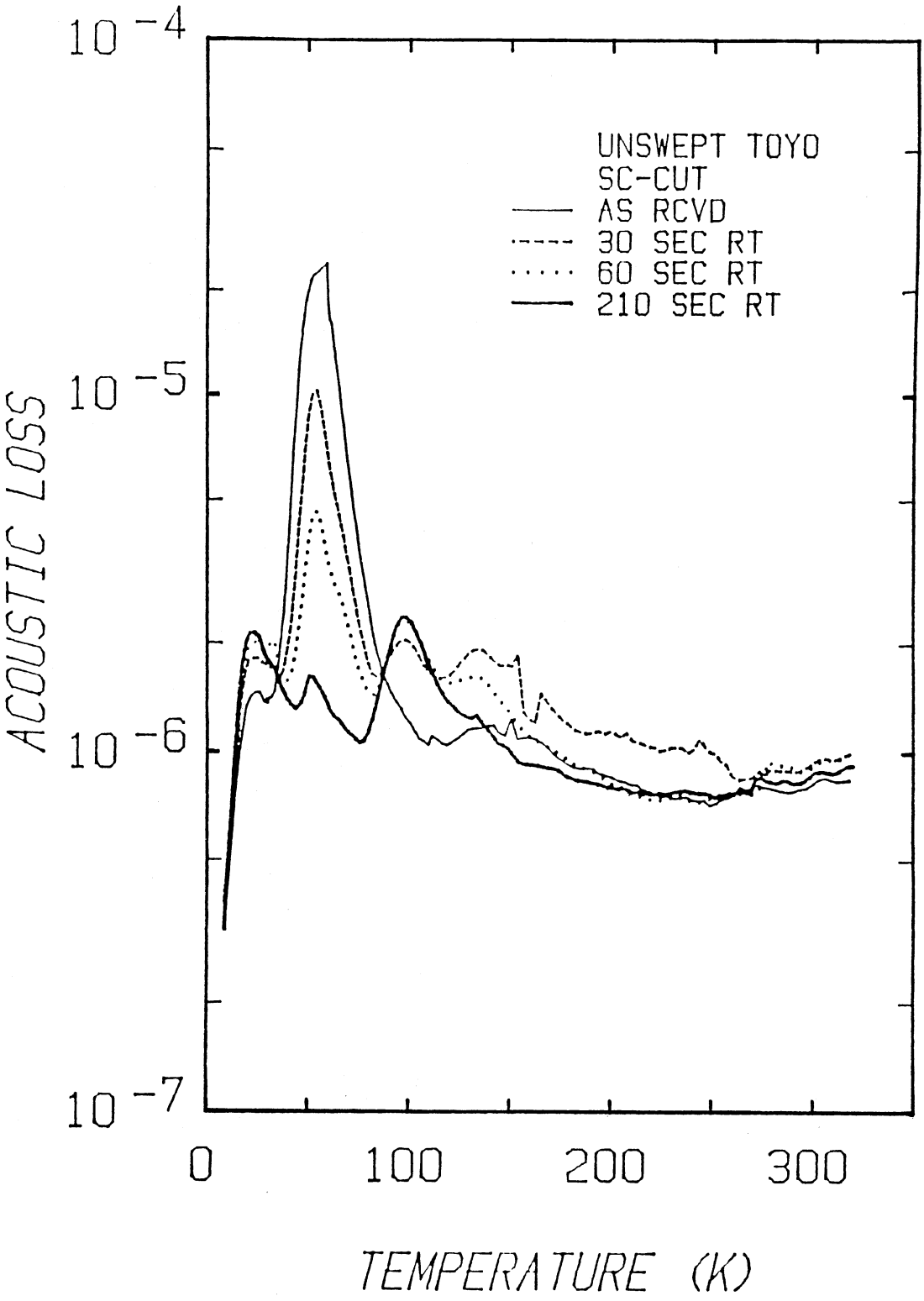

Figure 23. The Acoustic Loss Spectra of the Unswept SC-cut Crystal for a Series of Room Temperature Irradiations

be due to the normal variation of the aluminum content in different parts of the original quartz bar. The Al-Na^+ 135K loss peak is shown to be small as usual. The series of room temperature irradiations produced both the 23K and 100K loss peaks and reduced the Al-Na^+ 54K loss peak. The 54K loss peak decreased initially as $1.94 \times 10^{-5}\exp(-t/33)$ while the 23K peak grows as $6.1 \times 10^{-7}(1-\exp(-t/40))$ and the 100K peak as $10.4 \times 10^{-7}(1-\exp(-t/25))$ where t is the radiation time in seconds. The 23K loss peak is 10% lower than the 100K loss peak after the 210 second room temperature irradiation. The 100K loss peak seems to be saturated by the 100 second room temperature irradiation while the 23K loss peak by the 210 second room temperature irradiation. The 135K, β, loss peak was enhanced from 1.18×10^{-6} to 1.97×10^{-6} by the 30 second room temperature irradiation. The short room temperature irradiation moved some sodium from the Al-Na^+ orientation responsible for the 53K, α, peak to the Al-Na^+ orientation responsible for the β peak. However, the next series of room temperature irradiations destroyed this produced 135K peak.

Both the 23K and 100K loss peaks are essentially the same in the Li^+-swept, Na^+-swept, and unswept AT-cut Toyo crystals taken from the same bar, SQ-B. Thus, the strength of the two acoustic loss peaks seems to be characteristic of the crystal cut. Table 2 shows the strength of the 23K and 100K loss peaks and their ratio for the Li^+-swept AT-cut, Li^+-swept BT-cut, and unswept SC-cut Toyo crystals which are

TABLE II

THE STRENGTH OF THE 23K AND 100K LOSS PEAKS FOR THE Li-SWEPT AT-, Li-SWEPT BT-, AND UNSWEPT SC-CUTS TOYO CRYSTALS AND THEIR RATIO

	AT-CUT	BT-CUT	SC-CUT
23K	15×10^{-7}	5.7×10^{-7}	6.4×10^{-7}
100K	9.6×10^{-7}	26.9×10^{-7}	11.8×10^{-7}
100K/23K	0.6	4.7	1.8

fabricated from the same bar, SQ-B. The strength of each peak was calculated by substracting a background loss from the height of each loss peak when saturated by room temperature irradiations. The 100K loss peak is 2-3 times stronger in the BT-cut than either in the AT-cut or in the SC-cut while the 23K loss peak 2-3 times larger in the AT-cut than either in the BT-cut or in the SC-cut. Assuming the same defect concentration for all three cuts, this result shows that the defect responsible for the 100K loss peak, which is probably the Al-hole center, interacts with BT-cut more strongly than with either the AT-cut or SC-cut, and that the defect responsible for the 23K loss peak with AT-cut more strongly than either with either the BT-cut or with SC-cut. The strength of the two loss peaks in the SC-cut is weakest of the three cuts.

2. Loss Spectra: Low Temperature Irradiations

Figure 24 shows the acoustic loss spectra as a function of temperature over the 8-200K range for the Na^+-swept AT-cut Sawyer sample after 30 sec and 60 sec low temperature irradiations following the initial 210 sec room temperature irradiation. After this Na^+-swept AT-cut Sawyer sample reached saturation for the room temperature irradiation sequence low temperature irradiations were carried out at 80K. The control rack of the transmission system as well as the refrigerator rack was moved to the Van De Graaff room and the crystal resistance and temperature were monitored.

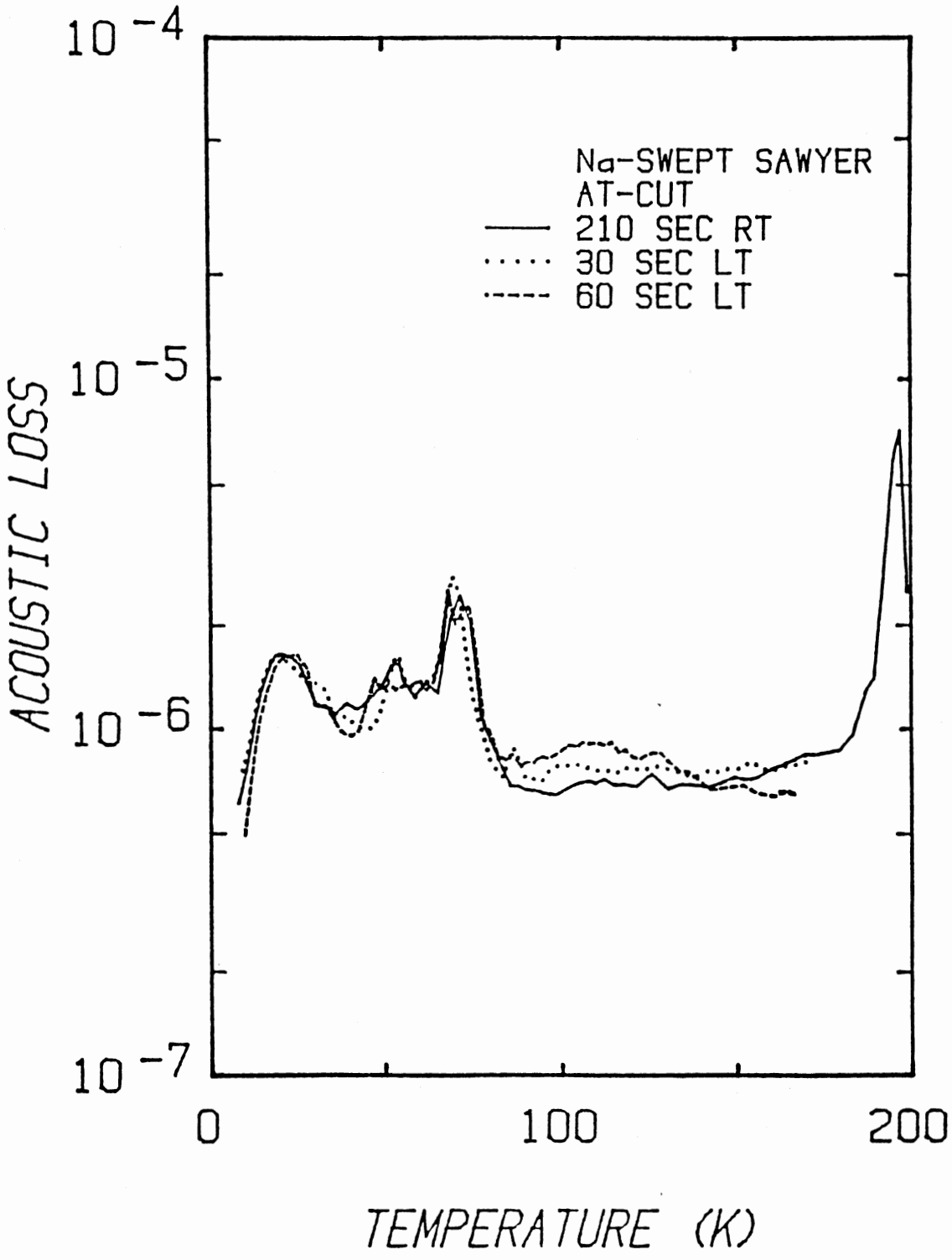

Figure 24. The Acoustic Loss Spectra for the Na^{+}-swept D14-45 Crystal for 30 sec and 60 sec Irradiations carried out at 80K following the Initial 210 second Room Temperature Irradiation

Initially, the sample was given a continuous 30 second irradiation at 80K and the crystal resistance was measured from 9K to 180K after cooling down to 9K. However, no significant change in resistance was observed. This might result from annealling of the low temperature radiation-induced centers by sample heating during the continuous irradiation. Therefore, the irradiation at 80K was repeated for 30 seconds with the 0.5 second pulsed shots spaced 15 seconds apart and its resistance was measured from 9K to 170K after cooling down to 9K. These data are shown as the dotted curve of 30 sec low temperature irradiation. After taking data up to 170K the sample was quickly cooled down to 80K and again irradiated for another 30 seconds with the 0.5 second pulsed shots. The data shown with the dashed curve was taken from 9K to 167K after the total 60 second low temperature irradiation. The 30 second low temperature irradiation at 80K increased the 100K loss peak previously produced by the room temperature irradiations and another 30 second low temperature irradiation further increased it. This 100K loss peak produced by the low temperature irradiation was annealed out after the sample was warmed up to room temperature. J. C. King first observed it and assigned it to the Al-hole center [16]. J. J. Martin showed it by infrared study of a H^+-swept blank taken from the same bar that a 30 second electron irradiation at 80K converted the Al-OH^- centers into Al-hole centers [31]. These results can be explained as follows. The room temperature

irradiations up to saturation completely converted the Al-Na^+ centers into a mixture of the Al-OH^- and Al-hole centers. A subsequent low temperature irradiation converted the Al-OH^- centers into Al-hole centers. These low temperature irradiations did not produce an observable 23K loss peak in this Na^+-swept crystal. Thus, this result shows that the 23K loss peak is probably not caused by the Al-hole center.

Figure 25 shows the acoustic loss spectra for a H^+-swept AT-cut Toyo sample in the as-H^+-swept condition and after a 30 second irradiation at 80K. The irradiation of the sample was performed without previous room temperature irradiation. The low temperature irradiation at 80K and the measurement of the acoustic loss were carried out as described in the discussion of Figure 24. The 30 second low temperature irradiation introduced a relatively large loss peak at 100K and smaller peaks at 23K and 135K. The 23K loss peak is slightly smaller than the 100K peak. This result is opposite to that observed in the previous Na^+-swept AT-cut Toyo and Sawyer samples for room temperature and low temperature irradiations. This H^+-swept Toyo sample has a much higher Al-OH^- content than the previous Na^+-swept Sawyer samples since the substitutional aluminum is compensated only by hydrogen. That is why the initially small 30 second low temperature irradiation has easily converted the Al-OH^- centers into the Al-hole centers, and produced the relatively large 100K loss peak compared to the

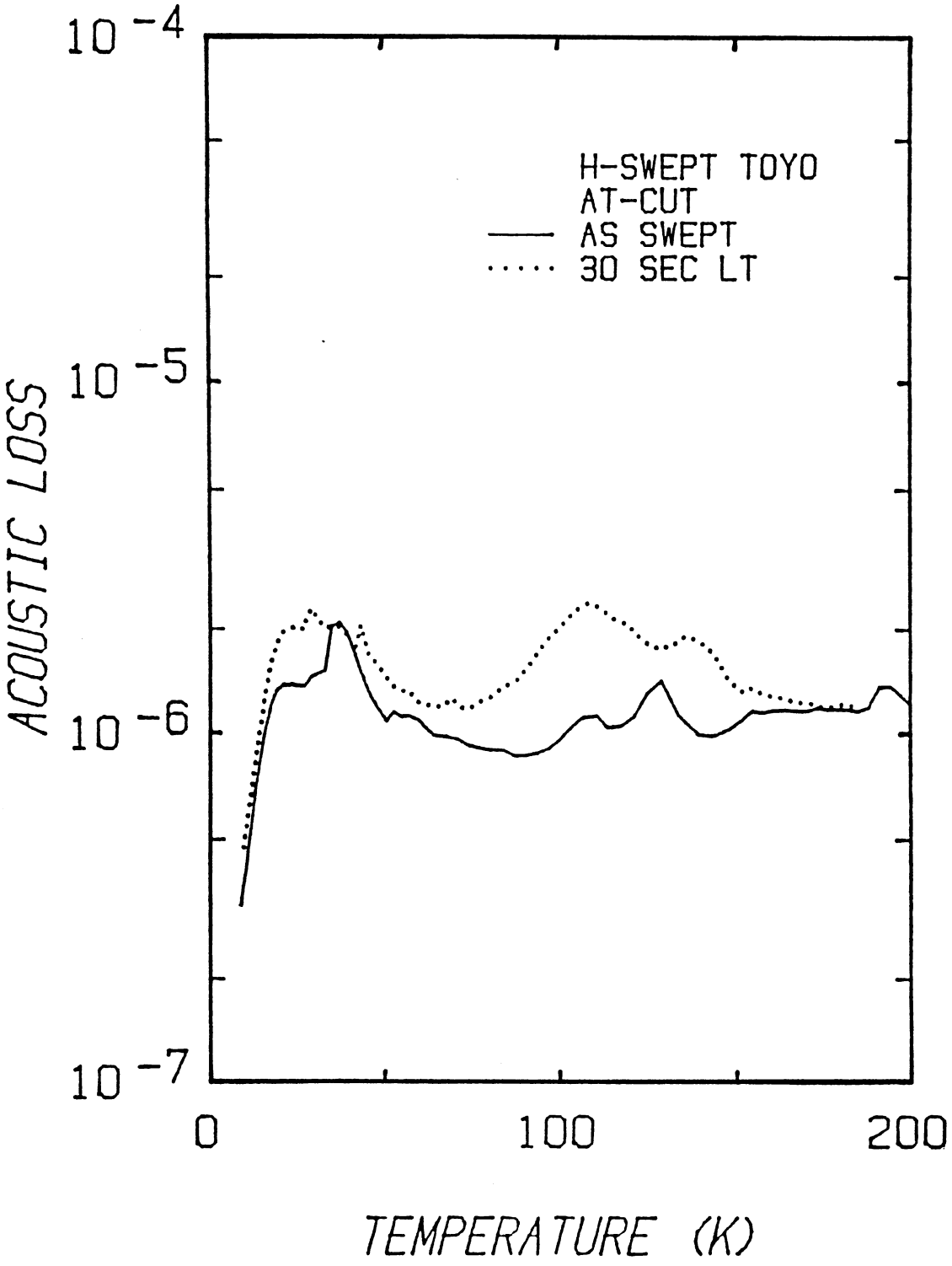

Figure 25. The Acoustic Loss Spectra for a H^+-swept Toyo SQ-B Crystal in the As-H^+-swept Condition and After a 30 second Irradiation performed at 80K

one for the previous Na^+-swept samples; the size of the produced 100K loss peak was proportional to the produced Al-hole centers. This result is supporting the assignment of the 100K loss peak to the Al-hole center by J. C. King. Furthermore, the reverse of the ratio of the 23K peak and the 100K loss peak again shows that the 23K loss peak is not probably due to the Al-hole center; if the Al-hole center is responsible for the 23K loss peak the production of the Al-hole centers will cause the growth of the 23K loss peak in a same rate as the 100K peak so that the ratio between the two loss peaks will be same as the one for the Na^+-swept samples. The 30 second low temperature irradiation did not saturate the production of the radiation-induced loss peaks.

Figure 26 shows the acoustic loss spectra for the Li^+-swept BT-cut Toyo crystal in as-swept condition, after 90 second room temperature irradiation, and after 80 second low temperature irradiation at 80K. After saturation with the 90 sec room temperature electron irradiation the sample was reirradiated at 80K. Both the 23K peak and the 100K loss peaks increased from 1.43×10^{-6} to 1.72×10^{-6} and from 3.07×10^{-6} to 4.91×10^{-6} respectively. This increase in the 100K peak is caused by the conversion of the Al-OH^- centers into Al-hole centers by the low temperature irradiation. The growth ratio is 0.51 for the 23K loss peak and 0.71 for the Al-hole 100K loss peak; thus, the Al-hole center grows slightly faster than the defect responsible for the 23K loss peak. This slower growth is consistent with

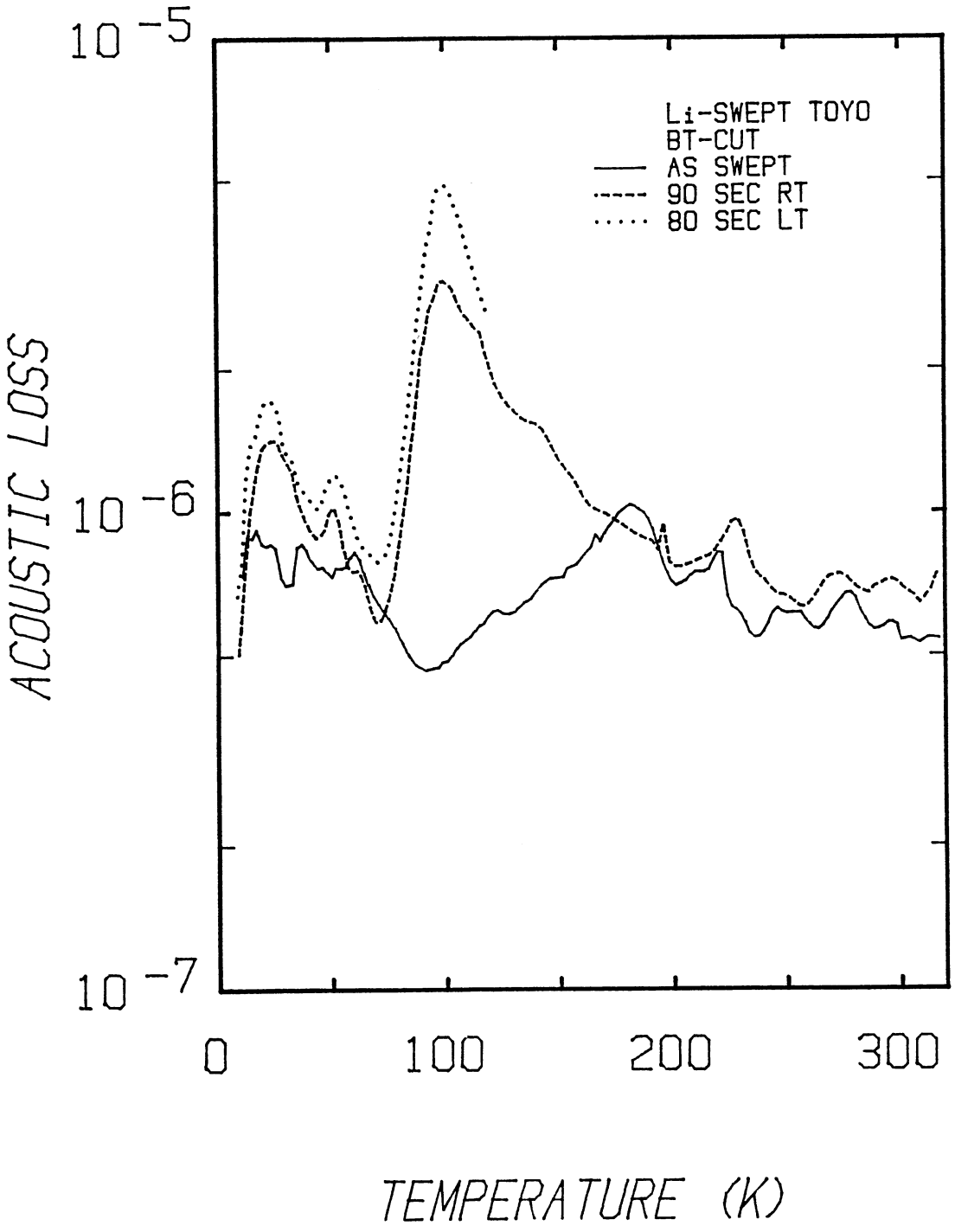

Figure 26. The Acoustic Loss Spectra for the Li^+-swept BT-cut Toyo Crystal in As-swept Condition, After 90 second Room Temperature Irradiation, and After 80 second Low Temperature Irradiation at 80K

our earlier results.

Figure 27 shows the acoustic loss versus temperature curves for the Li^+-swept AT-cut Toyo crystal after the 240 second room temperature irradiation to saturation, after 30 second and 60 second low temperature irradiations at 90K, and after annealing the sample at room temperature. The heavy solid curve shows the spectrum after the 240 sec room temperature irradiarion. The saturation of the sample indicates that most Al-Li^+ centers have been converted into Al-hole centers and Al-OH^- centers. The sample was then cooled to 90K, electron irradiated for 30 seconds, cooled to 9K, and the dashed curve taken as the sample was heated to 104K. The 30 sec low temperature irradiation increased the 100K loss peak from 1.58 X 10^{-6} to 2.4 X 10^{-6}, but slightly decreased the 23K loss peak. Then, the sample was again cooled to 90K, reirradiated for 60 seconds, cooled to 9K, and the light solid curve taken as the sample was heated to 115K. The 60 sec low temperature irradiation again increased the 100K loss peak from 2.4 X 10^{-6} to 2.75 X 10^{-6}, but did not change the 23K loss peak. The different behavior of the two loss peaks indicates that they are caused by different defects. The continuous growth of the 100K loss peak agrees well with the results of the previous low temperature irradiations for the H^+-swept AT-cut Toyo, the Li^+-swept BT-cut Toyo, and the Na^+-swept AT-cut Sawyer samples, and so supports the assignment of the 100K loss peak to the Al-hole center by J. C. King. After warming up to room temperature

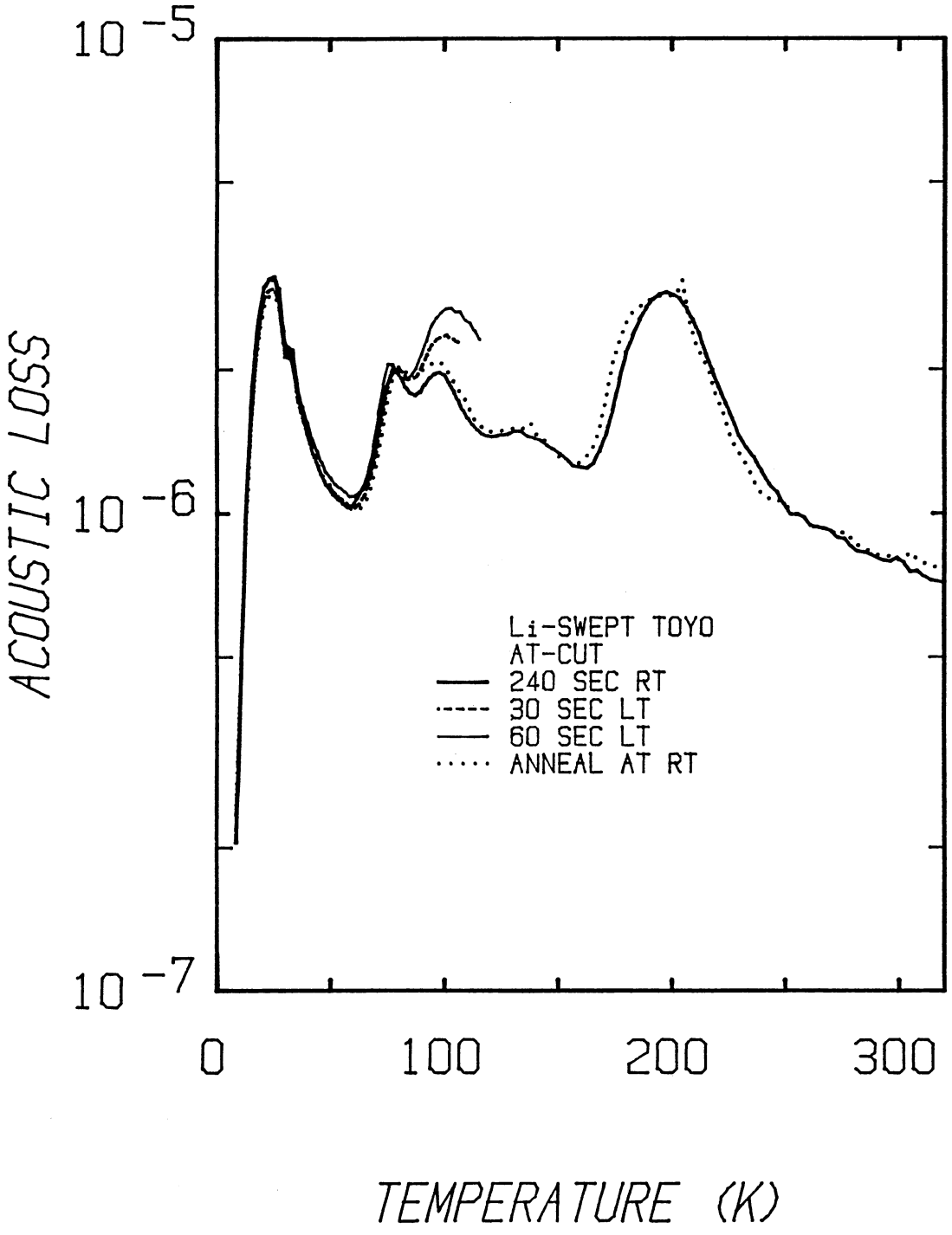

Figure 27. The Acoustic Loss versus Temperature Curves for the Li^+-swept AT-cut Toyo Crystal After the 240 second Room Temperature Irradiation to Saturation, After 30 second and 60 second Low Temperature Irradiations at 90K, and After Annealing the Sample at Room Temperature

the sample was cooled to 9K and the dotted curve taken as the sample was heated to 320K. The 23K loss peak slightly decreased below that after the 30 second low temperature irradiation. The 23K loss peak was not significantly changed by the low temperature irradiations. The portion of the 100K loss peak produced by the low temperature irradiation almost annealed out at room temperature. This result is consistent with the annealing characteristics of the Al-hole centers done with ESR technique by M. E. Markes and L. E. Halliburton [20].

After the unswept SC-cut Toyo sample had been irradiated to saturation at room temperature, the sample was reirradiated at 90K for 820 seconds, cooled to 8K, and the acoustic loss spectrum shown by the dashed curve in Figure 28 measured. The 820 sec low temperature irradiation at 90K doubled the 100K Al-hole center peak. The previous Li^+-swept AT-cut Toyo sample also showed a similar result. These results are consistent with the conversion of the Al-OH^- centers produced by the previous room temperature irradiation into Al-hole centers. The 23K loss peak showed only a very small increase as in the previous Li^+-swept AT-cut Toyo sample after the low temperature irradiation. These results again indicate that the two loss peaks respond differently to low temperature irradiation. Thus, it seems that the defect responsible for the 23K loss peak is not the Al-hole center. The small increase in the 54K loss peak is not understood.

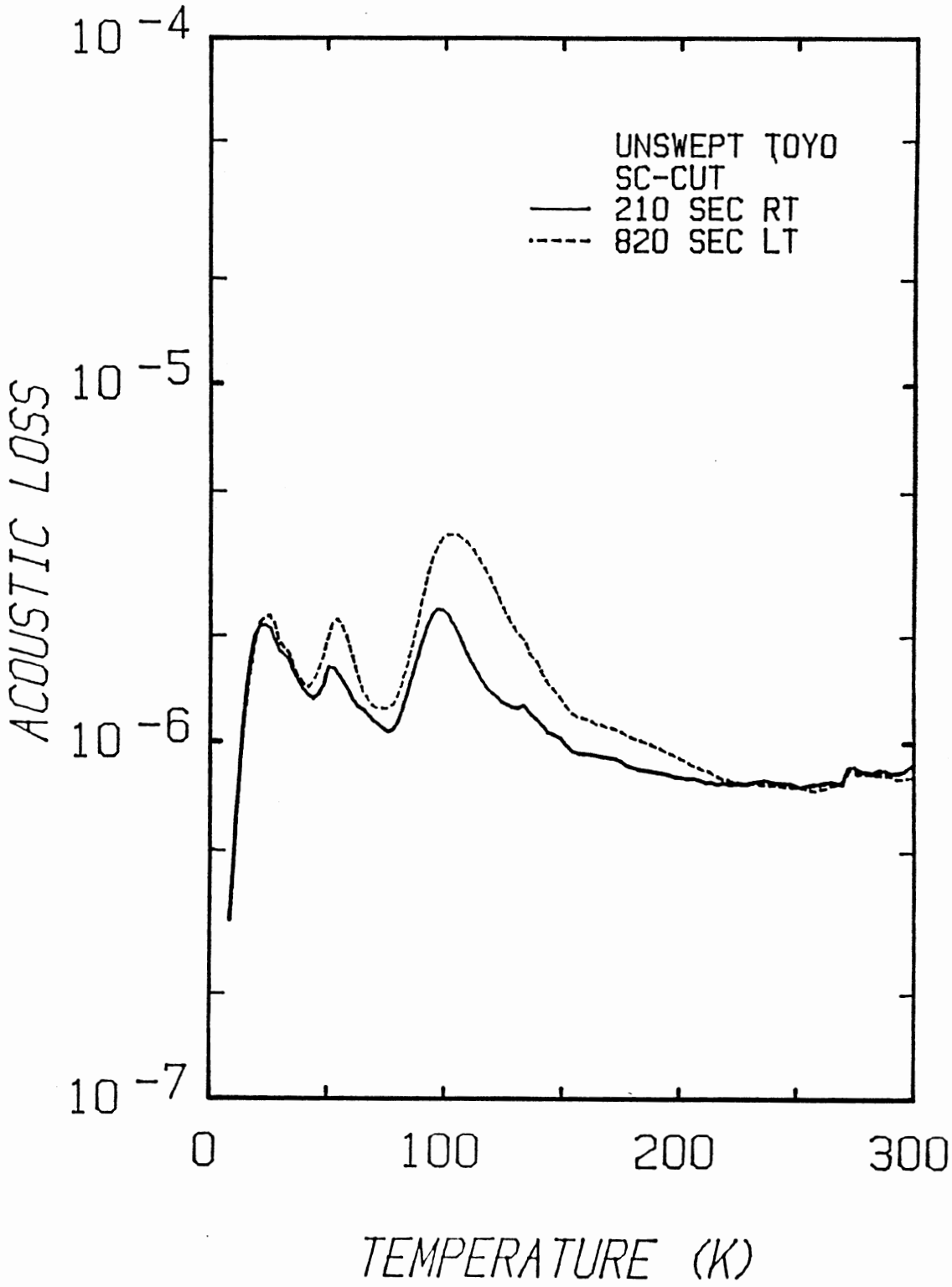

Figure 28. The Acoustic Loss Spectra for the Unswept SC-cut Toyo Sample After 210 second Room Temperature Irradiation to Saturation and After 820 second Low Temperature Irradiation at 90K

3. Production Curves

Figure 29 compares the reduction of the Al-Na^+ center versus radiation dose curves plotted on the log-linear scales for the Na^+-swept AT-cut Toyo sample and the unswept AT-cut Toyo sample. By 0.1 Mrad the Al-Na^+ center has been decreased to 37% in the Na^+-swept sample and 27% in the unswept sample of their initial heights. It shows that within 0.1 Mrad the Al-Na^+ center has been destroyed as $100e^{-10D}$ in the Na^+-swept sample and as $100e^{-13D}$ in the unswept sample, where D is radiation dose in Mrad. Both the Na^+-swept and unswept samples have been destroyed exponentially with smaller dose constants, K's, as radiation dose increases. Consequently, both the curves do not follow a single exponential decay and the Al-Na^+ center goes out more slowly in the Na^+-swept sample than in the unswept sample.

Figure 30 shows the reduction of the Al-Na^+ center as measured by the height of the 54K loss peak as a function of electron irradiation time for the Na^+-swept AT-cut Sawyer crystal. The irradiations were carried out at room temperature. The reduction initially shows an exponential decay of the Al-Na^+ center by the ionizing irradiations at room temperature. Within 100 second radiation time, this reduction is described by delta-loss = $11 \times 10^{-6}\exp(-0.012t)$ where t is the radiation time in seconds. This figure shows that between 150 seconds and 250 seconds of radiation time the reduction curve are straight and its slope becomes

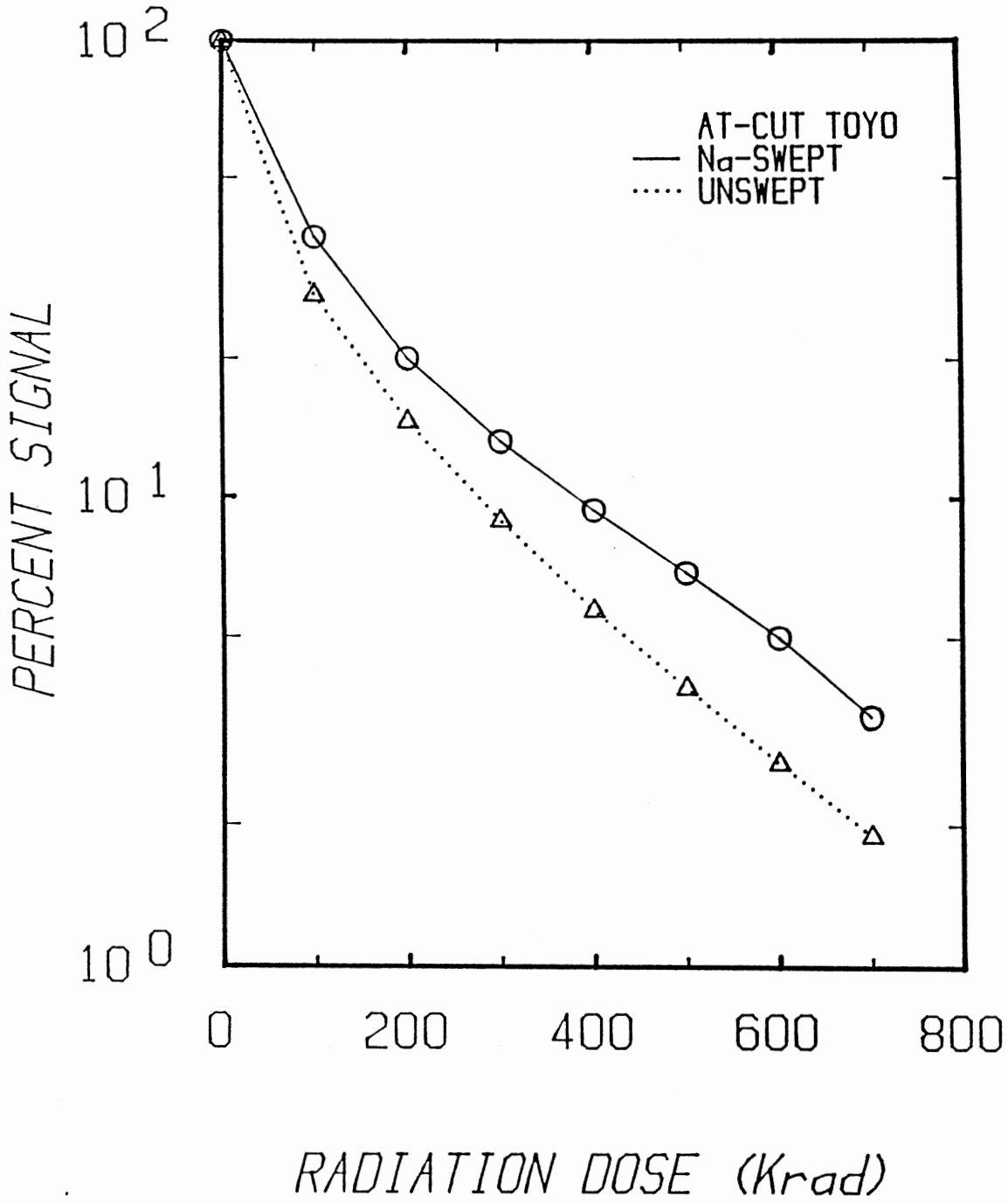

Figure 29. The Percentage Heights of the Al-Na^+ center Loss Peak in the Na^+-swept and Unswept AT-cut Toyo Crystals as a Function of Radiation Dose

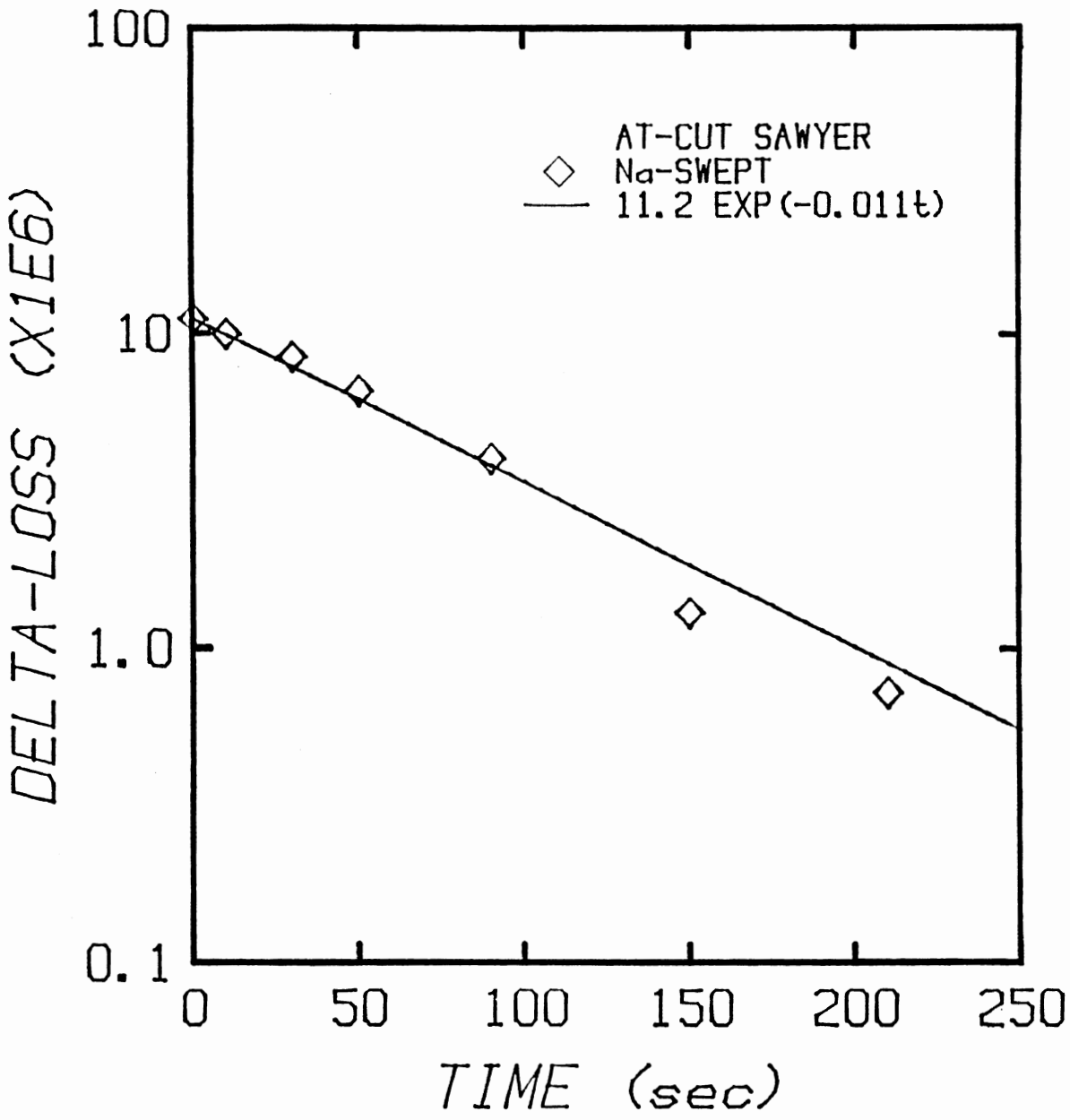

Figure 30. The Decrease in the Al-Na^+ center Concentration in the Na^+-swept AT-cut Sawyer as a Function of Electron Irradiation Time. The Irradiations were performed at Room Temperature

smaller. Thus, the Al-Na^+ center exponentially decreases with a smaller radiation time constant. Because of the large Al-Na^+ signal and interfering modes it was not possible to track the 100K Al-hole loss peak in this sample. However, the production study of the Al-OH^- center done by J. J. Martin with a 5 MHz 5th overtone AT-cut blank taken from the same Sawyer bar, SP-DD, also shows a exponential behavior [31]. This result can be explained by that a flood of the free electrons and holes produced by the ionizing irradiation destroyed the Al-Na^+ centers and produced a mixture of the Al-OH^- and Al-hole centers exponentially.

Figure 31 shows the growth of the Al-hole 100K loss peak and the 23K loss peak as a function of radiation time for the Li^+-swept BT-cut Toyo crystal. The irradiation of the sample was performed at room temperature. To calculate the delta-loss the height of the background loss was substracted from the height of the loss peak at each temperature. The solid curve was calculated from the equation, $\Delta Q^{-1} = 2.8 \times 10^{-6}(1-\exp(-0.03t))$ where t is radiation time. This curve follows the experimental data of the Al-hole 100K loss peak; thus, the Al-hole centers grows as $2.8 \times 10^{-6}(1-\exp(-0.03t))$ by room temperature irradiation. Since the 23K loss peak is about 1/5 the size of the 100K peak in this BT-cut crystal the production data shows considerably more scatter. However, as seen in Figure 31 the 23K loss peak seems to track the Al-hole 100K loss peak.

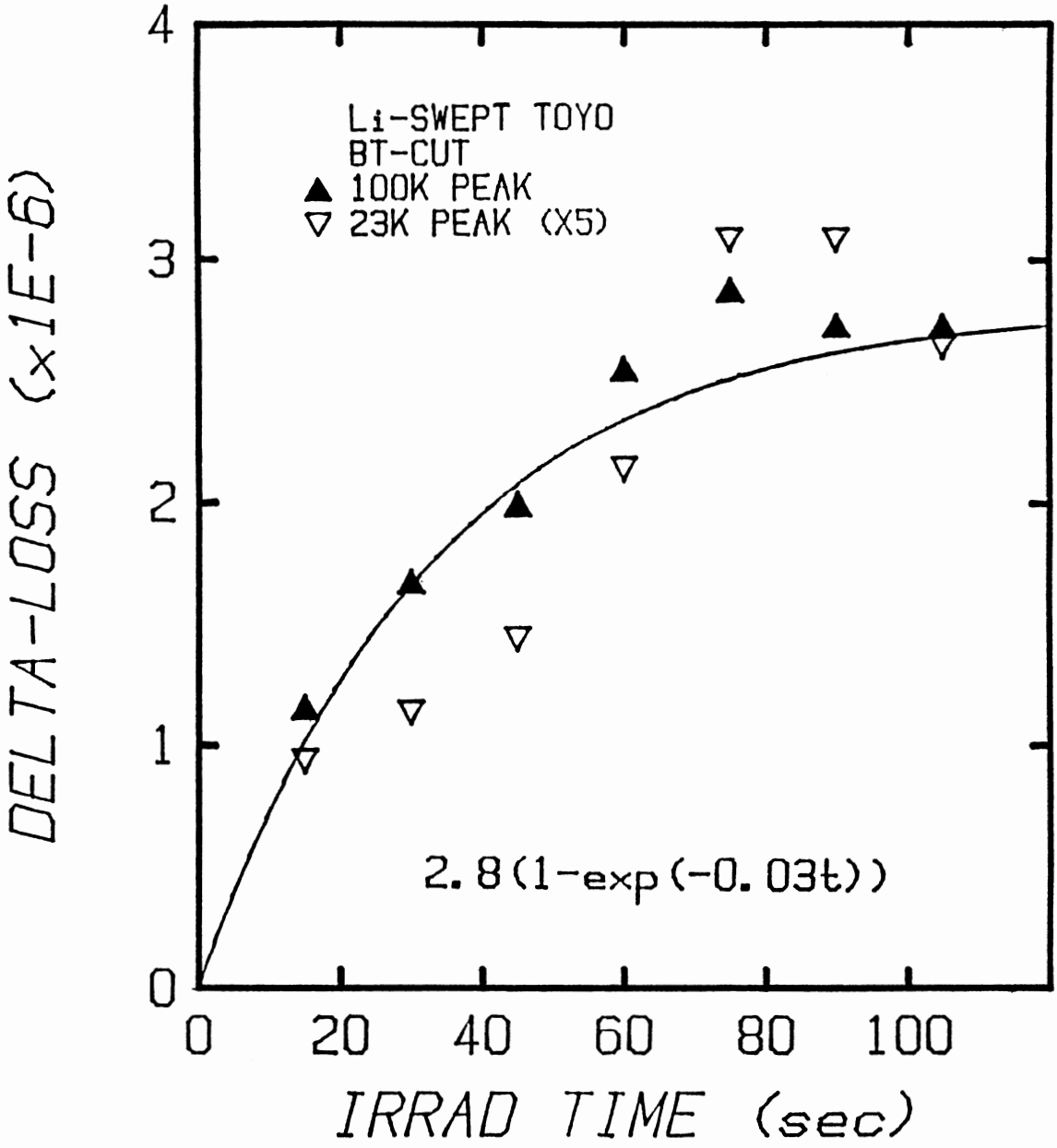

Figure 31. The Growth of the 100K Al-hole Center Peak and the 23K Loss Peak as a Function of Radiation Time for the Li^+-swept BT-cut Toyo SQ-B Series Crystal

Figure 32 shows the normalized destruction curve for the Al-Na^+ 54K loss peak and the normalized production curves for the 23K peak and the Al-hole 100K loss peak as a function of radiation time for the unswept SC-cut Toyo crystal. The Al-Na^+ 54K loss peak goes out initially as 100exp(-t/33), but becomes slower after 100 seconds of radiation time. This result are consistent with that of the Na^+-swept AT-cut Sawyer crystal described in Figure 30. The 100K loss peak grows faster than the 23K loss peak as in the Li^+-swept AT-cut, Li^+-swept BT-cut, and H^+-swept AT-cut Toyo crystals. This figure also shows that the Al-hole 100K loss peak may be saturated by the 100 second room temperature irrradiation while the 23K loss peak by the 210 second irradiation. A direct comparison of the production time contants for this SC-cut with that for the Li^+-swept AT-cut Toyo crystal can not be made because the radiation process was slightly changed.

4. Frequency Shifts

Figure 33 shows the frequency versus temperature curves for the Na^+-swept AT-cut Toyo crystal. The solid curve for the as-swept condition shows a sudden frequency drop of 110 ppm at 54K as expected. However, the 110 ppm frequency change is one half as large as the value predicted from the height of the 54K loss peak in Figure 19 by Equation (11) in Chapter 2. The dashed curve for the 2.08 Mrad irradiation does not show a frequency versus temperature inflection at

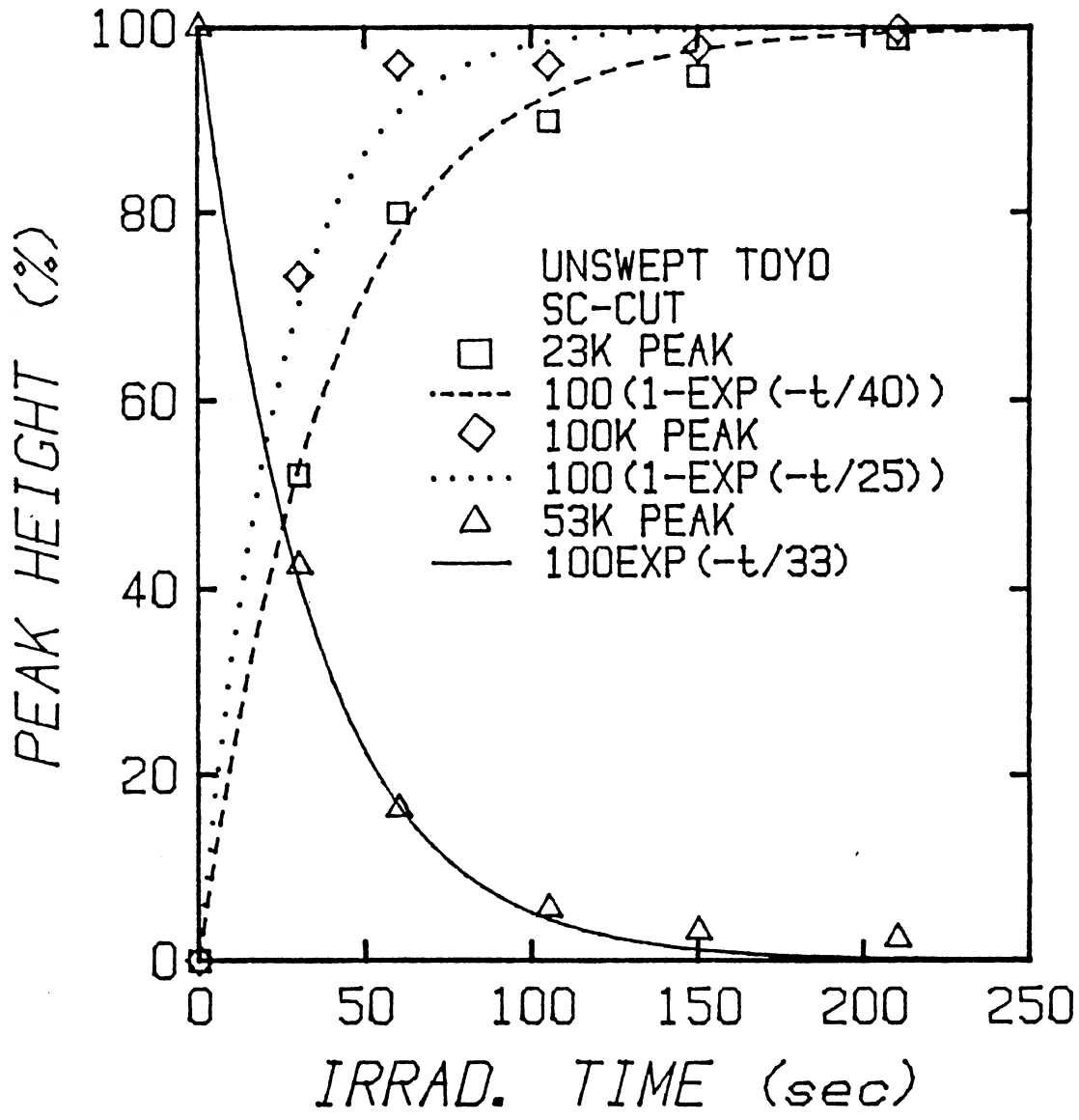

Figure 32. The Normalized Production Curves of the Al-Na^+ center, the Al-hole center, and the 23K Loss Peak for the Unswept SC-cut Toyo Crystal

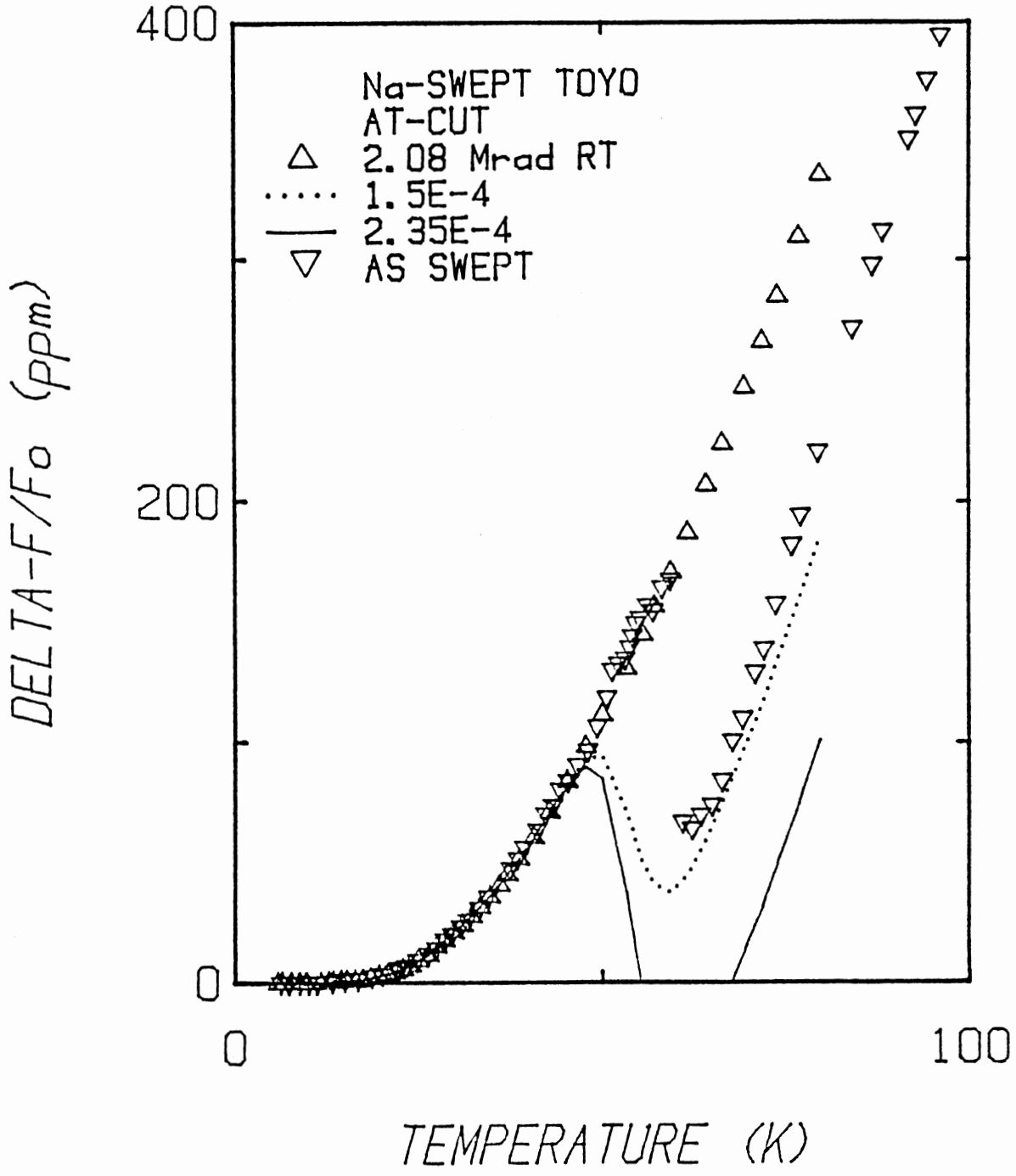

Figure 33. The Frequency versus Temperature Curves for the Na^+-swept AT-cut Toyo Crystal in the As-swept Condition and After the Gamma Irradiations

54K due to the almost complete removal of the Al-Na^+ 54K loss peak. The removal of the 54K loss peak causes a positive frequency shift as expected. If a new loss peak is introduced by irradiation it will cause a frequency drop above the peak temperature. When more than one loss peak, such as growth defect loss peaks and radiation-induced defect loss peaks, are present at temperatures below the operating temperature of crystal the frequency shifts corresponding to these peaks are summed according to Equation (12) in Chapter 2. Thus, the loss peaks produced by irradiation such as the 23K peak and the Al-hole center peaks cause negative frequency shifts; however, because of their small size they do not account for the much smaller observed shift. The frequency shift at room temperature is expected to be dominated by the positive shift due to the 54K loss peak since the size of the loss peaks causing the negative shifts is much smaller. The fractional frequency shift at room temperature is expected to be a 220 ppm positive frequency shift. However, Figure 33 shows a 35 ppm positive frequency shift at room temperature. This result is somewhat surprising. The smaller than expected shift may be an artifact due to the poorer frequency resolution of the log-decrement method, or the removal of the sample from the the cryostat for irradiation; or the small shift may be real.

The 54K loss peak in Figure 19 can be described by Equation (8) in Chapter 2 using 0.165 psec and 57 mV for the

relaxation time constant and activation energy respectively [32]. In the same way the frequency shift going through a loss peak can be described by Equation (11) in Chapter 2. Based on the over simplified assumption that the Al-Na^+ center 54K loss peak should account for the frequency shift in this Na^+-swept crystal the solid and dotted curves shown in Figure 34 were calculated by substracting the frequency shifts calculated by Equation (11) with $(1/Q)_{max}=2.35 \times 10^{-4}$ and 1.5×10^{-4} respectively from the experimental data points for the 2.08 Mrad dose. The solid curve overestimates the frequency shifts shown with the deltas in Figure 34 while the dotted curve gives a much better fit. Consequently, the as-Na^+-swept sample curve shows a greater slope above the 54K peak region, but its size is only a half of the one calculated from the 54k loss peak.

Figure 35 shows the fractional frequency offset versus temperature curves for the Na^+-swept AT-cut Sawyer crystal over the temperature range of 8-100K after a 210 second room temperature irradiation. Since the size of the 54K Al-Na^+ peak was reduced from 1.24×10^{-5} to 1.55×10^{-6}, the frequency shift of 11 ppm would be expected. Also, the frequency shift at the operating temperature of 54K was observed to be 11 ppm. This agreement of the expected and observed frequency offsets at 54K is encouraging when compared to that of the Na^+-swept AT-cut Toyo sample. In this case, the Na^+-swept Sawyer sample was not removed from the refrigerator for irradiation and the transmission method

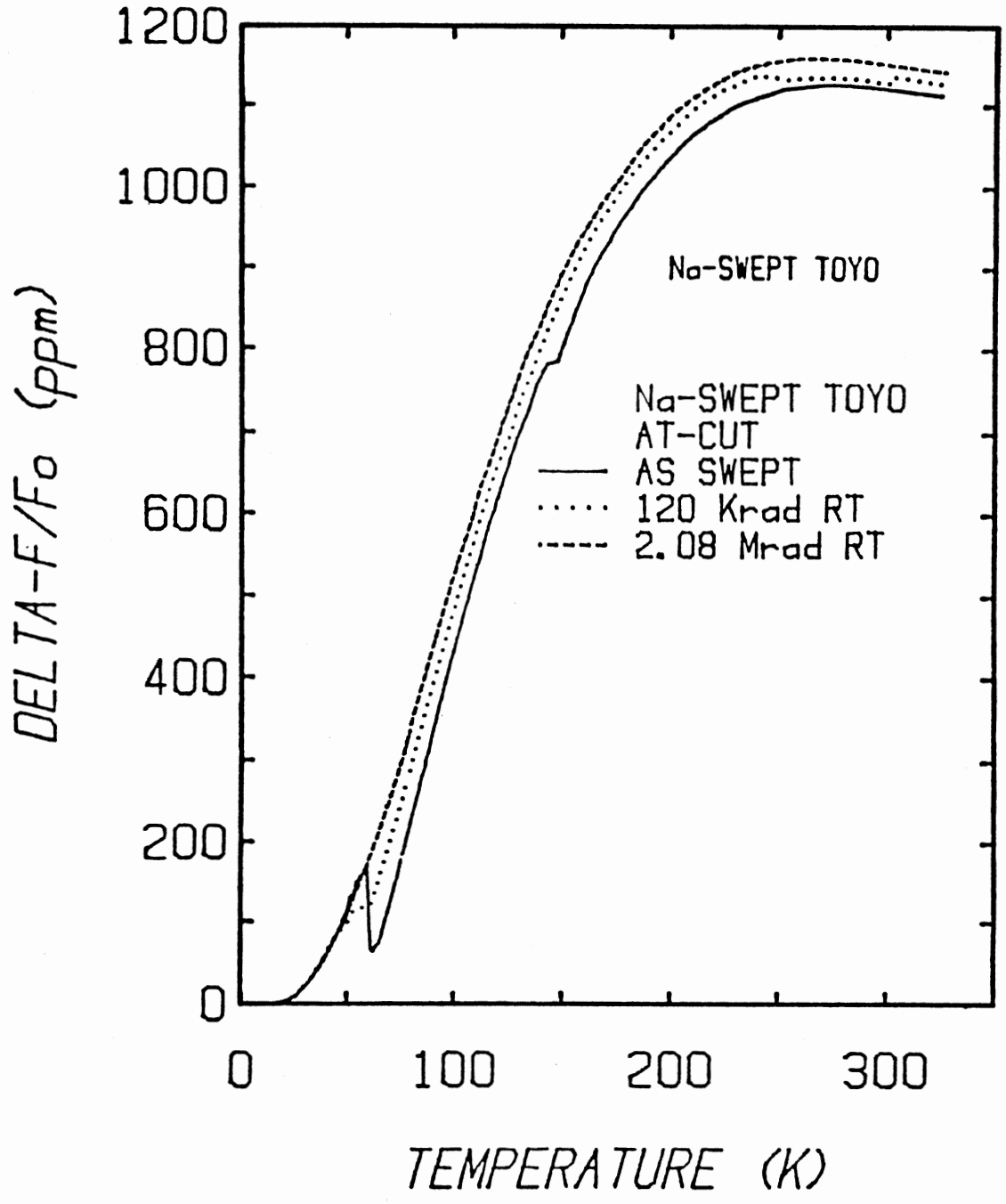

Figure 34. The Frequency versus Temperature Curves in Expanded Scale fot the Na^+-swept AT-cut Toyo Crystal After the Gamma Irradiation to Saturation and the Calculated Frequency Shifts from the 53K Loss Peak

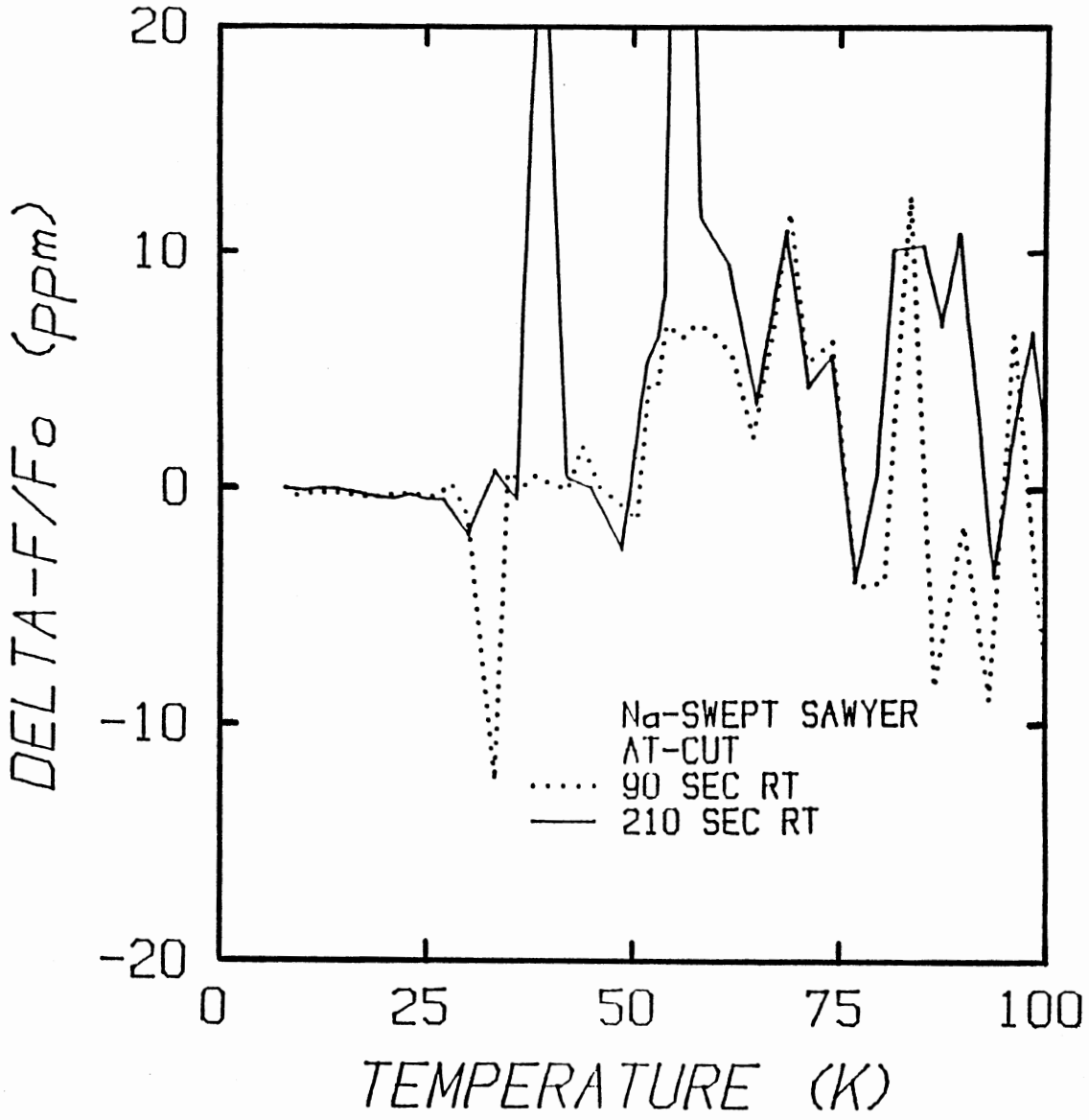

Figure 35. The Fractional Frequency Offset versus Temperature Curves for the Na^+-swept AT-cut Sawyer Crystal over the Temperature Range of 8K-100K after 210 second Room Temperature Irradiation

was used instead of the log-decrement method. Some frequency shifts above 54K might be caused by interfering modes.

Figure 36 shows the frequency versus temperature curves for the Na^+-swept AT-cut Sawyer crystal on an expanded scale for the 200-400K temperature range. In the discussion of Figure 33 the frequency shift at room temperature was expected to be mostly governed by the positive shift due to the 54K loss peak, but the observed frequency shift was much smaller than the predicted value from the the 54K peak. Again, the observed frequency shift of 2.6 ppm at room temperature is much smaller than the predicted value of 11 ppm from the 54K loss peak. However, it is encouraging that the ratio of the observed frequency shifts at the operating temperatures of 300K and 54K is similar to the one for the Na^+-swept AT-cut Toyo sample. The small frequency shift after irradiation between 200K and 250K might be due to the interfering modes at 200K and 250K. And the small frequency shift after irradiation above 300K might be due to the growth of the radiation-induced Na^+-related loss peak.

Figure 37 shows the fractional frequency offset versus temperature for the Li^+-swept BT-cut Toyo crystal after the 15 sec and 90 sec electron irradiation at room temperature. The observed frequency shift at the operating temperature of 100K is -2.3 ppm for the 15 second irradiation and -4.4 ppm for the 90 second irradiation. The frequency shift at 100K is expected to be -3.2 ppm for the 90 second irradiation

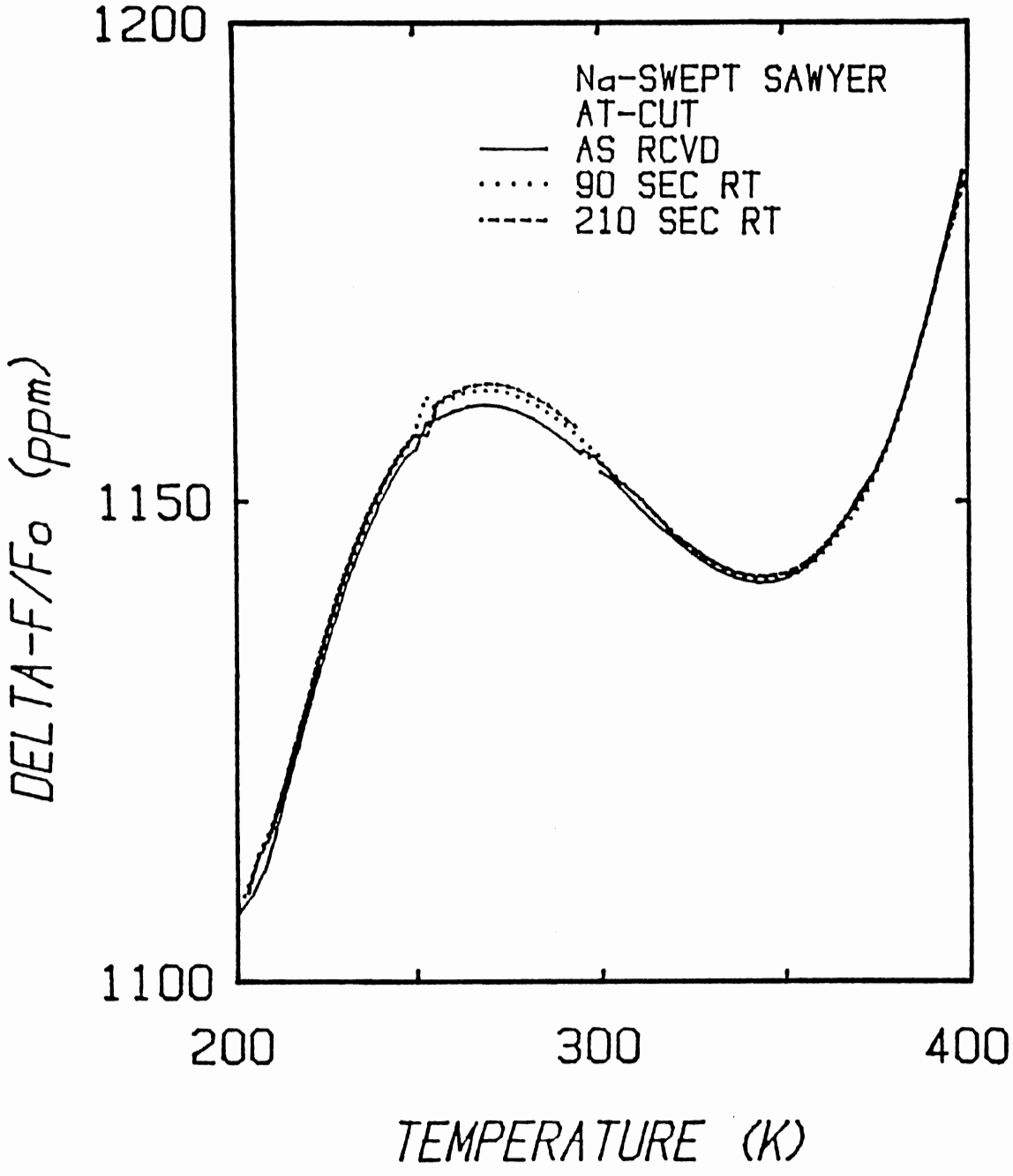

Figure 36. The Frequency versus Temperature Curves for the Na^+-swept AT-cut Sawyer Crystal for the 200K-400K Range

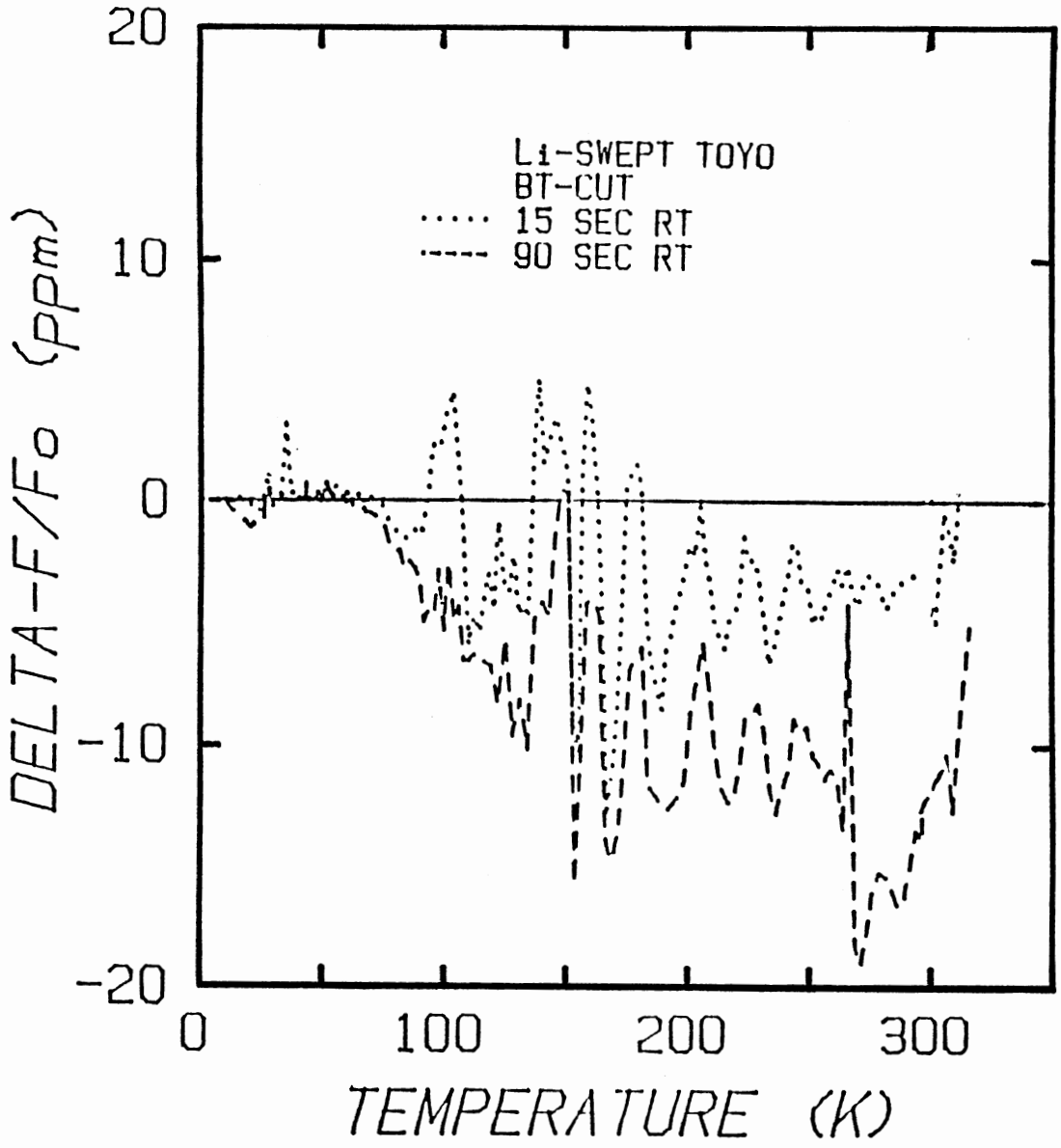

Figure 37. The Radiation-induced Fractional Frequency Offset for the Li^+-swept BT-cut Toyo Crystal

from the 23K and 100K loss peaks. The observed frequency at room temperature shows the expected value for the 15 second irradiation, but is 2.5 times as large as the expected value for the 90 second irradiation. This large frequency offset at room temperature may be due to unidentified loss peaks or interfering modes above 150K. This unidentified loss peaks are caused by some defects unidentified in acoustic loss spectrum which may be Al-related defects, germanium-related defects, or oxygen vacancy centers.

Figure 38 shows the fractional frequency shift for the Li^+-swept AT-cut Toyo sample as a function of temperature after the 240 second room temperature irradiation. The frequency shift at the operating temperature of 100K is expected to be -4 ppm based on the size of the 23K and 100k loss peaks in Figure 22 according to Equation (12) in Chapter 2. However, Figure 38 shows the negative frequency shift of -6 ppm at 100K. Figure 38 shows that the 200k loss peak caused by the interfering mode does not contribute the frequency shift at 200K. The frequency shift at room temperature is expected to be -5 ppm from the size of the acoustic loss peaks while the observed one is -4 ppm. This agreement is probably satisfactory.

Figure 39 shows the fractional frequency offset as a function of temperature for the unswept SC-cut Toyo crystal after the 30 sec and 210 sec room temperature irradiations. At 54K the positive frequency shift due to the destruction of the large Al-Na^+ 54K loss peak is calculated to be 23

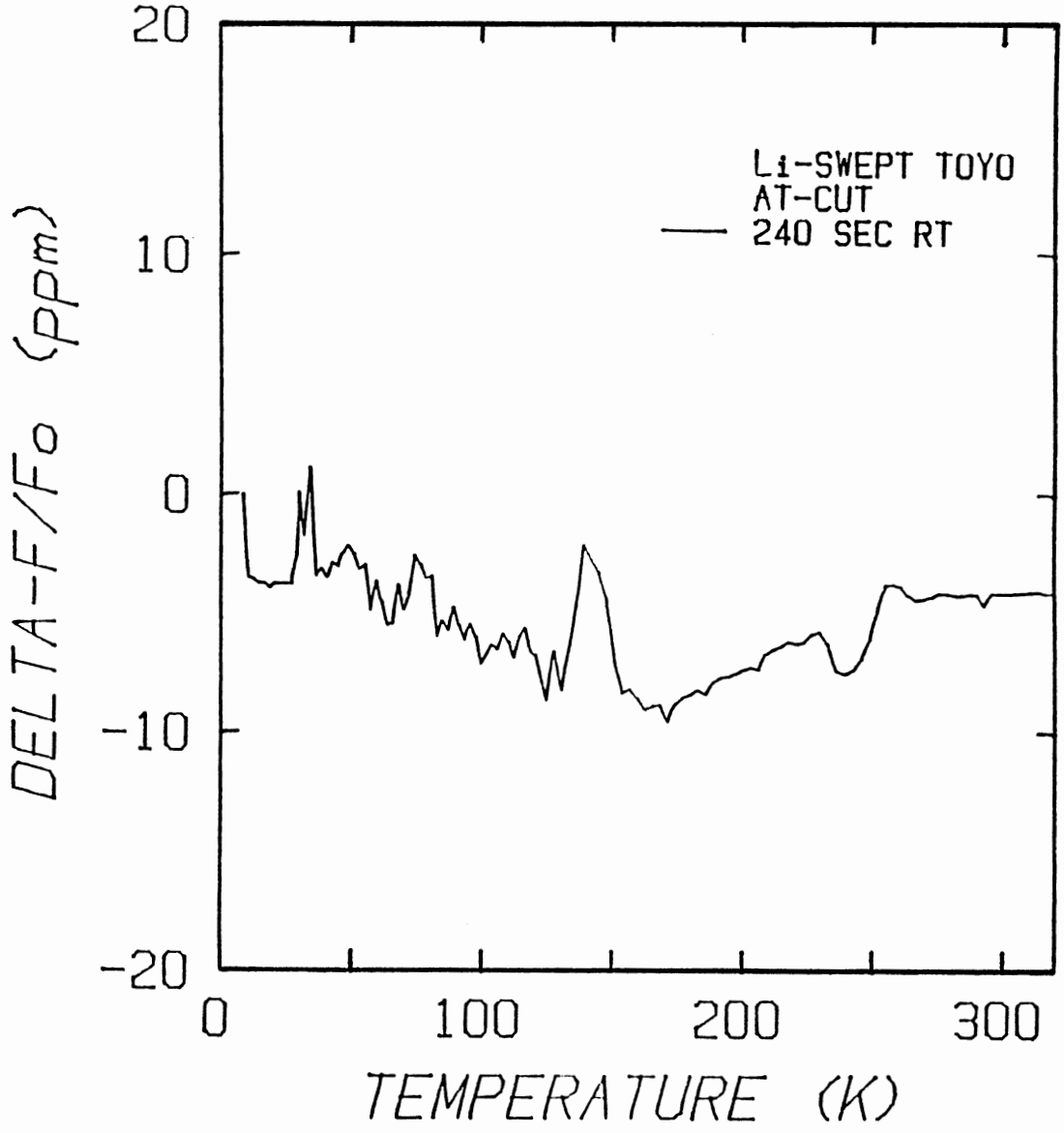

Figure 38. The Fractional Frequency Shift for the Li^+-swept AT-cut Toyo Sample as a Function of Temperature After the 240 second Room Temperature Irradiation

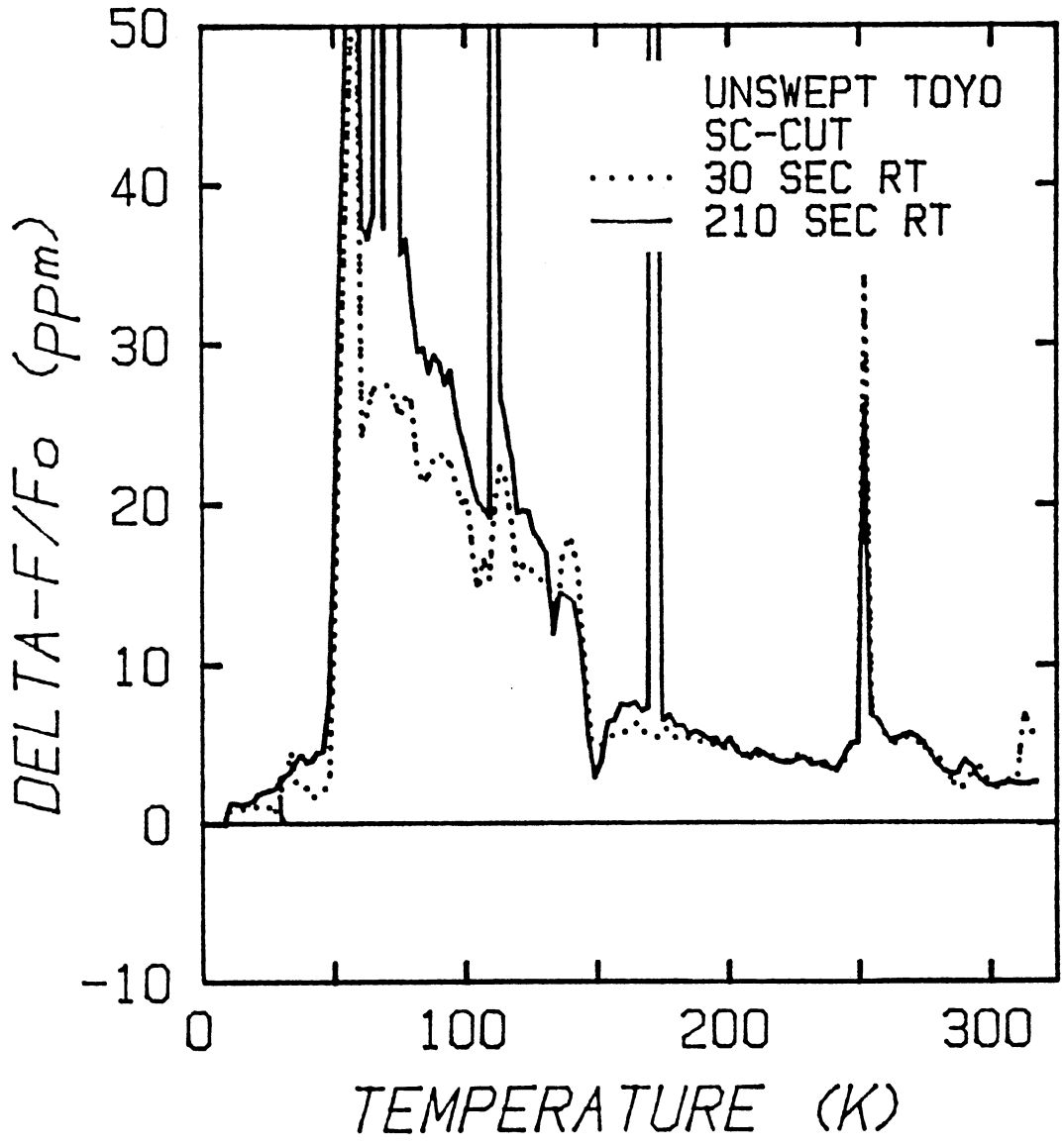

Figure 39. The Fractional Frequency Offset for the Unswept SC-cut Toyo Crystal for Two Room Temperature Irradiations

ppm, and the negative frequency shift due to the 23K loss peak to be -0.6 ppm. Thus, the 23 ppm of the frequency shift at 54K is predicted from the two loss peaks. However, the observed frequency shift at 54K shows about 37 ppm. At room temperature the frequency shift is calculated to be 22 ppm while the observed frequency shift is about 3 ppm. The ratio of the observed frequency shift to the expected value is 1.4 at the operating temperature of 54K and 0.14 at room temperature. The observed frequency shift at room temperature is only 14% of the expected value, which approximately matches with the Na^+-swept samples but a lot smaller than the Li^+-swept samples.

Figure 40 shows the fractional frequency offset for the low temperature irradiation of the unswept SC-cut Toyo crystal. The offset is taken from the frequency data measured after the 210 sec room temperature irradiation to saturation. At the operating temperature of 100K the observed frequency shift is about -10 ppm while the the frequency shift is calculated to be -2 ppm from the 54K and 100K loss peaks. At room temperature the observed frequency shift is -1.7 ppm while the calculated frequency shift is -2 ppm. The observed frequency shifts 87% of the predicted value at room temperature, but 5 times larger than the predicted value at 100K. This large difference at 100K between the observed and the predicted values may be due to the larger frequency shift according to the 54K loss peak than the frequency shift according to the 100K loss peak as

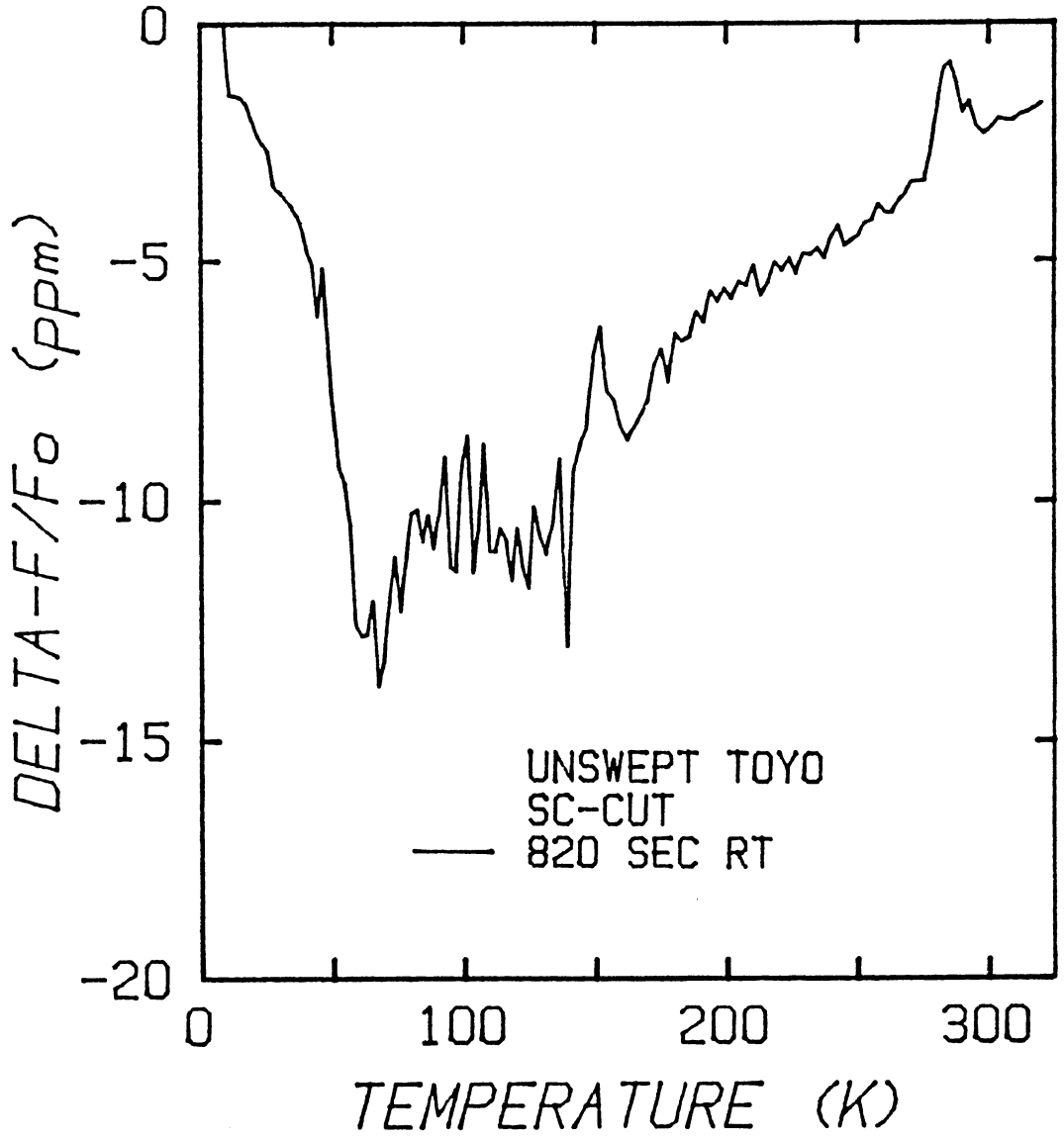

Figure 40. The Fractional Frequency Offset for the Subsequent Low Temperature Irradiation after Room Temperature Irradiation to

shown. The frequency shift due to the 54K loss peak is supposed to be smaller than the one due to the 100K loss peak. Thus, the produced 54K loss peak by the low temperature irradiation in Figure 39 may be due to a interfering mode.

CHAPTER IV

CONCLUSIONS

The large 53K loss peak, which is caused by the Al-Na^+ center, appears in the Na^+-swept and unswept samples, but not in the H^+-swept and Li^+-swept samples. The size of this peak scales with the aluminum concentration in the sample. A series of the ionizing irradiation at room temperature destroys the 53K loss peak. The 53K loss peak goes out as exp(-KD), where K is a constant and D is a radiation time or a radiation dose; however, the radiation constant, K, becomes smaller as the radiation dose goes to saturation. The reduction of the 53K loss peak causes a positive frequency shift. The observed frequency shift agrees with the expected value at the operating temperature of 53K, but is about 20% of the expected value at room temperature.

The 100K loss peak is produced by irradiation at room temperature and subsequent low temperature irradiation after saturation. However, an initial low temperature irradiation without previous room temperature irradiation failed to produce the 100K loss peak in the Li^+-swept sample while it produduced the 100K loss peak in the H^+-swept sample. Since the H^+-swept sample and the Li^+-swept sample after room temperature irradiation to saturation have high Al-OH^-

contents and the Li^+-swept sample before room temperature irradiation has a very small Al-OH^- content, it appears that room temperature irradiation destroys the Al-alkali centers and produces a mixture of the Al-hole and Al-OH^- centers and low temperature irradiation readily converts Al-OH^- centers into Al-hole centers. The 100K loss peak produced by room temperature irradiation does not anneal out at room temperature while the 100K loss peak produced by low temperature irradiation does. The 100K loss peak is 2-3 times stronger in BT-cut crystal than in AT-cut crystal. Thus, the 100K loss peak can be tracked most easily in BT-cut crystal as a function of radiation dose. For room temperature irradiation the 100K loss peak grows as $(1-\exp(-K'D))$. The production and growth patterns and annealing behavior of the 100K loss peak indicate that it is caused by Al-hole centers. The growth of the 100K loss peak causes a negative frequency shift at room temperature.

The 23K loss peak is produced together with the 100K loss peak by room temperature irradiation and subsequent low temperature irradiation after room temperature irradiation to saturation. However, the 23K loss peak does not change much in the Na^+-swept AT-cut Sawyer, Li^+-swept AT-cut Toyo, and unswept SC-cut Toyo samples according to subsequent low temperature irradiation; its production behavior is different from that of the 100K loss peak. The 23K loss peak is 2-3 times larger in AT-cut crystal than either in BT-cut crystal or in SC-cut crystal. Thus, the 23K loss peak can

be tracked most easily in an AT-cut crystal. The 23K loss peak grows according to the form $(1-\exp(-K''D))$ as the 100K loss peak. However, the constant K'' is smaller than constant K' of the 100K loss peak; it grows slower than the 100K loss peak. The reverse of the size of the 23K loss peak and the 100K loss peaks in the H^+-swept AT-cut sample, different production behavior from the 100K loss peak, and slower growth rate than the 100K loss peak indicate that the 23K loss peak is not due to the same center as the 100K loss peak. The 23K loss peak causes a negative frequency shift.

The small 135K, β, loss peak associated with the Al-Na^+ 53K loss peak is present in the Na^+-swept and unswept samples. This loss peak decays with radiation dose at room temperature.

The other 135K loss peak, which is probably associated with the Al-hole 100K loss peak, grows with radiation dose in the Li^+-swept samples. This 135K loss peak is also enhanced by subsequent low temperature irradiation.

The 340K and 305K loss peaks are produced by room temperature irradiation in the Na^+-swept and Li^+-swept samples respectively. These loss peaks are small, and grows in and out with radiation dose.

The new 107K loss peak is produced in the Li^+-swept sample by initial low temperature irradiation. It was destroyed by room temperature irradiation or anneal at room temperature. This 107K loss peak is definitely not the 100K loss peak when compared to the 100K loss peak produced by room temperature irradiation.

FUTURE WORK

1. By applying a DC field at 23K and at 100K the potential wells associated with these loss peaks will be changed and also the defects responsible for these loss peaks will be perturbed. Thus, we can monitor the modified loss peaks at 23K and 100K. This information may give us the information to identify the defects responsible for these two loss peaks; if these two loss peaks are caused by the same defect, Al-hole, they will change in the same way.

2. The conversion of radiation time into radiation dose for Van de Graaff accelerator was not done during this study. It is desired to directly compare results from both electron and gamma-ray irradiations.

3. The experiments with the H^+-swept sample shows that the Al-OH^+ center can be easily destroyed by low temperature irradiation. Further low temperature irradiations of the H^+-swept sample will give the growth information of the Al-hole center. Also room temperature irradiation with the H^+-swept sample may give us the information how the Al-OH^- center responds to room temperature irradiation.

4. From ESR studies it was known that some defects can be produced by the sequence of the irradiation at

intermediate temperature between 150K and 300K and low temperature irradiation at 80K. It seems that this defect are stable under liquid nitrogen temperature. So we may monitor a new loss peak caused by this defect if we irradiate a sample by following this sequence.

5. The Li^+-swept BT-cut sample gives a strong 100K loss peak when compared to the AT-cut sample. In the Na^+-swept AT-cut sample the 100K loss peak used to be small, so that the growth study of the 100K loss peak as a function of radiation dose was very difficult. However, in the Na^+-swept BT-cut sample the 100K loss peak may be easily tracked as a function of radiation dose.

REFERENCES

[1] Cady, W. G. Piezoelectricity, Vols. 1 and 2 (Dover Publications, New York, 1964).

[2] EerNisse, E. P., Proc. 30th Annual Symposium on Freq. Control, pp.8(1976).

[3] Kusters, J.: Adams, C.; Yoshida, H.; and Leach, J., Proc. 31st Annual Symposium on Freq. Control, pp.3(1977).

[4] Boemmel, H. E.; Mason, W. P.; and Warner, A. W. Phys. Rev., 99, 1894(1955).

[5] Boemmel, H. E.; Mason, W. P.; and Warner, A. W. Phys. Rev., 102, 64(1956).

[6] King, J. C. Bell System Tech. J., 38, 573(1959).

[7] King, J. C. Final Rept. DA 36-039 SC-64586, Bell Telephone Lab. Inc., (1960).

[8] Jones, C. K. and Brown, C. S. Proc. Phys. Soc. (London), 79, 930(1962).

[9] Fraser, D. B. J. Appl. Phys., 35, 2913(1964).

[10] Martin, J. J. Proc. 38th Annual Symposium on Frequency Control, 16, (1984).

[11] King, J. C. and Sander, H. H. IEEE Trans. Nucl. Sci., NS-19, 23(1972).

[12] Martin, J. J.; Halliburton, L. E.; and Bossoli, R. B. Proc. 35th Annual Symposium on Frequency Control, 317, (1981).

[13] Martin, J. J. and Doherty, S. P. Proc. 34th Annual Symposium on Frequency Control, 81, (1980).

[14] Sibley, W. A.; Martin, J. J.; Wintersgill, M. C.; and Brown, J. D. J. Appl. Phys., 50, 5449, (1979).

[15] Markes, M. E. and Halliburton, L. E. J. Appl. Phys. 50, 12(1979).

[16] Doherty, S. P.; Martin, J. J.; Armington, A. F.; and Brown, R. N. J. Appl. Phys., 51, 4164, (1980).

[17] Hallibuton, L. E.; Koumvakalis, N.; Markes, M. E.; and Martin, J. J. J. Appl. Phys., 52, 3565, (1981).

[18] Martin, J. J.; Hwang, H. B.; Bahadu, H. Proc. 39th Annual Symposium on Freq. Control, PP.266(1985).

[19] Berry, B. S. and Nowick, A. S. Physical Acoustics, Vol. 3, Part A, W. P. Mason Ed. (Academic Press, New York, 1966).

[20] Nowick, A. S. and Berry, B. S. Anelastic Relaxation in Crystalline Solids (Academic Press, New York, 1972).

[21] Kittel, C.; Knight, W. D.; and Rudermann, M. A. Mechanics, (Mcgraw-Hill, 1973)

[22] Halliburton, L. E.; Martin, J. J.; and Koehler, D. R. Precision Frequency Control, Vol. 1, E. A. Gerber and A. Ballato Ed. (Academic Press, New York, 1985), pp.37.

[23] King, J. C. and Koehler, D. R. Precision Frequency Control, Vol. 1, E. A. Gerber and A. Ballato Ed. (Academic Press, New York, 1985), pp.150.

[24] Klemens, P. G. Physical Acoustics, Vol. 3B, W. P. Mason Ed. (Academic Press, New York, 1965), pp.301.

[25] Akhieser, A. J. Phys. USSR 1, 277, (1939).

[26] Boemmel, H. E. and Dransfeld, K. Phys. Rev. 177, 1245, (1960).

[27] Woodruff, R. O. and Ehrenreich, H. Phys. Rev., 123, 1553, (1961).

[28] Mason, W. P. Physical Acoustics, Vol. 3B, W. P. Mason Ed. (Academic Press, New York,1965), pp. 235.

[29] Jalilian-Nosraty, M. and Martin, J. J. J. Appl. Phys., 52(2), 785, (1981).

[30] Chadderton, L. T. Radiation Damage In Crystals (Methuen & Co LTD, London, 1965) pp.161.

[31] Martin, J. J. (Private Communication), Mar. 1987, Oklahoma State University, Professor.

[32] Martin, J. J. J. Appl. Phys. 56, 2536(1984).

VITA

Ho Byong Hwang

Candidate for the Degree of

Doctor of Philosophy

Thesis: RADIATION STUDIES ON AL-RELATED DEFECT CENTERS IN QUARTZ CRYSTALS

Major Field: Physics

Biographical:

Personal Data: Born in Kimjae, Jeonbug, Korea, Septtember 6,1951. The son of Jongkyu and Jeongae Hwang. Married to Meeyoung Lee on June 8, 1980.

Education: Received Bachelor of Science degree in Physics from Jeonbug National University, Jeonju, Jeonbug, Korea, February 1974; received Master of Science degree in Physics from Oklahoma State University, Stillwater, Oklahoma, May 1985; completed requirements for the Doctor of Philosophy degree at Oklahoma State University, May 1987.

Professional Experience: Teaching Assistant, Department of Physics, Oklahoma State University, August 1981, to December 1983; Research Assistant, Department of Physics, Oklahoma State University, January 1984, to present.